Department of AERONAUTICS and ASTRONAUTICS
STANFORD UNIVERSITY

PHILIP M. BUCHEK

MODERN CONTROL TECHNIQUES IN ACTIVE FLUTTER SUPPRESSION USING A CONTROL MOMENT GYRO

MARCH
1974

This research was supported by the
National Aeronautics and Space Administration
under Grant NGL 05-020-498
and the Traineeship Program

SUDAAR
NO. 474

Department of Aeronautics and Astronautics
Stanford University
Stanford, California

MODERN CONTROL TECHNIQUES IN ACTIVE FLUTTER SUPPRESSION USING A CONTROL MOMENT GYRO

by

Philip M. Buchek

SUDAAR NO. 474

March 1974

This research was supported by the
National Aeronautics and Space Administration
under Grant NGL 05-020-498
and the Traineeship Program

ABSTRACT

PRECEDING PAGE BLANK NOT FILMED

The conventional solutions for increasing the flutter speeds of particular configurations have included structural modifications, mass balancing, and geometry changes, which generally result in increased structural weight and reduced aerodynamic efficiency. Flutter suppression by active control of aeroelastic modes with closed loop feedback of appropriate parameters is a relatively recent approach which can significantly reduce these design penalties. This thesis is concerned with the development of organized synthesis techniques, using concepts of modern control theory, for the design of active flutter suppression systems for two and three-dimensional lifting surfaces, utilizing a control moment gyro (CMG) to generate the required control torques.

Incompressible flow theory is assumed, with the unsteady aerodynamic forces and moments for arbitrary airfoil motion obtained by using the convolution integral based on Wagner's indicial lift function. Wagner's function is approximated in the analysis by a sum of exponential terms and two-dimensional strip theory is used to model the finite wing. This formulation enables Laplace transform techniques to be applied to the system of equations. Additional states, based on second and third order time derivatives of bending and torsional displacements, can be identified and thus allow the system to be placed into standard state variable form, with the state transition and control distribution matrices being real.

Using pole-assignment (arbritrary dynamics) techniques, the control system characteristics of the two-dimensional (typical section) wing are first examined to establish basic design trends with the results presented as a function of velocity on root locus diagrams. Linear optimal control theory is applied to find particular optimal sets of gain values which minimize a quadratic performance function. The closed loop system's response to impulsive gust disturbances and the resulting control power requirements are investigated, and the system eigenvalues necessary to minimize the maximum value of control power are determined. Full state feedback with scheduled gains is required to obtain this minimum value. Reduced feedback designs with constant gain values, which do not significantly increase power requirements, are also determined.

The vibrational properties of the wing in developing the three-dimensional analysis are described by a superposition of the "uncoupled" modes of pure bending and torsion. With

full state variable feedback, complete modal controllability (ie., arbitrary relocation of the system eigenvalues) of the system can be obtained with only a single CMG controller regardless of the number of assumed modes. The significant feedback parameters needed to obtain this control are determined as a function of structural and important CMG parameters and velocity. As was learned in the typical section analysis, the location of all the closed loop eigenvalues proved critical to particular designs, not only in meeting power level requirements, but also in influencing the occurrence of higher mode instability.

Conditions for system observability are discussed for both the typical section and three-dimensional wing cases.

ACKNOWLEDGEMENTS

I wish to thank my advisor, Dr. Samuel C. McIntosh, for his thorough review of the final manuscript. His constructive comments and suggestions have helped improve this presentation.

Thanks also go to Mrs. Bibby Schumann for her expeditious typing of the final draft of this thesis.

Particular gratitude is expressed to the National Aeronautics and Space Administration, who supported this research through their Traineeship Program and under NASA Grant NGL 05-020-498.

Especially, I would like to thank my wife, Pamela, for her unlimited patience and understanding and enthusiastic support and encouragement during the time required to complete this research.

TABLE OF CONTENTS

TABLE OF CONTENTS
(Continued)

LIST OF SYMBOLS

a	distance between typical-section datum and elastic axis in semichords; positive aft
A	matrix of weights on state variables, see Eq. 4.2
A_{ij}	characteristic-equation coefficients defined in Appendix C
b	typical-section semichord
B	matrix of weights on control variables, see Eq. 4.2
B_1	$1 + \mu$
B_2	$x_\alpha \mu - a$
B_3	$1 - 2a$
B_4	$\mu (\omega_h/\omega_\alpha)^2$
C	controllability matrix
$C(k)$	Theodorsen function
C_h, C_α	typical-section spring constants on h, α
$C_{h1}, C_{h2}, C_{\alpha 1}, C_{\alpha 2}$	modal spring constants on $h1$, $h2$, α_1, α_2
D_φ	denominator polynomial in rational approximation to $\varphi(\bar{s})$; $D_\varphi = \bar{s}^2 + d_1\bar{s} + d_0$
EI	flexural rigidity
F	open-loop dynamics matrix
F_{ij}	elements in open-loop dynamics matrix for typical-section, see Eq. 3-11
$F(k)$	real component of complex Theodorsen function

$F_{h1}, F_{h2}, F_{\alpha 1}, F_{\alpha 2}, F_{h1,\alpha 1}, F_{h2,\alpha 1}, F_{h1,\alpha 2}, F_{h2,\alpha 2}$	integrated modal weighting factors, see Eq. 5-16
$F(i,j)$	elements of two mode open-loop dynamics matrix, see Eq. 6-11
$f_{h1}, f_{h2}, f_{\alpha 1}, f_{\alpha 2}$	first and second bending and first and second torsional mode shapes, see Eqs. 5-7 to 5-10
f_1 to f_n	coefficients in open-loop characteristic equation, see Sect. 3.3
GJ	torsional rigidity
$G(k)$	imaginary component of complex Theodorsen function
G	control-distribution matrix, see Eq. 3-1
G_o	gyro parameter, $H_w/I_{Gz}\omega_\alpha$
G_1	gyro parameter, $H_w/\pi\rho b^4\omega_\alpha$
G_2	gyro parameter, G_oG_1
G_{o1}, G_{o2}	gyro parameter, $G_o f_{\alpha 1}(y_G)$, $G_o f_{\alpha 2}(y_G)$
G_{11}, G_{12}	gyro parameter, $\frac{G_1}{\ell} f_{\alpha 1}(y_G)$, $\frac{G_1}{\ell} f_{\alpha 2}(y_G)$
$\bar{G}_2$	gyro parameter, G_2/ℓ
g	control-distribution vector
g_1 to g_n	coefficients of desired characteristic equation, see Sect. 3.3
H	output distribution matrix, see Eq. 3-28
h	typical-section plunging degree of freedom, see Fig. 2.1
$h(y)$	span wise plunging degree of freedom, see Fig. 5.1

h_1, h_2	typical-section plunging states defined in Eqs. 3.3 and 3.4, in Chaps. 3 and 4; first and second bending mode deflections in Chap. 5
h_{11}, h_{12}	first bending plunging states defined in Eqs. 6.1 and 6.2
$\mathcal{H}$	Hamiltonian, see Sect. 4.1
H_w	CMG rotor angular momentum
I_a	typical-section moment of inertia about elastic axis
I_a'	I_a augmented by CMG moment of inertia about elastic axis
I_{G_z}	CMG gimbal moment of inertia
k	reduced frequency, $\omega b/U$
$\underline{K}$	feedback control gain vector
K_1 to K_{10}	feedback control gains
L	lift
L_D	disturbance lift in typical-section equations of motion
ℓ	span of wing
m	typical-section mass per unit span
m_G	CMG mass
m'	m augmented by CMG mass
M_D	disturbance moment about elastic axis
$M_{w/G}$	reaction moment of wing on CMG controller
N_φ	numerator polynomial in rational approximation for $\varphi(\bar{s})$; $N_\varphi = n_2\bar{s}^2 + n_1\bar{s} + n_o$

$\bar{P}$	dimensionless control power, $T_c\dot{\sigma}b/\omega_\alpha w_g$
R	matrix of open-loop characteristic equation coefficients, see Eq. 3.24
r_α	radius of gyration, $(I_\alpha/mb^2)^{\frac{1}{2}}$
$r_{\alpha 1}, r_{\alpha 2}, r_{\alpha G}$	radii of gyration, $\left[1 + \frac{I_{Gz}}{\ell I_\alpha}\frac{f_{\alpha 1}^2 (y_G)}{F_{\alpha 1}}\right]^{\frac{1}{2}} r_\alpha$
	$\left[1 + \frac{I_{Gz}}{\ell I_\alpha}\frac{f_{\alpha 2}^2 (y_G)}{F_{\alpha 2}}\right]^{\frac{1}{2}} r_\alpha$
	$\left[\frac{I_{Gz}}{\ell I_\alpha} f_{\alpha 1} f_{\alpha 2}(y_G)\right]^{\frac{1}{2}} r_\alpha$
s	complex frequency
$\bar{s}$	s/ω_α in Chaps. II, III, IV; $s/\omega_{\alpha 1}$ in Chaps. V, VI
S_α	static unbalance, product of airfoil mass and CM-EA distance
t	time
$\bar{t}$	tU/b in Chaps. II and V
T	kinetic energy
T_c	CMG control torque
$\bar{T}_c$	dimensionless control torque, $T_c b/I_{Gz}\omega_\alpha^2 w_g$
$\underline{u}_c$	control vector
$\bar{u}$	dimensionless speed, $U/b\omega_\alpha$
$\bar{u}_F$	dimensionless flutter speed
U	freestream speed
V	potential energy
w	local downwash on typical-section

W_g	gust velocity
w_g	impulse gust amplitude, feet
x	dimensionless chordwise typical-section coordinate
$\underline{x}$	state vector
x_α	dimensionless static unbalance, S_α/mb
$x_{\alpha 11}, x_{\alpha 12}$ $x_{\alpha 21}, x_{\alpha 22}$	dimensionless static unbalances, $\left[1 + \frac{m_G}{m\ell} \frac{f_{h1} f_{\alpha 1}(y_G)}{F_{h1,\alpha 1}}\right] x_\alpha$, $\left[1 + \frac{m_G}{m\ell} \frac{f_{h1} f_{\alpha 2}(y_G)}{F_{h1,\alpha 2}}\right] x_\alpha$, $\left[1 + \frac{m_G}{m\ell} \frac{f_{h2} f_{\alpha 1}(y_G)}{F_{h2,\alpha 1}}\right] x_\alpha$, $\left[1 + \frac{m_G}{m\ell} \frac{f_{h2} f_{\alpha 2}(y_G)}{F_{h2,\alpha 2}}\right] x_\alpha$,
y	wing spanwise coordinate
y_G	spanwise distance to CMG
α	typical-section pitching degree of freedom
$\alpha(y)$	spanwise pitching degree of freedom
α_1, α_2	typical section pitching states defined in Eqs. 3.5 and 3.6, used in Chaps. III and IV; first and second torsion mode deflections, used in Chap. V
α_{11}, α_{12}	first torsion pitching states defined in Eqs. 6.3 and 6.4
$\underline{\gamma}$	vector, whose elements are the differences between the desired and open-loop characteristic equation coefficients, see Eq. 3.25
μ	mass ratio, $m/\pi\rho b^2$
μ_1, μ_2, μ_G	mass ratios, $\left[1 + \frac{m_G}{m\ell} \frac{f_{h1}^2(y_G)}{F_{h1}}\right] \mu$,

	$\left[1 + \frac{m_G}{m_\ell} \frac{f_{h2}^2 (y_G)}{F_{h2}}\right]\mu$, $\left[\frac{m_G}{m_\ell} f_{h1} f_{h2} (y_G)\right]\mu$
$\xi_1, \xi_2, \xi_3, \xi_4$	aerodynamic lag states associated with rational approximation of $\varphi(\bar{s})$
ρ	freestream density
σ	CMG gimbal angle
σ_1, σ_2	gimbal-angle states defined in Eqs. 3.7 and 3.8
Φ	Wagner indicial function
ψ	Kussner indicial function
ω	frequency
ω_F	flutter frequency
ω_h, ω_α	typical-section uncoupled frequencies, $(C_h/m)^{\frac{1}{2}}$, $(C_\alpha/I_\alpha)^{\frac{1}{2}}$
$\omega_{h1}, \omega_{\alpha 1}$, $\omega_{h2}, \omega_{\alpha 2}$	modal uncoupled frequencies $(C_{h1}/m)^{\frac{1}{2}}$, $(C_{\alpha 1}/I_\alpha)^{\frac{1}{2}}$, $(C_{h2}/m)^{\frac{1}{2}}$, $(C_{\alpha 2}/I_\alpha)^{\frac{1}{2}}$
$\delta(y)$	dirac delta function
Δ	denominator in elements of two-mode, open-loop dynamics matrix, see Appendix D
λ	vector of lagrange multipliers
Θ	observability matrix
χ	characteristic equation of typical section, $u_c = 0$
χ_K	characteristic equation of controlled typical section
$\varphi(s)$	Laplace transform of $\dot{\Phi}(t)$, $s\Phi(s)$

I. INTRODUCTION

1.1 Background

Flutter can be defined as a self-excited, oscillatory instability of an elastic body in an airstream. Physically, this instability can occur when energy from the airstream is absorbed by the body more rapidly than it is dissipated by damping. The onset of the phenomenon is typically characterized by a flutter frequency and a critical airstream speed. Flight at airspeeds in excess of this critical flutter speed can result in catastrophic structural failure. The problem of increasing the flutter speed of particular configurations has in the past been generally solved at the expense of increased structural weight, through structural modification and mass balancing, or by reducing aerodynamic efficiency, through geometry changes. Weight penalties in the range of 10 to 25,000 pounds, for example, have been estimated (1,2) to meet flutter requirements in SST class vehicles.

In more recent years, a substantial amount of experience has been obtained in developing active control systems for gust alleviation and the suppression of low frequency, insufficiently damped structural modes of an aircraft. Refs. 3 and 4 are excellent survey papers of the work done in these areas. This experience, coupled with the potential performance payoffs available (1-5), has made the active suppression of the unstable flutter modes both feasible and desirable. Much of the work done in this latter area has occurred in the last 5 years, and some recent studies can be found in Refs. 6 through 11. In Ref. 6 a study, including analog simulation and wind tunnel tests, was done using an unswept, symmetric wing model to determine the basic characteristics of an active flutter control system. A simple aeroelastic model consisting of a cantilever plate with a follower force at its free end was analyzed both experimentally and theoretically in attempting to actively control flutter in Refs. 7 and 8. Analytical analyses of more complicated structural models applicable to the B-52 and F-4 respectively are described in Refs. 9 and 10, and in Ref. 11 a control system design based on aerodynamic energy is discussed. Each of these analyses, though detailed in many respects, considered rather simple sets of feedback parameters in designing their control systems. This approach, dictated primarily by sensor capabilities, ignores the possibility of using observors or estimators in determining unsensed parameters. The analyses have, therefore, been severely limited in a number of respects:

(1) the maximum available increase in flutter velocity with a particular set of controllers can be limited, (2) determining the gain values that produce this maximum flutter velocity increase can be tedious for complex systems, (3) selecting a control system design giving a particular flutter velocity increase while optimizing other pertinent design parameters is difficult, and (4) design procedures cannot be easily adapted to multi-input/multi-output systems. To remove some of these limitations, this thesis incorporates three goals:

(a) Develop and demonstrate organized synthesis techniques for the design of flutter suppression systems using concepts of modern control theory

(b) Using a control moment gyro as the primary control torque generator, indicate and illustrate design tradeoffs associated with the general development of a practical flutter suppression system

(c) Establish and identify attractive design features of the control moment gyro to warrant its consideration as a viable alternative to aerodynamic surfaces in producing control forces to suppress flutter modes.

1.2 Control Moment Gyro

Although not usually mentioned when possible methods for active flutter suppression are considered (4, 12), substantial experience has been obtained using control moment gyros (CMGs) for momentum exchange in the attitude control of space vehicles and satellites (13 - 19). To familiarize the reader with this type of control, the following is a brief description of the CMG, including some of the possible advantages to be obtained by its incorporation in a flutter suppression system.

The CMG consists basically of a rotor (or wheel) with a known constant magnitude of angular momentum, and a method by which the rotor can be precessed. As discussed more thoroughly in Ref. 18, the three basic configurations for the CMG are, as shown in Fig. 1-1, the one-degree-of-freedom, the two-degrees-of-freedom, and the twin gyro. The one- and two-degrees-of-freedom gyros consist of one rotor mounted so that it can be precessed about one or two axes respectively. These

systems, however, can have undesirable cross-coupling torques. The twin gyro consists of two counter-rotating gyro elements which are precessed through equal but opposite angles so that the control torque is always directed about a single axis. In a three-dimensional flutter analysis, the possibility does exist that cross-coupling torques occurring for the one degree-of-freedom gyro could be used to advantage. However, their inclusion in the flutter analysis introduces nonlinear terms into the equations of motion. Therefore to maintain linearity the twin-gyro control system will be used.

For space vehicle and satellite attitude control applications, the control moment gyro has been shown to have advantages in power, accuracy, response, and simplicity compared to reaction-wheel systems (16). Since output torque is proportional to input gimbal rate, the CMG can produce large moments on the airfoil at the relatively high flutter frequencies without requirements for large angular momenta, and hence, large size. The effectiveness is not influenced by the complex aerodynamic forces which depend upon Mach number and unsteady aerodynamic effects. Consequently, the mathematical complexities in the analysis are somewhat reduced. Furthermore, the inherent lag in the development of forces on aerodynamic surfaces does not occur with this system, which should result in a reduction in the amount of lead necessary for control and higher allowable controller bandwidth. Also, deflection angle of the gyro gimbal is an easily measured quantity and can be used directly as a feedback parameter and in estimating other states of the system.

1.3 Thesis Summary

In Chapter II, the equations of motion for the typical section (two-dimensional wing surface) and CMG controller are developed. Incompressible flow is assumed and the unsteady aerodynamics for arbitrary motion are represented by utilizing the Wagner indicial function. The open-loop characteristics of the system are examined with critical design parameters identified.

In Chapter III, the closed-loop characteristics of the system developed in Chapter II are determined. The system is placed in standard state variable form with the definition of two new states, and the controllability and observability of the system are discussed. Full state and reduced state feedback designs for various CMG sizes are determined.

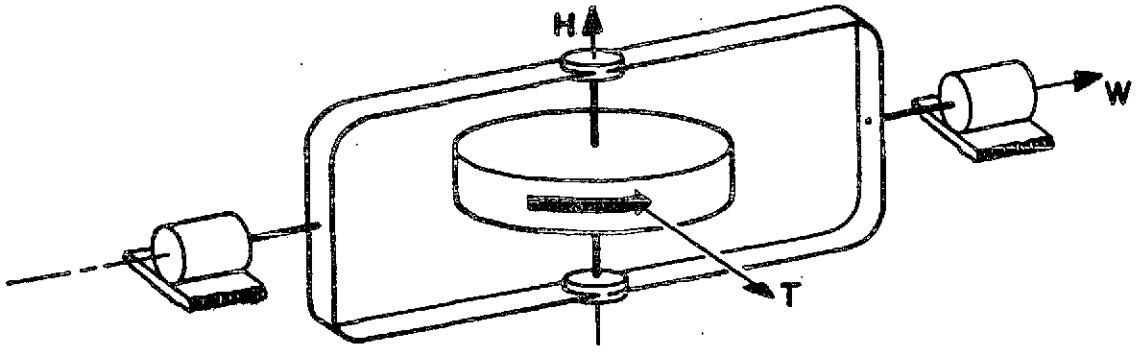

a. One Degree of Freedom

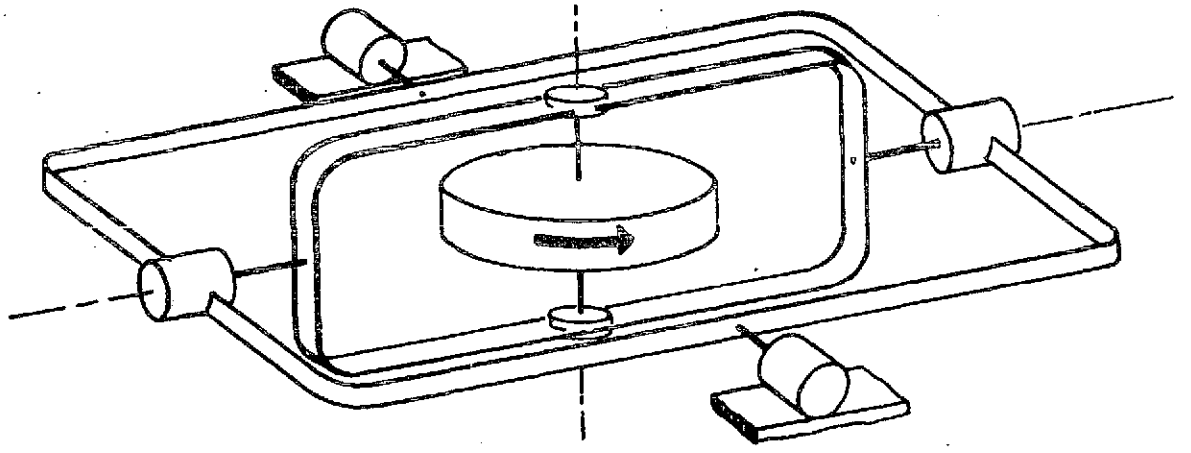

b. Two Degrees of Freedom

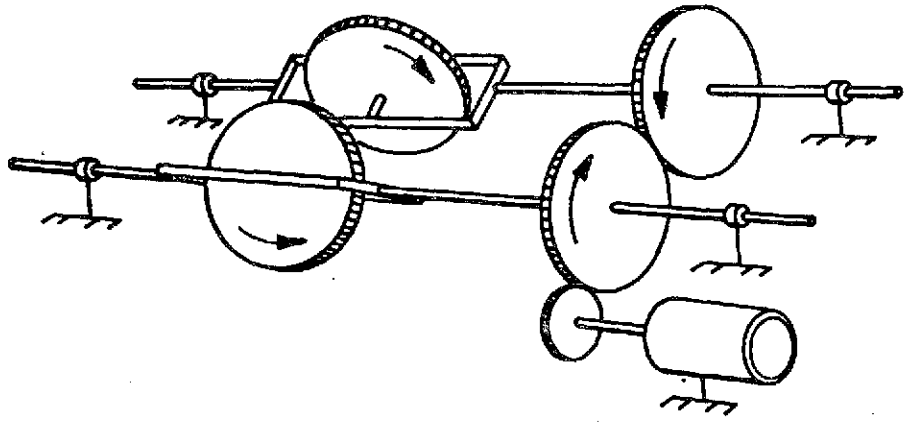

c. Twin Gyro

FIG. 1-1 CONTROL-MOMENT GYROS

In Chapter IV, optimum feedback systems based on a number of design criteria are determined. System response to gust inputs is also calculated.

In Chapter V, the equations of motion for a three dimensional, uniform cantilever wing are developed using assumed mode methods. Optimum orientation and location of the CMG on the wing are determined. The open loop characteristics of the system are calculated and comparisons are made with the two dimensional analysis.

In Chapter VI, the closed loop characteristics of the system are examined including a discussion of the effects on controllability and observability of increasing the number of vibrational modes in the analysis. Critical gains in full state feedback systems are identified, and a number of reduced state systems are determined. The problem of higher mode instabilities induced by the control is analyzed and methods for reducing the probability of its occurrence are discussed.

Chapter VII presents a summary of results, conclusions, and areas of further research.

II. TYPICAL SECTION WITH CMG: OPEN LOOP CONTROL CHARACTERISTICS

2.1 Wing-Controller Equations of Motion

The equations of motion of the typical wing section, illustrated in Fig. 2-1, appear in most aeroelastic references including Ref. 20, and will not be derived here. The equations of motion for the control-moment gyro are derived in Appendix B and their inclusion in the typical section equations is relatively straightforward. The resultant equations can be written

$$m'\ddot{h} + C_h h + S_\alpha \ddot{\alpha} = -L_D - L \tag{2-1}$$

$$S_\alpha \ddot{h} + I'_\alpha \ddot{\alpha} + C_\alpha \alpha + H_w \dot{\sigma} = M_D + M_\alpha \tag{2-2}$$

$$-H_w \dot{\alpha} + I_{Gz} \ddot{\sigma} = T_c \tag{2-3}$$

where the wing structural and geometric parameters, CMG parameters, and CMG orientation are defined in Fig. 2.1, the list of symbols, and Appendix B, respectively. The spin and precession axes of the gyro have been selected so the output torque generated by the CMG is about the elastic axis of the typical section. The effect of alternative orientations is discussed in Chap. V, when the three-dimensional case is considered. Structural damping contributions are considered negligible.

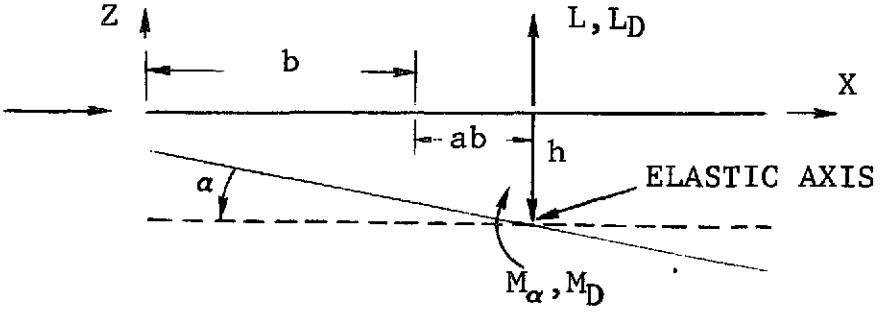

FIG. 2-1 TYPICAL SECTION GEOMETRY

For transient motion and incompressible flow, the expressions for aerodynamic lift and moment per unit span are (21)

$$L = \pi\rho b^2\left[\ddot{h} + U\dot{\alpha} - ba\ddot{\alpha}\right] \qquad (2\text{-}4)$$

$$+ 2\pi\rho bU \int_o^\tau \frac{d}{d\bar{t}}\left[\dot{h}(\bar{t}) + U\alpha(\bar{t}) + b(\tfrac{1}{2}-a)\dot{\alpha}(\bar{t})\right]\Phi(\tau - \bar{t})d\bar{t}$$

$$M_\alpha = \pi\rho b^2\left[ba\ddot{h} - Ub(\tfrac{1}{2} - a)\dot{\alpha} - b^2(\tfrac{1}{8} + a^2)\ddot{\alpha}\right] \qquad (2\text{-}5)$$

$$+ 2\pi\rho b^2 U(\tfrac{1}{2} + a)\int_o^\tau \frac{d}{d\bar{t}}\left[\dot{h}(\bar{t})+U\alpha(\bar{t})+b(\tfrac{1}{2}-a)\dot{\alpha}(\bar{t})\right]\Phi(\tau-\bar{t})d\bar{t}$$

where $\bar{t} = Ut/b$ is a dimensionless time measured in semi-chords traveled after the start of the motion at $t = 0$. The superscript dots, however, denote the derivative with respect to physical time, t. $\Phi(\bar{t})$ is the Wagner indicial admittance function describing the circulatory lift buildup after a sudden change in incidence, and is discussed in Appendix A.

Substituting Eqs. 2-4 and 2-5 into 2-1 and 2-2, and then dividing Eq. 2-1 by $\pi\rho b^3$ and Eq. 2-2 by $\pi\rho b^4$ produce the equations

$$\left[\mu + 1\right]\frac{\ddot{h}}{b} + \omega_h^2\,\mu\,\frac{h}{b} + (x_\alpha\mu - a)\ddot{\alpha} + \frac{U}{b}\dot{\alpha}$$

$$+ 2\,\frac{U}{b}\int_o^\tau \frac{d}{d\bar{t}}\left[\frac{\dot{h}}{b} + \frac{U}{b}\alpha + (\tfrac{1}{2}-a)\dot{\alpha}\right]\Phi(\tau - \bar{t})d\bar{t} = -L_D; \qquad (2\text{-}6)$$

$$(x_\alpha\mu - a)\frac{\ddot{h}}{b} + \left[r_\alpha^2\mu + (\tfrac{1}{8} + a^2)\right]\ddot{\alpha} + \frac{U}{b}(\tfrac{1}{2} - a)\dot{\alpha}$$

$$+ \omega_\alpha^2\mu r_\alpha^2\alpha - 2\,\frac{U}{b}\,(\tfrac{1}{2} + a)\int_o^\tau \frac{d}{d\bar{t}}$$

$$\times\left[\frac{\dot{h}}{b} + \frac{U}{b}\alpha + (\tfrac{1}{2} - a)\dot{\alpha}\right]\Phi(\tau - \bar{t})d\bar{t} + G_1\omega_\alpha\dot{\sigma} = M_D; \qquad (2\text{-}7)$$

$$-G_O\omega_\alpha\dot{\alpha} + \ddot{\sigma} = \frac{T_c}{I_{Gz}} \quad . \qquad (2\text{-}8)$$

In order to simplify future operations with these equations, Eq. 2-6 is multiplied by $(\frac{1}{2} + a)$ and added to Eq. 2-7, which yields

$$\left[x_\alpha\mu + \mu(\tfrac{1}{2} + a) + \tfrac{1}{2}\right]\frac{\ddot{h}}{b} + \omega_h^2\mu(\tfrac{1}{2} + a)\frac{h}{b} \qquad (2\text{-}7a)$$

$$+ \left[x_\alpha\mu(\tfrac{1}{2} + a) + r_\alpha^2\mu + \tfrac{1}{2}(\tfrac{1}{2}-a)\right]\ddot{\alpha} + \frac{U}{b}\dot{\alpha} + r_\alpha^2\omega_\alpha^2\mu\alpha + G_1\omega_\alpha\dot{\sigma} = 0.$$

Equations 2-6, 2-7a, and 2-8 are then the equations of motion for the wing-controller system.

2.2 Open-Loop Characteristics of Wing-Controller System

Taking the Laplace transform of the equations of motion, with the initial conditions and the disturbing force equal to zero, gives in matrix form

$$\begin{bmatrix} s^2[\mu+1+2\frac{U}{b}\Phi(s)]+\omega_h^2\mu & [x_\alpha\mu-a+\frac{U}{b}(1-2a)\Phi(s)]s^2+\left[\frac{U}{b}+2\frac{U^2}{b^2}\Phi(s)\right]s & 0 \\ [x_\alpha\mu+\mu(\frac{1}{2}+a)+\frac{1}{2}]s^2+\omega_h^2\mu(\frac{1}{2}+a) & [x_\alpha\mu(\frac{1}{2}+a)+r_\alpha^2\mu+\frac{1}{2}(\frac{1}{2}-a)]s^2+\frac{U}{b}s+r_\alpha^2\omega_\alpha^2\mu & G_1\omega_\alpha s \\ 0 & -G_0\omega_\alpha s & s^2 \end{bmatrix} \begin{bmatrix} \frac{h(s)}{b} \\ \alpha(s) \\ \sigma(s) \end{bmatrix} = \begin{bmatrix} 0 \\ 0 \\ \frac{T_c(s)}{I_{Gz}} \end{bmatrix} \qquad (2\text{-}9)$$

where $\Phi(s)$ is the Laplace transform of the indicial admittance function discussed in Appendix A.

It is of interest to examine the open-loop characteristics of this system with $T_c = 0$.

For convenience and to nondimensionalize all the parameters, the substitutions

$$\bar{s} = \frac{s}{\omega_\alpha}$$

$$\bar{u} = \frac{U}{b\omega_\alpha}$$

$$\varphi(\bar{s}) = \bar{s}\Phi(\bar{s}) = \frac{0.5\bar{s}^2 + 0.281\ \bar{u}\bar{s} + 0.01365\ \bar{u}^2}{\bar{s}^2 + 0.3455\ \bar{u}\bar{s} + 0.01365\ \bar{u}^2}$$

are made into Eq. 2-9, and the characteristic determinant becomes

$$\begin{vmatrix} (\mu+1)\bar{s}^2+2\bar{u}\varphi(\bar{s})\bar{s}+\left(\frac{\omega_h}{\omega_\alpha}\right)^2\mu & (x_\alpha-a)\bar{s}^2+\bar{u}\left[1+(1-2a)\varphi(\bar{s})\right]\bar{s}+2\bar{u}^2\varphi(\bar{s}) & 0 \\ \left[x_\alpha\mu+\mu(\frac{1}{2}+a)+\frac{1}{2}\right]\bar{s}^2+\left(\frac{\omega_h}{\omega_\alpha}\right)^2\mu(\frac{1}{2}+a) & \left[x_\alpha\mu(\frac{1}{2}+a)+r_\alpha^2\mu+\frac{1}{2}(\frac{1}{4}-a)\right]\bar{s}^2+\bar{u}\bar{s}+r_\alpha^2\mu & G_1\bar{s} \\ 0 & -G_o\bar{s} & \bar{s}^2 \end{vmatrix} = 0 . \quad (2\text{-}10)$$

The characteristic equation is written out in Appendix C and has the form

$$\begin{aligned} \bar{s}^2\Big\{ & A_6\bar{s}^6+\bar{u}A_5\bar{s}^5+(\bar{u}^2A_{41}+A_{42}+A_{43}G_2)\bar{s}^4+\bar{u}(\bar{u}^2A_{31}+A_{32}+A_{33}G_2)\bar{s}^3 \\ & +\left[\bar{u}^4A_{21}+\bar{u}^2A_{22}+A_{23}+(\bar{u}^2A_{24}+A_{25})G_2\right]\bar{s}^2 \\ & +\bar{u}\left[\bar{u}^2A_{11}+A_{12}+(\bar{u}^2A_{13}+A_{14})G_2\right]\bar{s} \\ & +\bar{u}^2(\bar{u}^2A_{01}+A_{02}+A_{03}G_2)\Big\} = 0 \quad , \end{aligned} \quad (2\text{-}11)$$

where the A coefficients are defined in Appendix C and are functions of μ, a, x_α, r_α^2, and $(\omega_h/\omega_\alpha)^2$, and G_2 is the gyro parameter equal to the product

$$G_1G_o = \frac{H_w^2}{\pi\rho b^4 I_{Gz}\omega_\alpha^2} .$$

In order to determine the effect of the CMG on the dynamic characteristics of a typical section, including flutter velocity, the following values were selected for the non-dimensional wing parameters (similar to those in Ref. 22)

μ	=	10.0
a	=	-0.4
x_α	=	0.2
r_α^2	=	0.25
$(\omega_h/\omega_\alpha)^2$	=	0.33 .

Substituting these values into Eq. 2-11 yields

$$\bar{s}^2\{24.88\bar{s}^6+15.97\ \bar{u}\bar{s}^5+(0.36\bar{u}^2+36.67+11.0\ G_2)\bar{s}^4$$
$$+\ \bar{u}(-1.31\ \bar{u}^2+17.84+4.8\ G_2)\bar{s}^3$$
$$+\ \left[-0.40\ \bar{u}^4+2.76\bar{u}^2+8.25+(0.71\bar{u}^2+3.3)G_2\right]\bar{s}^2$$
$$+\ \bar{u}\left[-0.085\bar{u}^2+2.85+(0.006\bar{u}^2+1.14)G_2\right]\bar{s}$$
$$+\ \bar{u}^2\left[-0.009\bar{u}^2+0.113+0.045\ G_2\right]\}$$
$$=\ 0. \qquad (2\text{-}12)$$

Figures 2-2a and 2-2b show a comparison of the root loci for this system for three values of G_2 including $G_2 = 0$, i.e., without CMG. The root loci are drawn for variations of the velocity parameter $\bar{u} = U/b\omega_\alpha$, which will imply, in this analysis, variations in U with ω_α and b held constant. Roots marked "x" indicate u = 0. From the figures, it can be seen that for the particular values chosen for the non-dimensional parameters, the critical roots associated with the onset of flutter correspond to the torsion branch of the root locus plot. The frequencies associated with the bending-torsion modes approach one another as the flutter velocity is approached for each case, which is a result often occurring in classical bending-torsion flutter. For increasing values of $\bar{u}$ beyond its flutter value, the frequencies corresponding to the bending and torsion branches of the root locus tend to converge to the same value. The roots that remain fixed at the origin for varying $\bar{u}$ are associated with presence of the CMG in the system.

For increasing values of G_2, corresponding increases in flutter velocity and flutter frequency occur. This can be seen more explicitly in Fig. 2.3 which shows that increasing G_2 from 0.0 to 5.0 results in increases for $\bar{u}_F$ from 1.65 to 3.35 and for ω_F/ω_α from 0.80 to 1.11. In general, increases in the value of G_2 would correspond to increasing the size of the CMG. However, for a constant value of angular momentum, increasing G_2 could correspond to a decreasing value of I_{Gz} with fixed angular momentum, which would be associated with a decreasing CMG size.

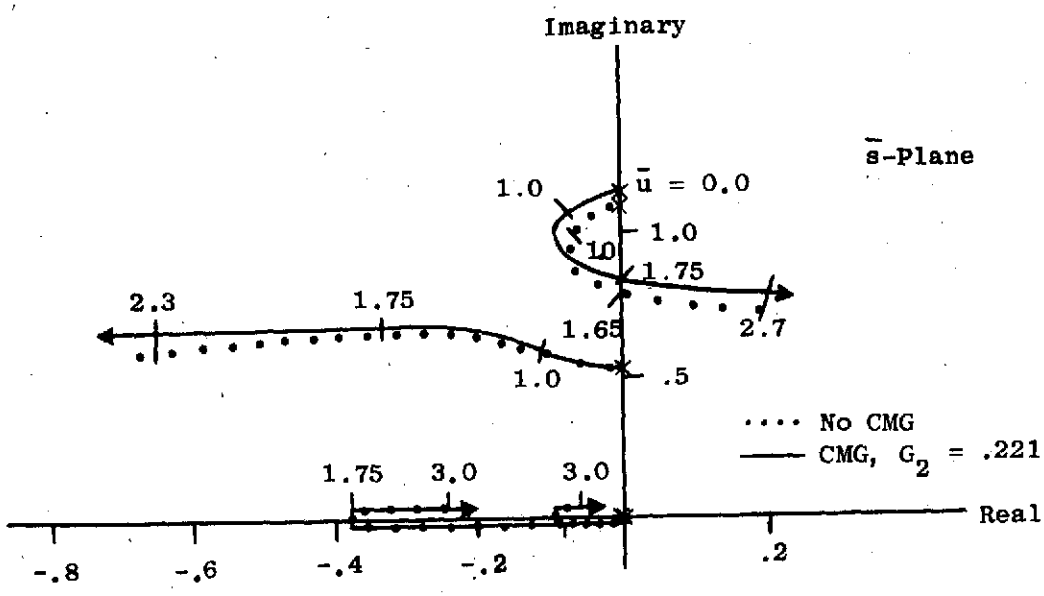

FIG. 2-2a ROOT LOCUS COMPARISON OF WING WITH AND WITHOUT CMG, G_2 = 0.221

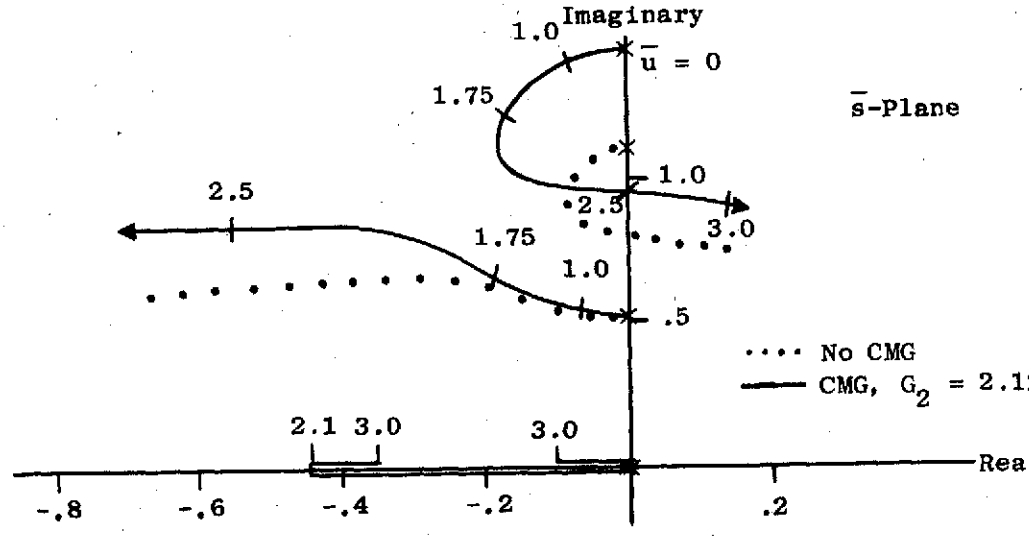

FIG. 2-2b ROOT LOCUS COMPARISON OF WING WITH AND WITHOUT CMG, G_2 = 2.12

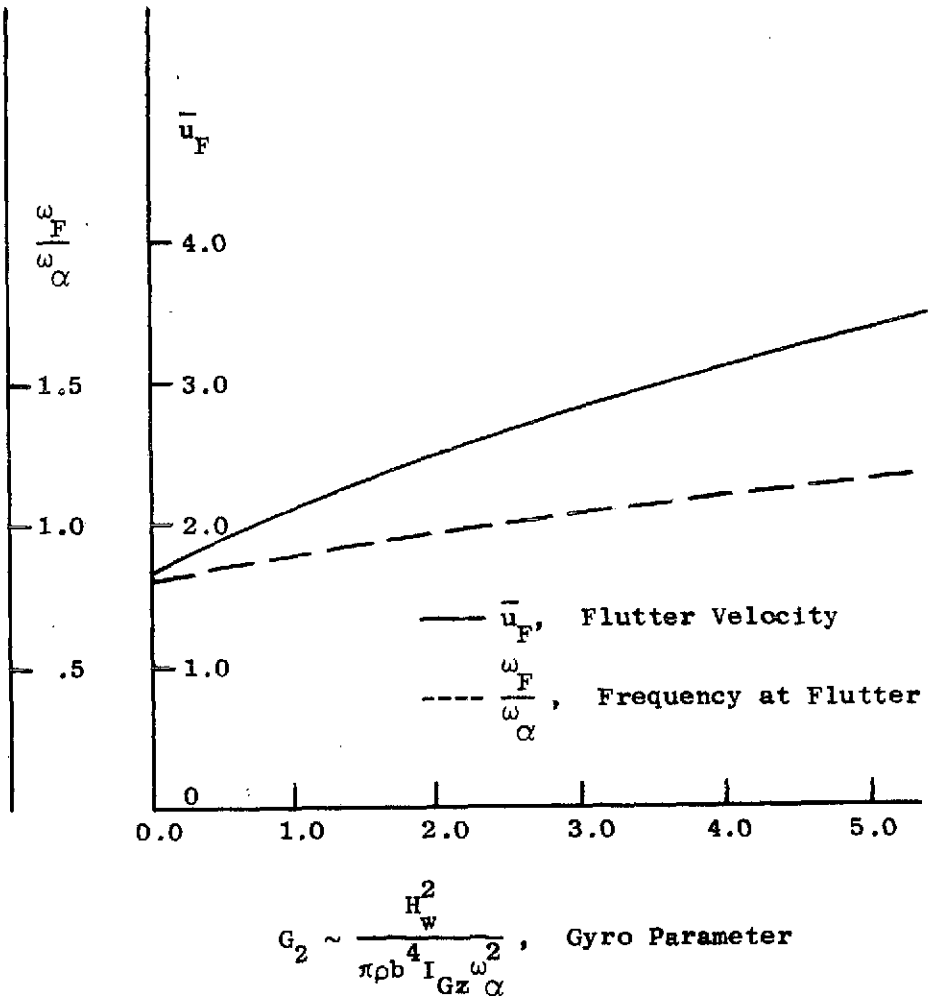

FIG. 2-3 VARIATION IN VELOCITY AND FREQUENCY AT FLUTTER WITH G_2

In the next chapter, the effect of feedback on this system will be examined.

III. FEEDBACK CONTROL OF TWO DIMENSIONAL WING-CONTROLLER SYSTEM

3.1 State Variable Formulation

The characteristic equation developed in the previous section is 8th degree, where the two roots located at the origin in Figs. 2-2a and 2-2b are associated with the presence of the CMG in the system. If feedback of the gimbal angle σ were not required, the degree of the characteristic equation could be reduced to seven. However, passive or active feedback of gimbal angle is necessary to maintain the validity of the small-gimbal-angle assumption in the equations of motion. Thus, the minimum number of states to define this system is eight. It would be advantageous for sensor and estimator design requirements if it were not necessary to obtain information on all states to adequately suppress the onset of flutter for reasonable increases in the velocity. To obtain some insight into which parameters are most significant in the control law, an analysis using arbitrary dynamics is done in this section. In this method, the eigenvalues of the uncontrolled system are shifted to arbitrary new locations using state variable feedback. This requires that the system be modally controllable with the particular set of states chosen to define the system. To determine the controllability of the system, the equations of motion (Eqs. 2-6, 2-7a, 2-8) are first put into standard state-variable matrix form, which can be written in general, with no disturbing forces

$$\dot{\underline{x}} = F\underline{x} + G\underline{u_c} \tag{3-1}$$

where $\underline{x}$ is the state vector and $\underline{u_c}$ the control vector. With $\varphi(\bar{s}) = N_\varphi/D_\varphi$, the first equation in Eqs. 2-9 is multiplied by D_φ, and then the inverse Laplace transformation of Eqs. 2.9 is taken assuming zero initial conditions. The resulting equations can be written

$$B_1\frac{\dddot{h}}{b} + (B_1d_1+1)\bar{u}\frac{\ddot{h}}{b} + (B_1d_o\bar{u}^2 + 2\bar{u}^2n_1 + B_4)\frac{\ddot{h}}{b}$$

$$+ \left[2n_o\bar{u}^3 + B_4d_1\bar{u}\right]\frac{\dot{h}}{b} + B_4d_o\bar{u}^2\frac{h}{b} + B_2\ddot{\alpha} + \bar{u}(B_2d_1 + B_3n_2 + 1)\ddot{\alpha}$$

$$+ \bar{u}^2(B_2 d_o + d_1 + B_3 n_1 + 1)\ddot{\alpha}$$

$$+ \bar{u}^3\left[d_o + B_3 n_o + 2n_1\right]\dot{\alpha} + 2n_o\bar{u}^4\alpha = 0 \quad ; \qquad (3\text{-}2a)$$

$$\left[B_2 + B_1(\tfrac{1}{2} + a)\right]\frac{\ddot{h}}{b} + B_4(\tfrac{1}{2} + a)\frac{h}{b} + \left[B_2(\tfrac{1}{2} + a) + r_\alpha^2\mu - \tfrac{1}{8} + a^2\right]\ddot{\alpha}$$

$$+ \bar{u}\dot{\alpha} + r_\alpha^2\mu\alpha + G_1\dot{\sigma} = 0; \qquad (3\text{-}2b)$$

$$-G_o\dot{\alpha} + \ddot{\sigma} = \frac{T_c}{I_{Gz}\omega_\alpha^2} . \qquad (3\text{-}2c)$$

Equations 3-2 are equivalent to Eqs. 2-6, 2-7a, and 2-8 insofar as they have the same characteristic equation. For certain nonzero initial conditions, the dynamic response of the two systems would be different.

Before writing Eqs. 3-2 in standard form, a decision must be made as to which quantities are considered states. There are many possible realizations of the system of equations, and the procedure here will be to select those states which would be the least complicated to individually sense, and can be explicitly identified. The following quantities are therefore selected as the states of the system:

$$h_1 = h \qquad (3\text{-}3)$$

$$h_2 = \dot{h}_1 \qquad (3\text{-}4)$$

$$\alpha_1 = \alpha \qquad (3\text{-}5)$$

$$\alpha_2 = \dot{\alpha}_1 \qquad (3\text{-}6)$$

$$\sigma_1 = \sigma \qquad (3\text{-}7)$$

$$\sigma_2 = \dot{\sigma}_1 \qquad (3\text{-}8)$$

$$\xi_1 = (B_1\frac{\dot{h}_2}{b} + B_2\dot{\alpha}_2) \qquad (3\text{-}9)$$

$$\xi_2 = \dot{\xi}_1 + (B_1 d_1 + 1)\bar{u}\frac{\dot{h}_2}{b} + \bar{u}(B_2 d_1 + 1 + B_3 n_2)\dot{\alpha}_2. \qquad (3\text{-}10)$$

Substituting Eqs. 3-3 to 3-10 into Eqs. 3-2 and writing in matrix form yields Eq. 3-11, where the F_{ij} are defined in Appendix C:

$$\begin{bmatrix} \dot{h}_1/b \\ \dot{h}_2/b \\ \dot{\alpha}_1 \\ \dot{\alpha}_2 \\ \dot{\sigma}_1 \\ \dot{\sigma}_2 \\ \dot{\xi}_1 \\ \dot{\xi}_2 \end{bmatrix} = \begin{bmatrix} 0 & 1 & 0 & 0 & 0 & 0 & 0 & 0 \\ \frac{B_2B_4(\frac{1}{2}+a)}{A_6} & 0 & \frac{B_2}{A_6}r_\alpha^2\mu & \frac{B_2}{A_6}\bar{u} & 0 & +\frac{B_2G_1}{A_6} & \frac{[B_2(\frac{1}{2}+a)+r_\alpha^2\mu+\frac{1}{8}+a^2]}{A_6} & 0 \\ 0 & 0 & 0 & 1 & 0 & 0 & 0 & 0 \\ -\frac{B_1B_4(\frac{1}{2}+a)}{A_6} & 0 & -\frac{B_1}{A_6}r_\alpha^2\mu & -\frac{B_1}{A_6}\bar{u} & 0 & -\frac{B_1G_1}{A_6} & -\frac{[B_2+B_1(\frac{1}{2}+a)]}{A_6} & 0 \\ 0 & 0 & 0 & 0 & 0 & 1 & 0 & 0 \\ 0 & 0 & 0 & G_0 & 0 & 0 & 0 & 0 \\ F_{71} & 0 & F_{73} & F_{74} & 0 & F_{76} & F_{77} & 1 \\ F_{81} & F_{82} & F_{83} & F_{84} & 0 & F_{86} & F_{87} & 0 \end{bmatrix}$$

$$\times \begin{bmatrix} h_1/b \\ h_2/b \\ \alpha_1 \\ \alpha_2 \\ \sigma_1 \\ \sigma_2 \\ \xi_1 \\ \xi_2 \end{bmatrix} + \begin{bmatrix} 0 \\ 0 \\ 0 \\ 0 \\ 0 \\ 1 \\ 0 \\ 0 \end{bmatrix} \frac{T_c}{I_{Gz}\omega_\alpha^2} \quad . \qquad (3\text{-}11)$$

3.2 System Controllability

A necessary and sufficient condition for arbitrary relocation of the system eigenvalues by state-variable feedback (i.e., modal controllability) is that the so-called controllability matrix be nonsingular. The controllability matrix is defined to be,

$$C = \left[G \mid FG \mid \cdots \mid F^{n-1}G \right] . \qquad (3\text{-}12)$$

where n is the number of states defining the system. It can be shown that this matrix is nonsingular for the parameters selected in this analysis with G_1, $G_o > 0$, $\bar{u} \geq 0$.

Thus, using only one CMG-controller and full state feedback, the flutter velocity can theoretically be increased to any value by just making all the real parts of the system eigenvalues have negative values. This generally, is not only true for systems utilizing a CMG controller, but also can be shown to be the case if a single aerodynamic surface were to be used. This is contrary to implications given in Ref. 11, in which Nissim states that the typical section system "has two degrees of freedom, translation (bending) and rotation (torsion). Therefore, two control surfaces are required in order to maintain precise control of the two degrees of freedom of the main surface." However, implicit in that requirement, although it is not entirely clear what is meant by precise, is that the number of feedback parameters is limited to only four quantities, α, $\dot{\alpha}$, h, and $\dot{h}$.

3.3 Full-State Feedback Gain Determination

Another method for determining if the system is modally controllable is to actually solve for the feedback gains in the control law, which relocate the eigenvalues to selected locations. Obviously, if the gains can be determined, the system is modally controllable. Two methods will be given for the determination of the required feedback gains. The first is rather straightforward and can be generally more convenient to use on low order systems, since the evaluation of the controllability matrix is not required, and actually the system equations need not be arranged in state variable form. The second method is mathematically more involved, but provides a generalized format for more conveniently calculating the gains in a large order system. The description of this method is based on the procedure outlined in Ref. 25. The control law will be assumed to be of the general form

$$\frac{T_c}{I_{Gz}\omega_\alpha^2} = K_1 \frac{h_1}{b} + K_2 \frac{h_2}{b} + K_3 \alpha_1 + K_4 \alpha_2$$

$$-K_5\sigma_1 - K_6\sigma_2 + K_7\xi_1 + K_8\xi_2 \qquad (3\text{-}13)$$

or in vector notation

$$\frac{T_c}{I_{Gz}\omega_\alpha} = u_c = -\underline{K}^T \underline{x} = -\begin{bmatrix} -K_1, -K_2, -K_3, -K_4, +K_5, +K_6, -K_7, -K_8 \end{bmatrix} \begin{bmatrix} h_1 \\ h_2 \\ \alpha_1 \\ \alpha_2 \\ \sigma_1 \\ \sigma_2 \\ \xi_1 \\ \xi_2 \end{bmatrix} \tag{3-14}$$

The basic problem of selecting gains to arbitrarily place the system eigenvalues can be stated as follows:

Given the single-input system

$$\dot{\underline{x}} = F\underline{x} + \underline{g}u_c \tag{3-15}$$

(where for application to Eq. 3-11, u_c is a scalar and $\underline{g}$ is a vector) with the characteristic polynomial for $u_c = 0$,

$$\chi(s) = \det(sI-F) = s^n + f_1 s^{n-1} + \cdots\cdots f_n, \tag{3-16}$$

find the gain vector $\underline{K}$ such that the characteristic polynomial of the system

$$\dot{\underline{x}} = (F - \underline{g}\underline{K}^T)\underline{x} \tag{3-17}$$

has the specified form

$$\chi_K(s) = s^n + g_1 s^{n-1} \cdots\cdots g_n \ . \tag{3-18}$$

Whenever the system contains a small number of states, a solution for the gains can sometimes be generated more

conveniently by directly expanding the characteristic determinant of Eq. 3-16 and equating the coefficients of like powers of s with those of the desired characteristic equation, Eq. 3-18. For example, for the particular system described in Eq. 3-11, a solution can be developed by substituting the Laplace transform of Eq. 3-13 into the transform of Eq. 3-2 which results in the following characteristic determinant:

$$\begin{vmatrix} B_1\bar{s}^4 + \bar{u}(B_1d_1+1)\bar{s}^3 + [(B_1d_o+2n_1)\bar{u}^2+B_4]\bar{s}^2 & B_2\bar{s}^4 + (B_2d_1+1+B_3n_2)\bar{u}\bar{s}^3 & 0 \\ \quad + (2\bar{u}^3n_o+B_4d_1\bar{u})\bar{s} + B_4d_o\bar{u}^2 & \quad + (B_2d_o+d_1+B_3n_1+1)\bar{u}^2\bar{s}^2 & \\ & \quad + (d_o+B_3n_o+2n_1)\bar{u}^3\bar{s} + 2n_o\bar{u}^4 & \\ [B_2 + B_1(\tfrac{1}{2}+a)]\,\bar{s}^2 + B_4(\tfrac{1}{2}+a) & [B_2(\tfrac{1}{2}+a)+r_\alpha^2\mu+\tfrac{1}{8}+a^2]\bar{s}^2 + \bar{u}\bar{s} + r_\alpha^2\mu & G_1\bar{s} \\ -K_8B_1\bar{s}^3 + [-K_7B_1-K_8\bar{u}(B_1d_1+1)]\bar{s}^2 & -K_8B_2\bar{s}^3 + [-K_7B_2-K_8\bar{u}(B_2d_1 & \bar{s}^2+K_6\bar{s}+K_5 \\ \quad - K_2\bar{s}-K_1 & \quad + 1+B_3n_2)]\bar{s}^2 & \\ & \quad - (K_4+G_o)\bar{s} - K_3 & \end{vmatrix} = \chi_K \quad (3\text{-}19)$$

Expanding this determinant and equating coefficients establishes eight equations, which can be solved simultaneously for the eight gains to arbitrarily relocate the eigenvalues of the system.

For large order systems the above approach could be tedious, and a procedure more amenable to computerized solution is needed. The following method is presented from Ref. 25. From Eq. 3-17

$$\begin{aligned} \chi_K(s) &= \det\,(sI - F + \underline{g}\,\underline{K}^T) \\ &= \det\,(sI - F)(I + (sI - F)^{-1}\,\underline{g}\,\underline{K}^T) \\ &= \det\,(sI - F)\cdot\det\,(I + (sI - F)^{-1}\underline{g}\,\underline{K}^T) \\ &= \chi(s)\cdot\,(1 + \underline{K}^T(sI - F)^{-1}\,\underline{g}) \end{aligned} \quad (3\text{-}20)$$

Hence,

$$\chi_K(s) - \chi(s) = \chi(s) \cdot \underline{K}^T(sI - F)^{-1}\, \underline{g}$$

$$= \gamma_1\, s^{n-1} + \cdots\cdots \gamma_{n-1}\, s + \gamma_n \qquad (3\text{-}21)$$

where

$$K^T(sI - F)^{-1}\underline{g} = \frac{\gamma_1 s^{n-1} + \cdots\cdots \gamma_{n-1}s + \gamma_n}{s^n + f_1 s^{n-1} \cdots\cdots \quad f_n} \quad .$$

Now, as can be directly verified,

$$(sI - F)^{-1} = \frac{1}{\chi(s)}\left[s^{n-1} + (F + f_1 I)s^{n-2} + (F^2 + f_1 F + f_2 I)s^{n-3}\right.$$

$$\left. + \cdots + (F^{n-1} + f_1 F^{n-2} + \cdots f_{n-1} I)\right] \qquad (3\text{-}22)$$

Substituting Eq. 3-22 into Eq. 3-21 and equating coefficients of like powers of s gives the following system of equations:

$$\begin{aligned}
\gamma_1 &= \underline{K}^T\underline{g} \\
\gamma_2 &= \underline{K}^T F\underline{g} + f_1\underline{K}^T\underline{g} \\
\gamma_3 &= \underline{K}^T F^2\underline{g} + f_1\underline{K}^T F\underline{g} + f_2\underline{K}^T\underline{g} \\
&\vdots \\
\gamma_n &= \underline{K}^T F^{n-1}\underline{g} + f_1\underline{K}^T F^{n-2}\underline{g} + \cdots\cdots f_{n-1}\underline{K}^T\underline{g}
\end{aligned} \qquad (3\text{-}23)$$

This can be written in matrix form as

$$\underline{\gamma} = \begin{bmatrix} 1 & & & \\ f_1 & 1 & & \\ f_2 & f_1 & 1 & \\ \vdots & \ddots & \ddots & \ddots \\ f_{n-1} & \cdots & f_2 & f_1 & 1 \end{bmatrix} \begin{bmatrix} \underline{K}^T\underline{g} \\ \underline{K}^T F\underline{g} \\ \vdots \\ \underline{K}^T F^{n-1}\underline{g} \end{bmatrix} = R \begin{bmatrix} \underline{g}^T \\ \underline{g}^T F^T \\ \vdots \\ \underline{g}^T F^{T(n-1)} \end{bmatrix} \underline{K}$$

$$= RC^T\underline{K} \qquad (3\text{-}24)$$

where C is the controllability matrix, and $\underline{\gamma}$ is the vector whose elements are the differences in the coefficients of the characteristic polynomials defined in equations 3-16 and 3-18, i.e.,

$$\underline{\gamma} = \begin{bmatrix} g_1 - f_1 \\ g_2 - f_2 \\ \vdots \\ g_n - f_n \end{bmatrix} . \qquad (3\text{-}25)$$

Thus, the gain vector can now be obtained from Eq. 3-24:

$$\underline{K} = C^{-T}R^{-1}\underline{\gamma} \qquad (3\text{-}26)$$

This will have a solution, since R is clearly non-singular and, for the controllable system that is considered here, C is non-singular.

3.4 Design by Arbitrary Dynamics (Pole Placement)

An extensive parametric study was done, utilizing equations obtained from Eq. 3-19, in order to determine some of the characteristics of the wing-controller system. Variations in $\bar{u}$, G_2, and root locations were considered. Although later design specifications may dictate additional requirements on the root locations, the one stability criterion established for arbitrary root placement was that the minimum negative value of the real part of any root would be greater than $0.05\omega_\alpha$ when $\bar{u}$ is greater than its critical value for the wing without the CMG (i.e., $\bar{u} > 1.65$). Consequently, two particular situations arose in the analysis, depending on the values of G_2 and $\bar{u}$: (1) one conjugate pair of roots had positive real parts or did not meet the stability criterion, and thus, to maintain an adequate stability level, these roots plus the two roots at the origin (Fig. 2-2) had to be relocated by proper selection of the control gains; (2) all roots except those at the origin met the stability criterion, with no positive real roots. The roots that are relocated in order to meet the stability criterion will be referred to as the critical roots. When judging the merits of various root locations for particular values of G_2 and $\bar{u}$, the relative size of each set of control gains was the basis of comparison, with smaller gains implying a more desireable design. Though not a direct indication of the quality of a particular design, the size of the gains do provide a measure of the relative minimum values of the torque and power requirements among designs constrained to the same stability criterion. This is verified by the results of Chap. 4. Low gain values also facilitate the determination of adequate reduced feedback systems, since elimination of certain feedbacks as unnecessary can be made when their values are negligible. The following results and conclusions were obtained from the parametric analysis

a. The lowest gain values are obtained when only the critical roots are relocated and are placed as near to the imaginary axis as allowed by the stability criterion.

b. When relocating only the roots at the origin, the values of the gains are reduced by placing the roots on the real axis.

c. When there are four critical roots, the gain values can be reduced (1) by proper adjustment of the imaginary part of roots originally located at the origin,

and (2) by relocating the torsion-branch roots at approximately the same distance from the origin as they were with no control.

d. Gain scheduling, in which the gains are made a function of freestream velocity, can be used to reduce the gain values over a range of velocities. Depending on the value of G_2, all the gains need not be scheduled, but even with reduced scheduling, the added complexity may be prohibitive for a particular design. The following three examples illustrate the effects of gain scheduling. Since the wing is stable without the CMG for $\bar{u} < 1.65$, only the feedback characteristics for $\bar{u} > 1.65$ were considered of interest.

Table 3-1 shows, as a function of velocity and for three values of G_2, the gains needed to place the eigenvalues of the system at the desired new locations as shown in Figs. 3-1, 3-2, and 3-3. The root locations were chosen to produce minimum gain values using the guidelines indicated above in a, b, and c. In the characteristic equation, all the gains except K_5 and K_6 appear multiplied by the gyro term, G_1. Thus in Table 3-1, $\bar{K}_i = G_1 K_i$ is used as a convenient parameter to describe the feedback characteristics, since, for a given G_2 and set of root locations, $\bar{K}_i$ will remain constant for variations in G_1 and G_o. Figures 3-1 to 3-3 show three different control situations:

(1) $G_2 = 0.221$: There are four critical roots for all $\bar{u}$.

(2) $G_2 = 3.8$: For each $\bar{u}$ except $\bar{u} = 3.0$, only two critical roots exist.

(3) $G_2 = 2.12$: For $\bar{u} \leq 2.4$ there are two critical roots, and for $\bar{u} > 2.4$ there are four critical roots.

For $G_2 = 3.8$, the gains remain relatively constant over the range of velocities considered except at $\bar{u} = 3.0$. This indicates that a set of constant gains could be selected which would place the roots in approximately the same locations. For $G_2 = 0.221$,

Table 3-1

SCHEDULED GAINS FOR FLUTTER SUPPRESSION TO $\bar{u} = 3.0$

$\bar{u}$	$\bar{K}_i = G_1 K_i$							
	$\bar{K}_1$	$\bar{K}_2$	$\bar{K}_3$	$\bar{K}_4$	K_5	K_6	$\bar{K}_7$	$\bar{K}_8$
				(1) $G_2 = 0.221$				
1.75	.043	.070	-.110	-.060	.148	.207	-.021	-.002
2.0	.062	.118	-.203	-.105	.231	.340	-.030	-.016
2.3	.082	.166	-.195	-.000	.291	.456	-.036	-.018
2.5	.098	.198	-.140	- 0.0	.317	.522	-.039	-.020
2.7	.115	.236	-.086	.05	.332	.582	-.061	-.021
3.0	.127	.317	-.070	.06	.300	.665	-.042	-.022
				(2) $G_2 = 2.12$				
1.9	.014	.025	.231	.032	.005	.10	0.0	.006
2.1	.014	.024	.235	.035	.006	.10	0.0	.005
2.3	.015	.023	.241	.040	.006	.10	0.0	.005
2.5	.015	.020	.035	-.265	.024	.2175	-.0164	-.0201
2.7	.091	.163	.056	-.300	.071	.339	-.024	-.022
3.0	.145	.315	.109	-.360	.105	.490	-.026	-.026
				(3) $G_2 = 3.80$				
1.9	.026	.045	.415	.058	.008	.10	0.0	.011
2.1	.026	.042	.422	.063	.008	.10	0.0	.010
2.3	.027	.041	.431	.071	.009	.10	0.0	.009
2.5	.029	.042	.445	.082	.010	.10	0.0	.009
2.7	.033	.046	.464	.098	.012	.10	0.0	.009
3.0	.010	.013	.257	-.285	.016	.197	-.011	-.0155

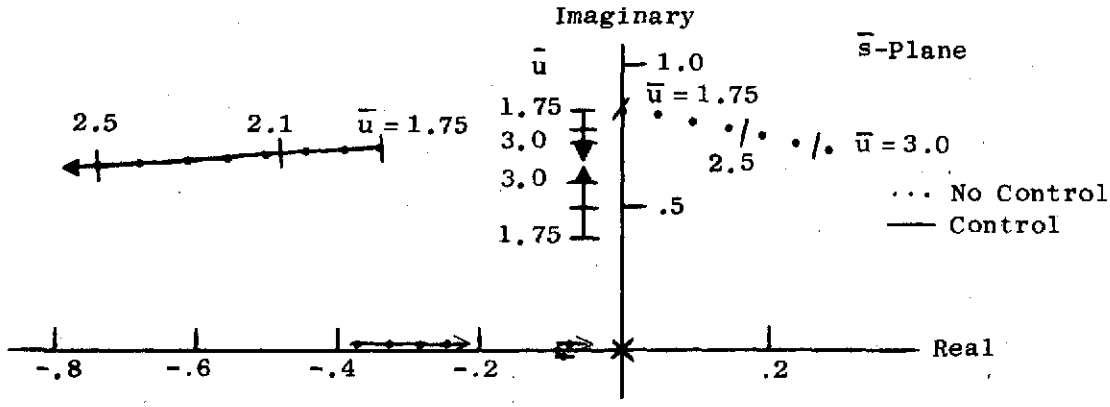

FIG. 3-1 ROOT LOCATIONS FOR $G_2 = 0.221$

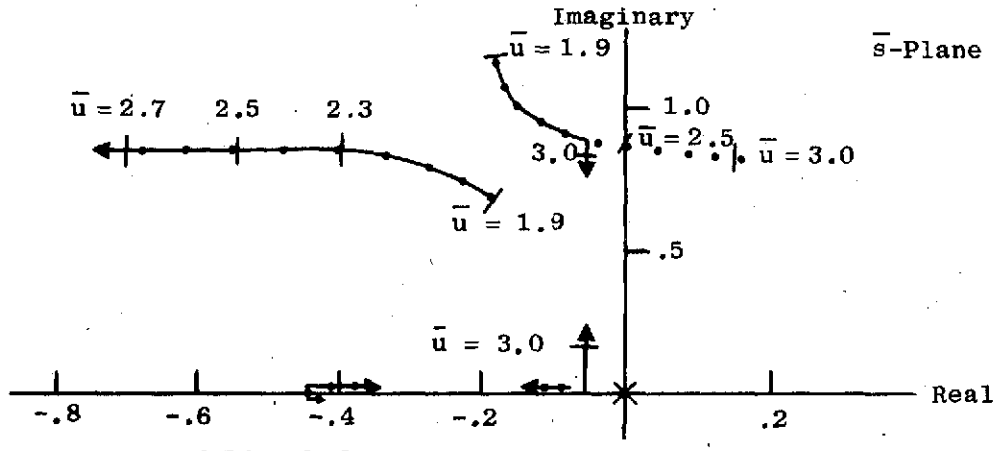

FIG. 3-2 ROOT LOCATIONS FOR $G_2 = 2.12$

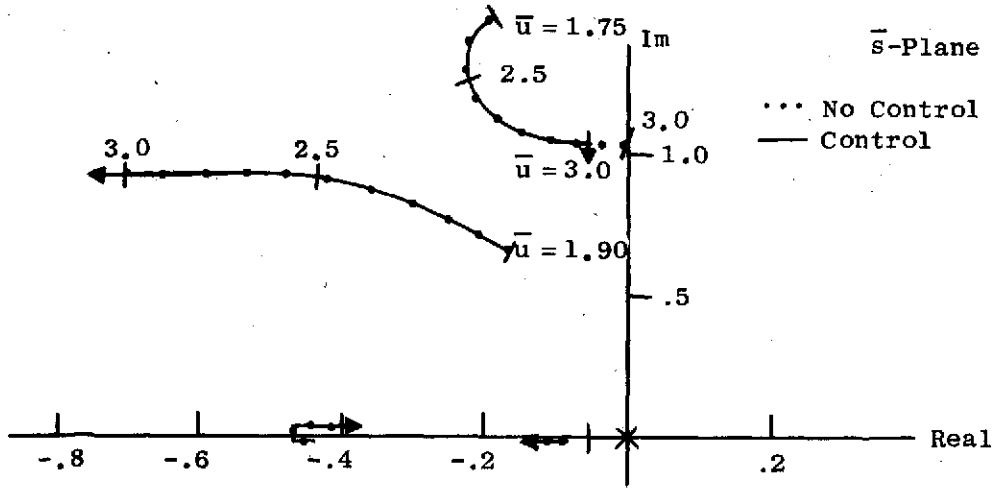

FIG. 3-3 ROOT LOCATIONS FOR $G_2 = 3.8$

each of the gains varies somewhat, with only feedbacks of $\dot{h}$ and $\dot{\sigma}$ having a significant variation with velocity. For $G_2 = 2.12$, each gain does show significant variation with velocity, caused primarily by the change from two to four critical roots as the value of $\bar{u}$ increases beyond 2.4.

Figures 3-4, 3-5, and 3-6 show a comparison of the root loci for $G_2 = 0.221$, 2.12, and 3.8 respectively, using constant gains and gain scheduling. Figure 3-6 shows that constant gains can be used with very little change in the root locus. Figure 3-4, $G_2 = 0.221$, shows that there is very little change in the noncritical roots using constant gains. The critical roots become located on either side of their scheduled value. For $G_2 = 2.12$, Fig. 3-5 shows what differences may result when using constant gains. The roots corresponding to the torsion branch of the root locus with constant gains follow the bending branch associated with scheduled gains, and the bending branch of the root locus with constant gains results in the critical flutter condition.

Thus, it appears that to obtain the best results using constant gains, the value of G_2 should be selected to give an open-loop flutter velocity greater than the maximum flutter velocity desired for a particular application.

e. Relaxing the stability criterion, such that the critical roots can be placed nearer the imaginary axis, can result in reduced values for the gains. The size of the gains, however, may not provide an accurate measure of the relative values of the torque and power among designs constrained to different stability criterion.

f. Although feedback of eight states is necessary to place exactly the set of roots at a desired location for particular values of velocity and G_2, adequate stability can be achieved with reduced-feedback systems. A number of possible designs using various combinations of the feedback parameters can be developed, depending on the values of

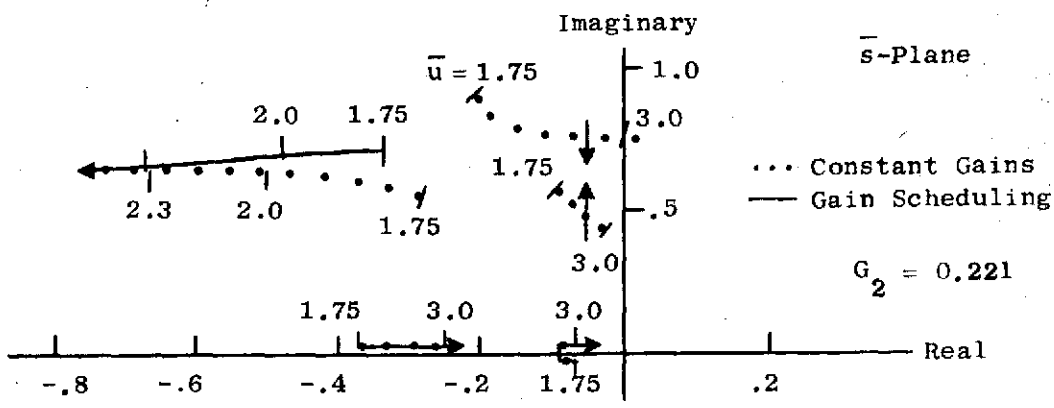

FIG. 3-4 ROOT LOCUS COMPARISON BETWEEN CONSTANT AND SCHEDULED GAINS

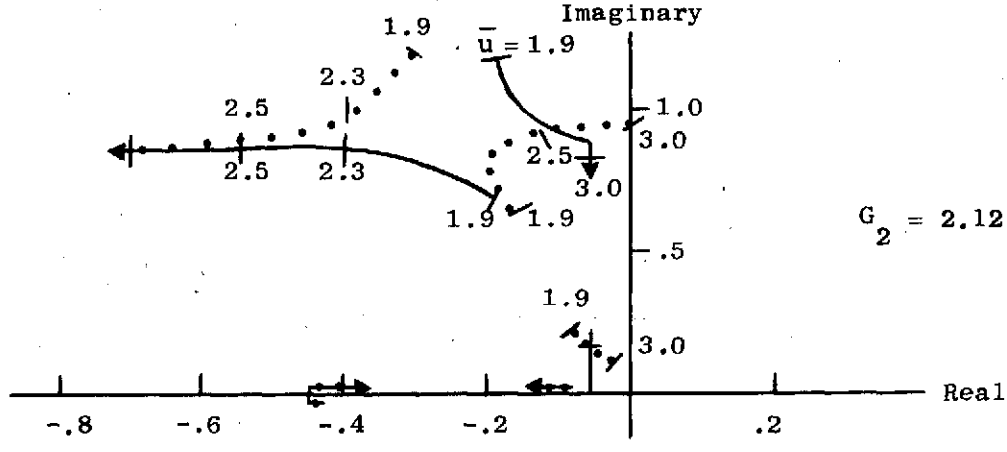

FIG. 3-5 ROOT LOCUS COMPARISON BETWEEN CONSTANT AND SCHEDULED GAINS

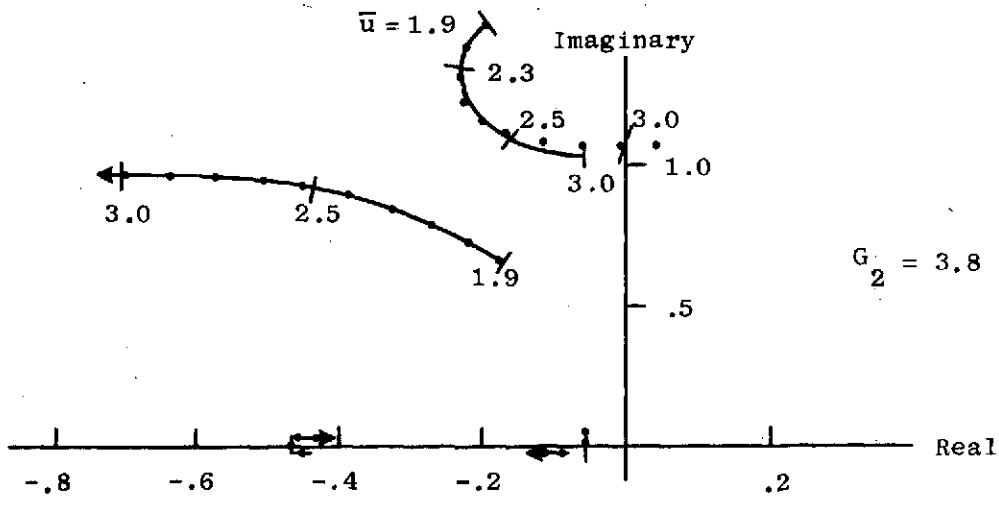

FIG. 3-6 ROOT LOCUS COMPARISON BETWEEN CONSTANT AND SCHEDULED GAINS

$\bar{u}$, G_2 and the eigenvalues of the system. One example of a reduced-feedback system can be obtained from Table 3-1 for $G_2 = 3.8$. The significant gains correspond to feedback of α and $\dot{\sigma}$, and a design using only these two feedbacks, along with σ to null the gyro, results in a root locus very similar to the eigenvalues shown in Fig. 3-6.

The simplest feedback system for any value of G_2 can be determined by examining the characteristic determinant, Eq. 3-19. It can be seen that feedback of $\dot{\alpha}(K_4)$ has the same influence on the roots in the characteristic equation as G_0. Consequently, increasing the value of the gain parameter $\bar{K}_4$ is equivalent to increasing G_2. Figure 3-7 shows the root locus for a system using only two feedbacks characterized by the gains

$$(\bar{K}_4 + G_2) = 3.8$$

$$K_5 = 0.10$$

For $G_2 = 3.8$, this system reduces to one requiring the feedback of only σ.

A comparison of the response characteristics of this system with systems using all eight states as feedbacks will be done in Chap. 4.

3.5 System Observability

In the preceding analysis, total knowledge of all the necessary states for use in the control laws was assumed. This information could be obtained through sensor measurements or through a properly designed estimator if it were not possible or convenient to measure directly the desired states. The sensor problem would be reduced to a minimum if all the states could be estimated from one measurement, the most convenient of which would be σ. If the state of a system at any time can be uniquely determined by the available measurements, the system is considered observable. The observability of the wing-controller system, assuming only σ is measured, can be qualitatively determined by examining Eqs. 3-2. Mathematically, observability can be determined

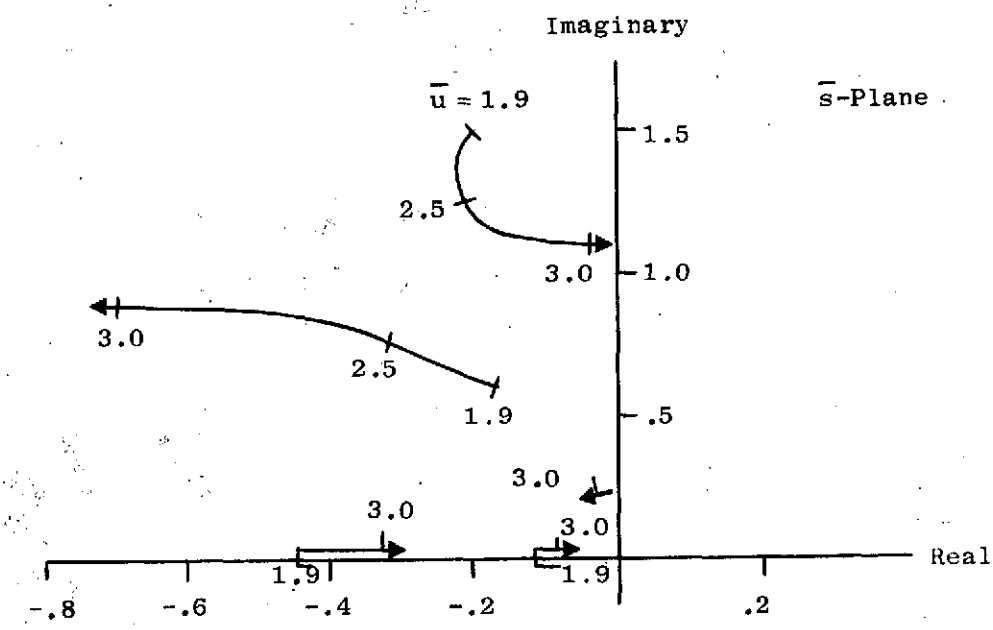

FIG. 3-7 REDUCED FEEDBACK ROOT LOCUS $(\bar{K}_4 + G_2) = 3.8$

by the requirement that the observability matrix be non-singular. The observability matrix is defined to be

$$\Theta = \begin{bmatrix} H \\ \hline HF \\ \hline \\ \hline HF^{n-1} \end{bmatrix} \qquad (3\text{-}27)$$

where H is the output matrix defined from

$$\underline{y} = H\underline{x} \qquad (3\text{-}28)$$

and $\underline{y}$ is the measured quantity. With only σ measured,

$$H = \begin{bmatrix} 0 & 0 & 0 & 0 & 1 & 0 & 0 & 0 \end{bmatrix}. \qquad (3\text{-}29)$$

It can be shown that the observability matrix is non-singular for the parameters selected in this analysis for G_o, $G_1 > 0$, $\bar{u} \geq 0$.

Thus, it appears σ may be the only quantity necessary to measure, since stability can be achieved with only σ feedback. If more control of the eigenvalue locations is desired, the other states can be estimated from this measurement.

IV. SYSTEM DESIGN USING OPTIMAL CONTROL

4.1 Optimal Control Using Quadratic Synthesis

In Section 3.4, the relative values of the gains in the control law were used as a basis for comparing various eigenvalue locations. A criterion more directly associated with system performance, which results in stable, linear feedback control, can be obtained by minimizing a cost function made up of integral quadratic forms in the state and control. Determining the control requirements in this case is basically similar to the optimal regulator problem as discussed in Ref. 26. The following is a brief description of this method.

As has been shown previously, the equations of motion can be written in the form

$$\dot{\underline{x}} = F\underline{x} + G\underline{u}_c . \tag{4-1}$$

It is desired to minimize a cost function of the form

$$J = \frac{1}{2}\int_o^\infty (\underline{x}^T A\underline{x} + \underline{u}_c{}^T B\underline{u}_c)dt \tag{4-2}$$

where superscript T indicates the matrix transpose, and A and B are symmetric weighting matrices selected to obtain "acceptable" levels of $\underline{x}$ and $\underline{u}_c$. The control $\underline{u}_c$ which minimizes J can be obtained by solving Eq. 4-1 simultaneously with the Euler-Lagrange equations

$$\dot{\underline{\lambda}}^T = -\frac{\partial \mathcal{H}}{\partial \underline{x}} \tag{4-3}$$

$$\frac{\partial \mathcal{H}}{\partial \underline{u}_c} = 0 \tag{4-4}$$

where

$$\mathcal{H} = \tfrac{1}{2}\underline{x}^T A\underline{x} + \tfrac{1}{2}\underline{u}_c{}^T B\underline{u}_c + \underline{\lambda}^T(F\underline{x} + G\underline{u}_c)$$

and $\underline{\lambda}$ is a vector of Lagrange multipliers.

Substituting for $\dot{x}$ in Eqs. 4-3 and 4-4 yields

$$\dot{\underline{\lambda}} = - A\underline{x} - F^T\underline{\lambda} \tag{4-5}$$

$$\underline{u_c} = - B^{-1}G^T\underline{\lambda}. \tag{4-6}$$

Substituting Eq. 4-6 into 4-1 and combining with Eq. 4-5 gives

$$\begin{bmatrix} \dot{\underline{x}} \\ \dot{\underline{\lambda}} \end{bmatrix} = \begin{bmatrix} F & -GB^{-1}G^T \\ -A & -F^T \end{bmatrix} \begin{bmatrix} \underline{x} \\ \underline{\lambda} \end{bmatrix} \tag{4-7}$$

One method of solving Eq. 4-7 is by using the substitution $\underline{\lambda} = S\underline{x}$, where S is a matrix. This results for the regulator problem in determining the steady-state solution of a matrix Riccati equation for S of the form,

$$SF + F^TS - S^TGB^{-1}G^TS + A = 0 \tag{4-8}$$

The feedback gain matrix, K, in the control law $\underline{u_c} = -K\underline{x}$ is then obtained from

$$K = B^{-1}G^TS. \tag{4-9}$$

Another method of solution is by eigenvalue decomposition as described in Ref. 27.

Obviously, critical to any solution of this problem is the choice of weighting matrices. One "rule of thumb" in selecting A and B is to choose diagonal matrices whose elements are equal to

$$\frac{1}{(x_{i_{max}})^2} \quad \text{and} \quad \frac{1}{(u_{c_{max}})^2}$$

respectively, where $x_{i_{max}}$ and $u_{c_{max}}$ are the maximum "acceptable" values of x_i, the elements of state vector, and $\underline{u_c}$ respectively. It must be remembered, of course, that the weighting matrices are only relative, and the actual maximum values and their relative sizes occurring in practice will depend on the system response to initial conditions and disturbances.

As a first step in this introductory analysis, the diagonal elements of A are considered to be very small with respect to B, so that no restrictions are placed on the state behavior other than stability, and therefore the design that essentially minimizes $\int_0^t \underline{u}_c^2 \, dt$ is being determined. The matrix A can be positive semi-definite to the extent that it cannot be identically zero, since, as can be seen from Eq. 4-2, the solution degenerates to the case, $\underline{u}_c = 0$.

Table 4-1 shows the feedback gains for $G_2 = 0.221$ as a function of velocity, resulting from a solution of the optimal control problem.

A root locus of the critical roots is shown in Fig. 4-1. The noncritical roots, as might have been expected, are left unchanged in the controlled case, and are not shown in the figure.

TABLE 4-1

GAINS FROM OPTIMAL CONTROL ANALYSIS $G_2 = 0.221$

$\bar{K}_i = G_1 K_i$

$\bar{u}$	$\bar{K}_1$	$\bar{K}_2$	$\bar{K}_3$	$\bar{K}_4$	K_5	K_6	$\bar{K}_7$	$\bar{K}_8$
1.75	-.005	-.010	-.028	-.039	.001	.057	-.003	-.006
2.3	-.166	-.026	-1.26	-1.22	.001	.555	-.038	-.168
2.5	-.202	.052	-1.56	-1.45	.001	.687	-.037	-.182
2.7	-.232	.136	-1.81	-1.63	.001	.807	-.037	-.187
3.0	-.272	.260	-2.13	-1.84	.001	.971	-.039	-.186

For a particular value of $\bar{u}$, it can be seen that if the system instability is due to eigenvalues equal to $R \pm jI$, then to minimize J, the roots in the controlled case should be placed at $-R \pm jI$. Thus, as the value of u increases, the real root of the critical eigenvalue should be placed increasingly farther into the left-half plane. Similar results occur also for larger values of G_2 and can be repeated on a simpler level by looking at a simple second order system with negative damping. For example, consider

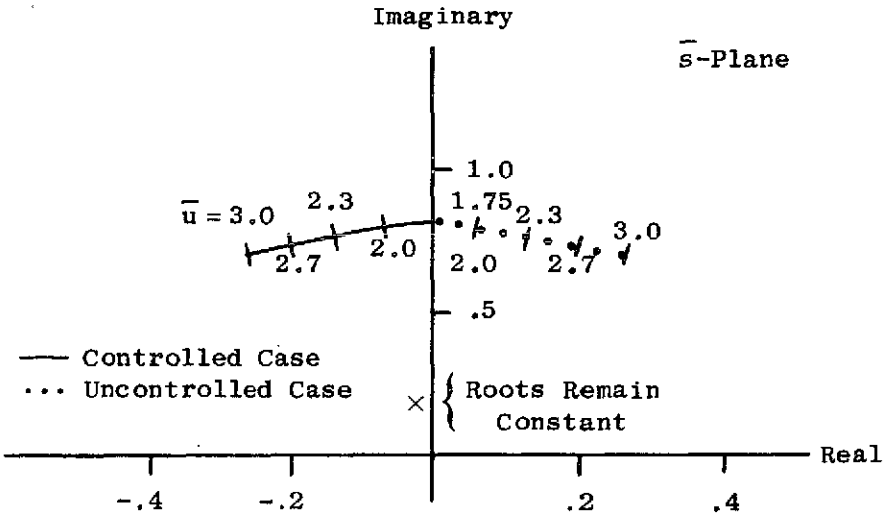

FIG. 4-1 ROOT LOCUS FROM OPTIMAL CONTROL ANALYSIS
G_2 = 0.221

$$\ddot{\underline{x}} - 2R\dot{\underline{x}} + \omega_o^2 \underline{x} = \underline{u}_c .$$

For $\underline{u}_c = 0$, the eigenvalues are

$$s = R \pm jI$$

with

$$I = \sqrt{\omega_o^2 - R^2}$$

To minimize

$$J = \int_0^\infty (\underline{x}^T A \underline{x} + b\underline{u}_c^2) dt$$

with the diagonal elements of A small,

$$\underline{u}_c \cong -4R\dot{\underline{x}}.$$

The resulting eigenvalues are

$$s = -R \pm jI.$$

Since six of the eight roots remain essentially unchanged in the higher-order system when going from the uncontrolled to the controlled case, this system takes on characteristics similar to those of a simple harmonic system.

The large gain values appearing in Table 4-1 as compared to those in Table 3-1 are in part due to the tighter control requirements resulting from moving the pair of critical roots farther into the left-half plane. Primarily, however, the large values are due to the relocation of the roots originally at the origin. It was found in Section 3.4 that proper placement of these roots can result in lower gains (and for the particular value of G_2 used in this analysis, large gains result for placement of these roots near the real axis). Thus, whether gain values can be used to indicate a desirable design as was done in Section 3.4 depends on what particular function is being optimized.

Because of the placement of the critical roots in achieving the minimum integrated value of control torque, the initial values of torque tend to be large. This feature of the design can be partially alleviated by redesigning the

control for larger values of G_2. In fact, for practical design considerations, the maximum values of torque and power may be more critical parameters than the time integral of control torque. The effects on these parameters and other response characteristics resulting from variations in $\bar{u}$, G_2, and root locations are investigated in Section 4.2.

4.2 System Response to Gust Impulse

The aerodynamic lift and moment produced by gust-like disturbances in the airstream are a major source of external loads on a lifting surface. The lift and moment disturbances created by an impulsive upward gust striking the leading edge at time $t = 0$ can be described by (20)

$$L_D = 2\pi\rho b U^2 \int_0^\tau \frac{d}{d\bar{t}} \left[\frac{W_g}{U}(\bar{t})\right] \psi(\tau - \bar{t})d\bar{t} \quad (4\text{-}10)$$

$$M_D = 2\pi\rho b^2(\tfrac{1}{2} + a)U^2 \int_0^\tau \frac{d}{d\bar{t}} \left[\frac{W_g(\bar{t})}{U}\right] \psi(\tau - \bar{t})d\bar{t} \quad (4\text{-}11)$$

where $W_g = w_g\delta(t)$ is the impulsive gust velocity, and $\psi(\tau)$ is the Kussner indicial function for a sharp-edged gust. Substituting for L_D and M_D in Eqs. 2-6 and 2-7 results in

$$\left[\mu + 1\right]\frac{\ddot{h}}{b} + \omega_h^2 \mu \frac{h}{b} + (x_\alpha \mu - a)\ddot{\alpha} + \frac{U}{b}\dot{\alpha}$$

$$+ 2\frac{U}{b}\int_0^\tau \frac{d}{d\bar{t}}\left[\frac{\dot{h}}{b} + \frac{U}{b}\alpha + (\tfrac{1}{2} - a)\dot{\alpha}\right]\Phi(\tau - \bar{t})d\bar{t}$$

$$= -2\frac{U^2}{b^2}\int_0^\tau \frac{d}{d\bar{t}}\left[\frac{W_g}{U}(\bar{t})\right]\psi(\tau - \bar{t})d\bar{t}\ ; \quad (4\text{-}12)$$

$$(x_\alpha\mu - a)\frac{\ddot{h}}{b} + \left[r_\alpha^2\mu + \tfrac{1}{8} + a^2\right]\ddot{\alpha} + \frac{U}{b}(\tfrac{1}{2} - a)\dot{\alpha} + \mu\omega_\alpha^2 r_\alpha{}^2\alpha$$

$$- 2\frac{U}{b}(\tfrac{1}{2} + a)\int_0^\tau \frac{d}{d\bar{t}}\left[\frac{\dot{h}}{b} + \frac{U}{b}\alpha + (\tfrac{1}{2} - a)\dot{\alpha}\right]\Phi(\tau - \bar{t})d\bar{t}$$

$$+ G_1\omega_\alpha\dot{\sigma}$$

$$= 2\frac{U^2}{b^2}\left(\tfrac{1}{2}+a\right)\int_o^\tau \frac{d}{d\bar{t}}\left[\frac{W_g}{U}(\bar{t})\right]\psi(\tau-\bar{t})d\bar{t}\ ; \qquad (4\text{-}13)$$

$$-G_o\omega_\alpha\dot{\alpha} + \ddot{\sigma} = \frac{Tc}{I_{Gz}}\ . \qquad (4\text{-}14)$$

As before, adding the product of Eq. 4-13 and $(\frac{1}{2}+a)$ times Eq. 4-12, rearranging terms, and taking the Laplace transform gives

$$\left[(\dot{\mu}+1)\bar{s}^2 + 2\bar{u}\varphi(\bar{s})\bar{s} + \left(\frac{\omega_h}{\omega_\alpha}\right)^2\mu\right]\frac{h(\bar{s})}{b}$$

$$+\left\{(x_\alpha^2\mu - a)\bar{s}^2 + \left[1+(1-2a)\varphi(\bar{s})\right]\bar{u}\bar{s} + 2\varphi(\bar{s})\bar{u}^2\right\}\alpha(\bar{s})$$

$$= -2\bar{u}^2\frac{W_g(\bar{s})}{U}\psi(\bar{s}); \qquad (4\text{-}15)$$

$$\left\{\left[x_\alpha^2\mu + \mu\left(\tfrac{1}{2}+a\right)+\tfrac{1}{2}\right]\bar{s}^2 + \left(\frac{\omega_h}{\omega_\alpha}\right)^2\mu\left(\tfrac{1}{2}+a\right)\right\}\frac{h(\bar{s})}{b}$$

$$+\left\{\left[x_\alpha^2\mu\left(\tfrac{1}{2}+a\right) + r_\alpha^2\mu + \tfrac{1}{2}\left(\tfrac{1}{4}-a\right)\right]\bar{s}^2 + \bar{u}\bar{s} + r_\alpha^2\mu\right\}\alpha(\bar{s})$$

$$+ G_1\bar{s}\sigma(\bar{s}) = 0; \qquad (4\text{-}16)$$

$$-G_o\bar{s}\alpha(\bar{s}) + \bar{s}^2\sigma(\bar{s}) = \frac{T_c(\bar{s})}{I_{Gz}\,\omega_\alpha{}^2}. \qquad (4\text{-}17)$$

Multiplying Eq. 4-15 by D_φ and substituting the general control law, Eq. 3-13 gives in matrix form

$$
\begin{bmatrix}
B_1\bar{s}^4+\bar{u}(B_1d_1+1)\bar{s}^3+(B_1d_o\bar{u}^2+2n_1\bar{u}^2+B_4)\bar{s}^2 & B_2\bar{s}^4+(B_2d_1+1+B_3n_2)\bar{u}\bar{s}^3 & 0 \\
\quad +(2\bar{u}^3n_o+B_4d_1\bar{u})\bar{s}+B_4d_o\bar{u}^4 & \quad +(B_2d_o+d_1+B_3n_1+1)\bar{u}^2\bar{s}^2 & \\
 & \quad +(d_o+B_3n_o+2n_1)\bar{u}^3\bar{s}+2n_o\bar{u}^4 & \\
\left[B_2+B_1(\tfrac{1}{2}+a)\right]\bar{s}^2+B_4(\tfrac{1}{2}+a) & \left[B_2(\tfrac{1}{2}+a)+r_\alpha^2\mu+\tfrac{1}{8}+a^2\right]\bar{s}^2+\bar{u}\bar{s}+r_\alpha^2\mu & G_1\bar{s} \\
-K_8B_1\bar{s}^3+\left[-K_7B_1-K_8\bar{u}(B_1d_1+1)\right]\bar{s}^2 & -K_8B_2\bar{s}^3+\left[-K_7B_2-K_8\bar{u}(B_2d_1+1\right. & \bar{s}^2+K_6\bar{s}+K_5 \\
\quad -K_2\bar{s}-K_1 & \quad \left.+B_3n_2)\right]\bar{s}^2-(K_4+G_o)\bar{s}-K_3 &
\end{bmatrix}
$$

$$
\times \begin{bmatrix} \frac{h(\bar{s})}{b} \\ \alpha(\bar{s}) \\ \sigma(\bar{s}) \end{bmatrix} = \begin{bmatrix} -2\bar{u}^2\frac{W_g}{U}D_\varphi\Psi(\bar{s}) \\ 0 \\ 0 \end{bmatrix} . \qquad (4\text{-}18)
$$

The Laplace transforms of the solutions for $\alpha(t)$, $h(t)$, and $\sigma(t)$ are

$$
\begin{aligned}
\alpha(\bar{s}) = \frac{2u^2}{\chi_K}\left(\frac{W_g(\bar{s})}{U}\right)\Psi(\bar{s})D_\varphi\Bigg(&\left[B_2+B_1(\tfrac{1}{2}+a)+\bar{K}_8B_1\right]\bar{s}^4 \\
&+\left\{\bar{K}_7B_1+\bar{K}_8(B_1d_1+1)\bar{u}\right. \\
&\left.+K_6\left[B_2+B_1(\tfrac{1}{2}+a)\right]\right\}\bar{s}^3 \\
&+\left\{B_4(\tfrac{1}{2}+a)+K_5\left[B_2+B_1(\tfrac{1}{2}+a)\right]+\bar{K}_2\right\}\bar{s}^2 \\
&+\left[K_6B_4(\tfrac{1}{2}+a)+\bar{K}_1\right]\bar{s}+K_5B_4(\tfrac{1}{2}+a)\Bigg) ; \qquad (4\text{-}19)
\end{aligned}
$$

$$\sigma(\bar{s}) = -\frac{2\bar{u}^2}{\chi_K G_1}\left(\frac{W_g(\bar{s})}{U}\right) D_\varphi \psi(\bar{s})\Bigg(-\bar{K}_8 A_6 \bar{s}^5 - \left[\bar{K}_7 A_6 + (A_{5D}+d_1 A_6 + n_2 A_{5N})\bar{K}_8\right]\bar{s}^4$$
$$+ \Bigg\{\left[B_2 + B_1(\tfrac{1}{2}+a)\right](\bar{K}_4+G_2) + \bar{K}_8\left[B_2 B_4(\tfrac{1}{2}+a) - \bar{u}^2(B_1 d_1+1) - r_\alpha^2 \mu B_1\right]$$
$$-\bar{K}_2\left[B_2(\tfrac{1}{2}+a) + r_\alpha^2\mu + \tfrac{1}{8} + a^2\right] - \bar{u}\bar{K}_7 B_1\Bigg\}\bar{s}^3$$
$$+ \Bigg\{\left[B_2 + B_1(\tfrac{1}{2}+a)\right]\bar{K}_3 + \left[B_2 B_4(\tfrac{1}{2}+a) - r_\alpha^2\mu B_1\right]\bar{K}_7$$
$$- \bar{K}_2\bar{u} - \bar{K}_1\left[B_2(\tfrac{1}{2}+a) + r_\alpha^2\mu + \tfrac{1}{8} + a^2\right]$$
$$+ \bar{u}\bar{K}_8\left[B_4(\tfrac{1}{2}+a)(B_2 d_1 + 1 + B_3 n_2) - r_\alpha^2\mu(B_1 d_1 + 1)\right]\Bigg\}\bar{s}^2$$
$$+ \Big\{B_4(\tfrac{1}{2}+a)(\bar{K}_4+G_2) - \bar{u}\bar{K}_1 - r_\alpha^2\mu\bar{K}_2\Big\}\bar{s}$$
$$+ \Big\{B_4(\tfrac{1}{2}+a)\bar{K}_3 - r_\alpha^2\mu\bar{K}_1\Big\}\Bigg); \qquad (4\text{-}20)$$

$$\frac{h(\bar{s})}{b} = -\frac{2\bar{u}^2}{\chi_K}\frac{W_g(\bar{s})}{U} D_\varphi \psi(\bar{s})\Bigg(\Big\{\left[B_2(\tfrac{1}{2}+a) + r_\alpha^2\mu + \tfrac{1}{8} + a^2\right] + \bar{K}_8 B_2\Big\}\bar{s}^4$$
$$+ \Big\{K_6\left[B_2(\tfrac{1}{2}+a) + r_\alpha^2\mu + \tfrac{1}{8} + a^2\right] + \bar{u}$$
$$+ \left[\bar{K}_7 B_2 + \bar{K}_8\bar{u}(B_2 d_1 + 1 + B_3 n_2)\right]\Big\}\bar{s}^3$$
$$+ \Big\{r_\alpha^2\mu + K_6\bar{u} + K_5\left[B_2(\tfrac{1}{2}+a)r_\alpha^2\mu + \tfrac{1}{8} + a^2\right] + (\bar{K}_4+G_2)\Big\}\bar{s}^2$$
$$+ \Big\{K_6 r_\alpha^2\mu + K_5\bar{u} + \bar{K}_3\Big\}\bar{s} + K_5 r_\alpha^2\mu\Bigg); \qquad (4\text{-}21)$$

where χ_K denotes the characteristic equation. ψ, like $\Phi(\bar{t})$, is a transcendental function and must be approximated so that $\psi(\bar{s})$ can be determined and Eqs. 4-19, 4-20, and 4-21 can be inverted. The most familiar form is

$$\psi(\bar{t}) = 1 - 0.5e^{-.13\bar{t}} - 0.50e^{-\bar{t}} \qquad (4\text{-}22)$$

Its Laplace transform is

$$\psi(\bar{s}) = \frac{0.565\bar{u}\bar{s} + 0.13\bar{u}^2}{(\bar{s}+0.13\bar{u})(\bar{s}+\bar{u})} \qquad (4\text{-}23)$$

The torque required for control, T_c is determined from inverting Eq. 4-17, and the power used by the gyro torquer is

simply the product of control torque times gimbal rate, $\dot{\sigma}$. Figures 4-2 and 4-3 show the control torque and power response to an impulsive gust striking the leading edge. Two convenient non-dimensional parameters are presented, $\bar{T}_c$ and $\bar{P}$ (see List of Symbols). For three values of G_2, 0.221, 2.12, and 3.8, the feedback gains used in this analysis correspond to the values in Table 3-1 for $\bar{u} = 2.5$, and the value of G_1 is assumed constant at 3.5.

As can be seen from the figures, the maximum values of the torque and power parameters tend to decrease with increasing G_2. The control torque and power are damped much faster for $G_2 = 3.8$, where the real root associated with the torsion branch of the root locus is farther in the left-half plane (Fig. 3-3).

The response of the gyro gimbal angle to a gust impulse is illustrated in Fig. 4-4. For the same set of roots, the maximum values of σ for each value of G_2 are approximately the same. These maximum values, which equal approximately 0.2 for the three cases considered, indicate the possibility (for large values of w_g/b corresponding to large gusts or small wing chords) that the small-angle approximation introduced in Appendix B to linearize the equations may become invalid. For example, $G_1 = 3.5$, $G_2 = 2.12$, $w_g/b = 3.0$ results in

$$\sigma_{max} = 33 \text{ deg.}$$

To obtain the effect of varying G_2 on maximum power requirements, a parametric optimization study was done in which the root locations corresponding to the smallest absolute value of maximum power for varying values of G_2 and $\bar{u}$ were calculated. For each G_2 and $\bar{u}$ the minimum power values occurred for approximately those root locations associated with minimum gain values. The results are shown in Fig. 4-5. Small values of G_2 correspond to situation (1) as discussed in Section 3.4 in which four critical roots exist. The large values of control torque are needed not only to null the gyro gimbal, but to provide energy to increase the flutter velocity of the system. For large values of G_2, there are only two critical roots associated with the gyro gimbal angle. The minimum value of the power parameter, $\bar{P}$, for a particular $\bar{u}$ occurs at the transition between two and four critical roots. This minimum corresponds to the actual minimum power required if $I_{Gz}\omega_\alpha^3$ remains constant as G_2 is varied.

To obtain an actual estimate of power required, the

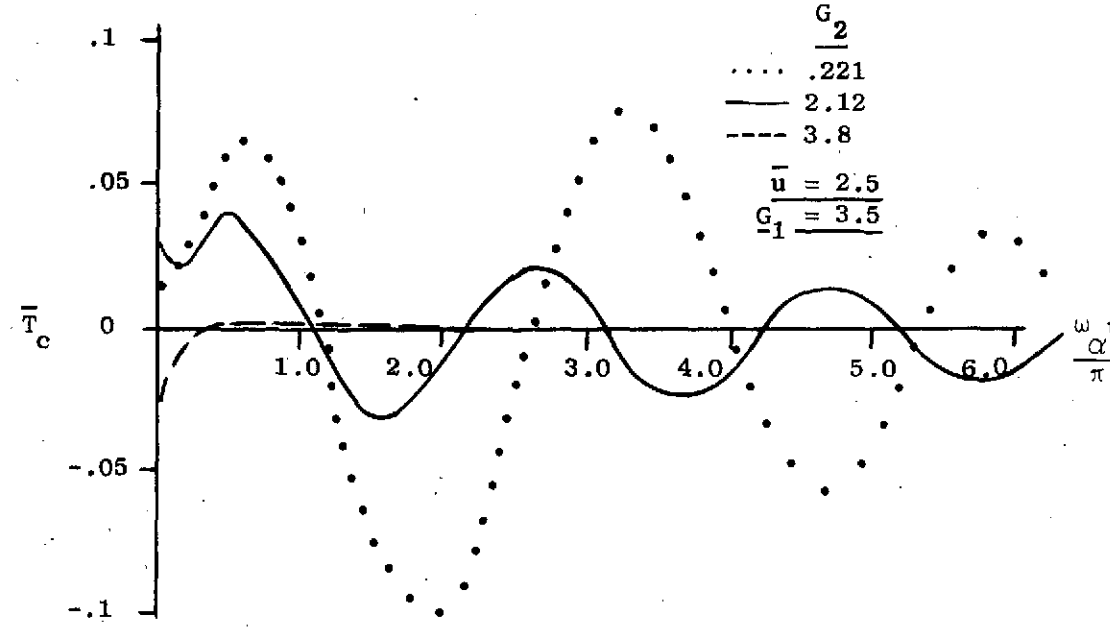

FIG. 4-2 TORQUE RESPONSE TO GUST IMPULSE

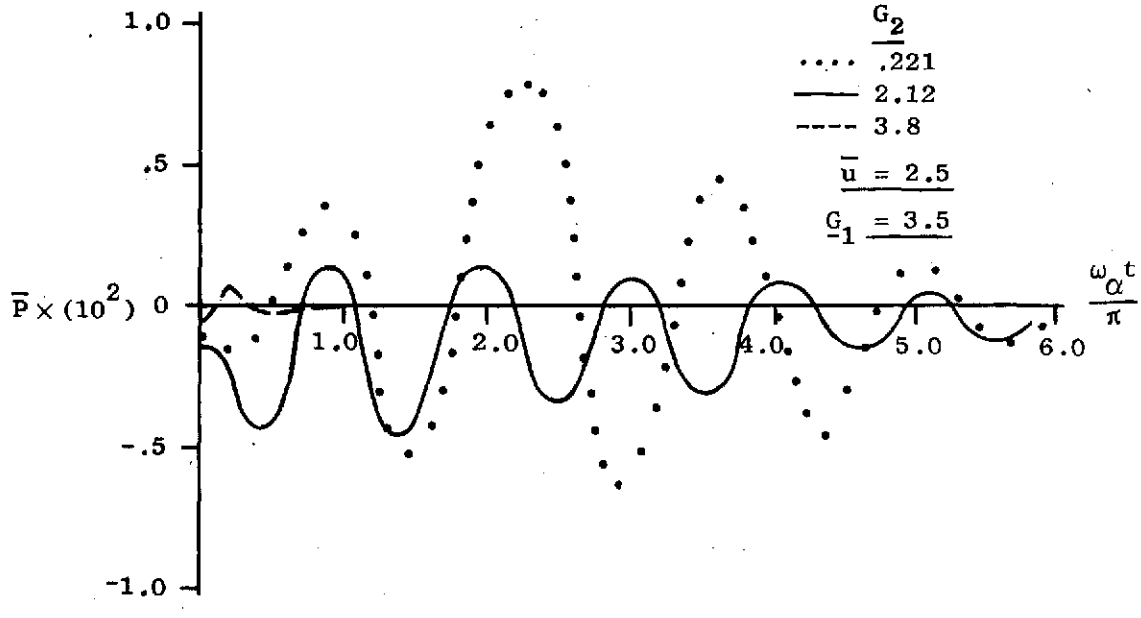

FIG. 4-3 POWER RESPONSE TO GUST IMPULSE

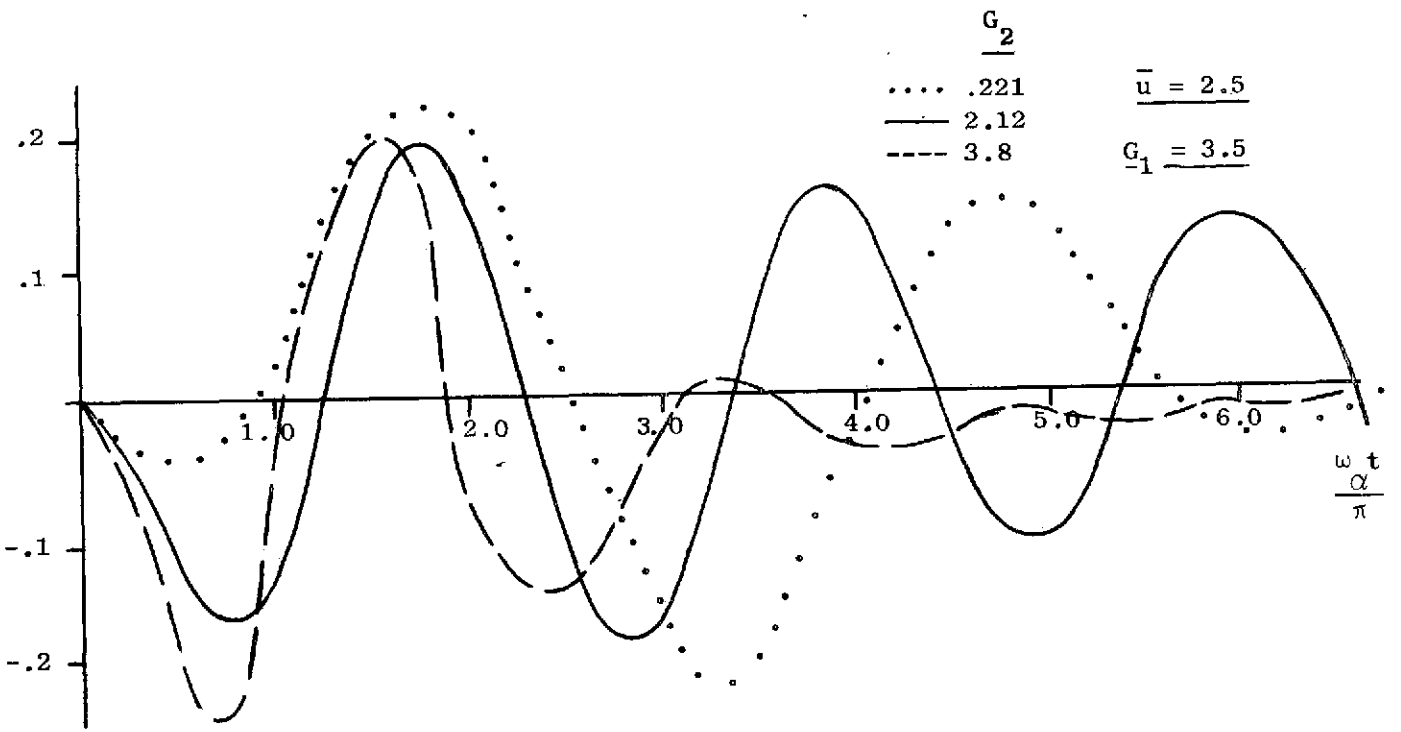

FIG. 4-4 GIMBAL ANGLE RESPONSE TO GUST IMPULSE

following set of values was selected, compatible with the chosen values of G_1 and G_2:

TABLE 4-2

G_2	=	3.8
H_w	=	6.0 $\frac{\text{kg-m}^2}{\text{sec}}$
I_{Gz}	=	0.09 kg-m^2
ω_α	=	10 Hz
b	=	1.5 ft.

The corresponding maximum value of power is 0.007 HP.

Also shown in Fig. 4-5 are the values of power associated with two of the reduced feedback cases discussed in Sec. 3-4, and identified on the figure. These values indicate that by proper selection of the root locations a reduction in feedback complexity can be made without a significant increase in power requirements (illustrated by ⊙). However, since the system eigenvalues cannot be arbitrarily determined with reduced feedback systems, the noncritical root locations and the stability level of the controlled system may be sufficiently altered to produce increased power requirements. The maximum gimbal angles corresponding to the root locations used to determine Fig. 4-5 are shown in Fig. 4-6. The minimum values of σ for each u occur at the value of G_2 corresponding to the minimum value of $\bar{P}$ in Fig. 4-5. These two curves indicate that selecting a value of G_2 corresponding to a value of u_F equal to the maximum desired flutter velocity results in the "best" design, with regard to minimizing values of power, while keeping variations of σ to a minimum. This, of course, would be subject to size constraints on the CMG itself. The large values of $\sigma/(w_g/b)$ may be prohibitive for any practical design. These values can be reduced by relocating the critical and noncritical roots of the system with corresponding increases in power requirements. From Eq. 4-20, it can be seen that increases in G_1, holding G_2 constant, can also result in a decrease in σ. These would be some of the many tradeoffs to be made in the more detailed design procedure used when developing an actual system.

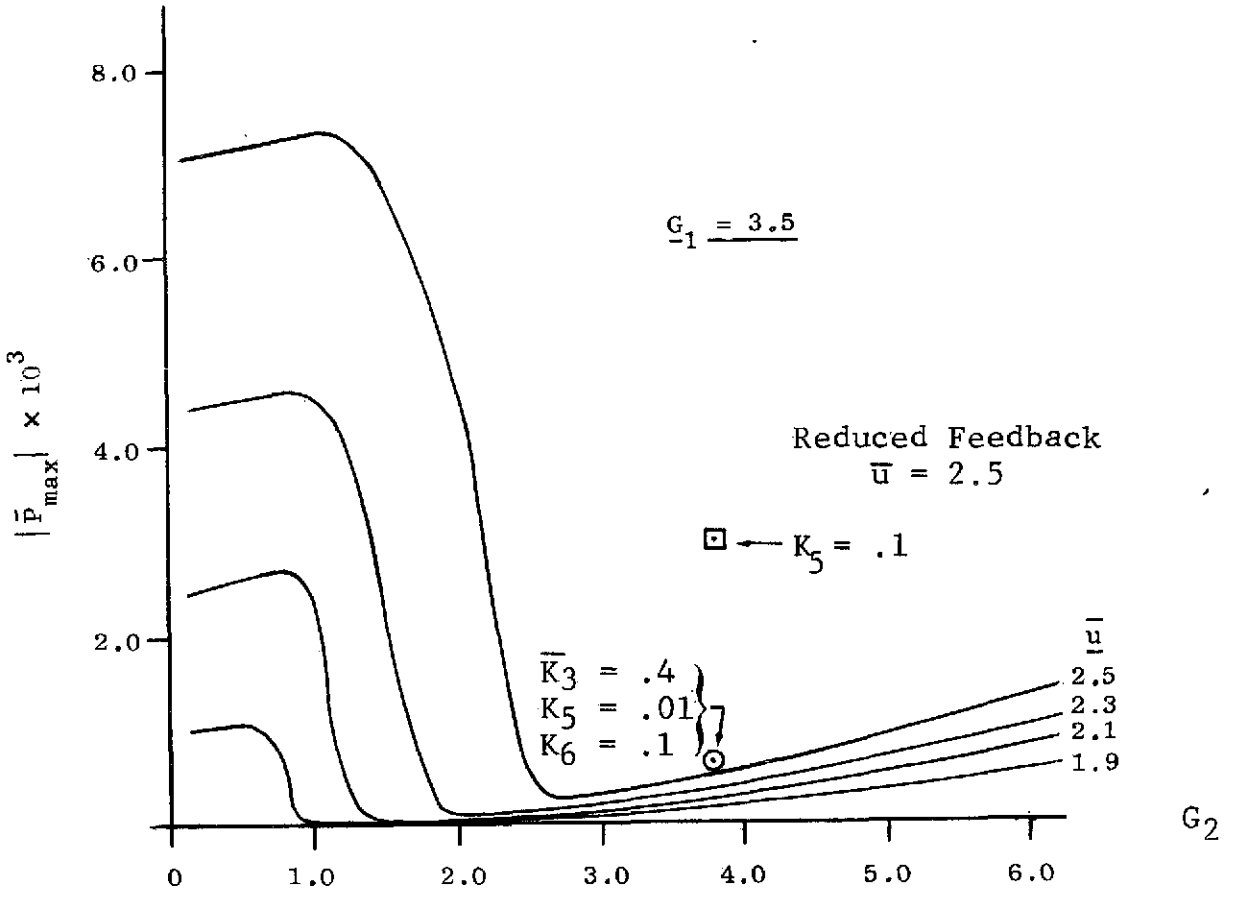

FIG. 4-5 MINIMIZED MAXIMUM POWER RESPONSE TO GUST IMPULSE

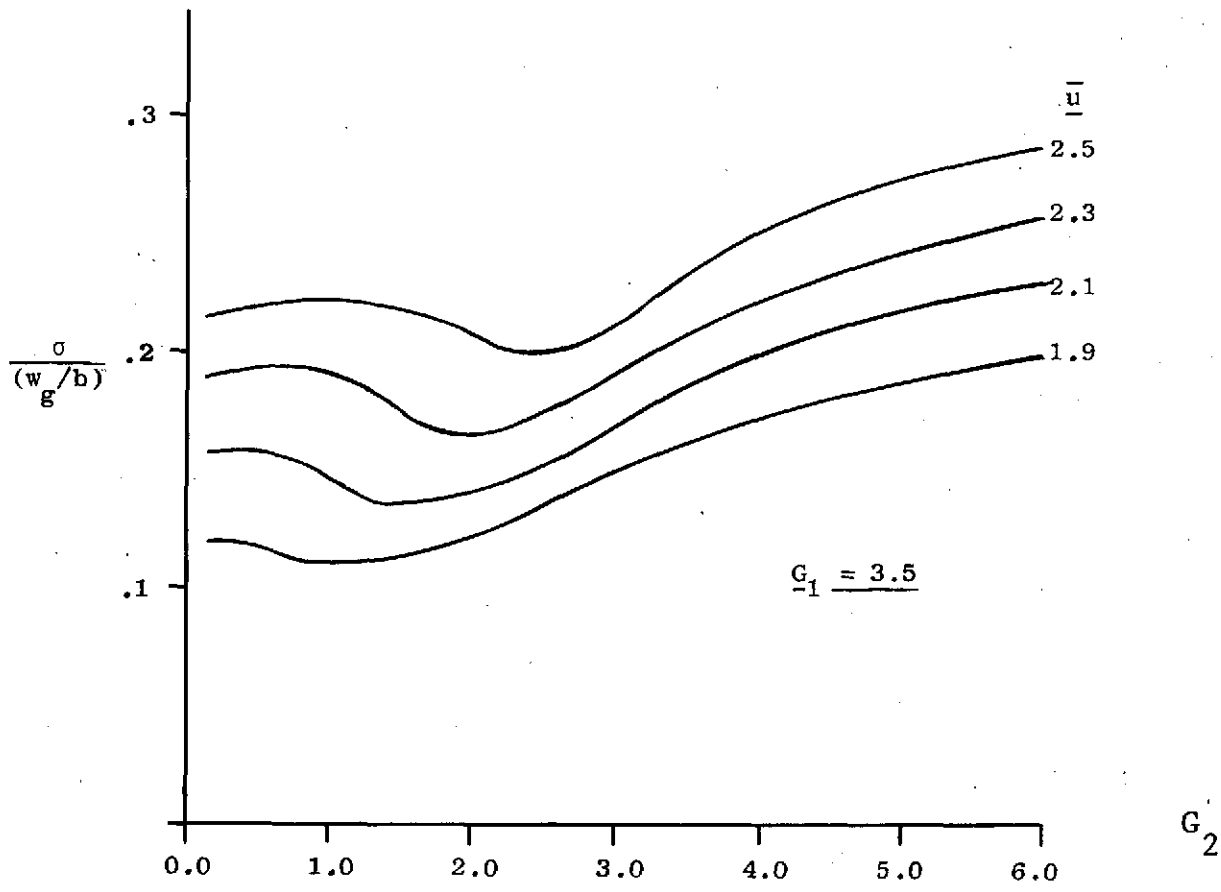

FIG. 4-6 MAXIMUM GIMBAL ANGLE CORRESPONDING TO THE MINIMIZED MAXIMUM POWER RESPONSE

V. OPEN-LOOP CONTROL CHARACTERISTICS OF A THREE-DIMENSIONAL CANTILEVER WING WITH CMG CONTROLLER

5.1 CMG Orientation

The basic approach to the design analysis of the three dimensional wing parallels the typical section analysis developed in Chap. II. The wing geometry is shown in Fig. 5-1. It is assumed to be an unswept, constant chord, cantilever wing, with rigid chordwise sections, having a straight elastic axis and uniform structural properties. Before developing the equations of motion for the wing controller system, the most effective orientation of the CMG should be determined. As can be seen from Figure 5-2, six possible orientations exist, depending on the direction of the gyro's precession and spin axes (for illustrative purposes, only a single rotor of the twin-gyro controller is shown). To be most effective, the output torque produced by the CMG on the wing, $M_{G/W}$, should be directed about an axis of rotation of the wing (i.e., the X or Y axis). Thus, cases 5-2b and 5-2e, which provide moments about the Z-axis, would obviously not be a suitable choice. A preliminary analysis has also shown, for the particular set of parameters selected in this thesis (see Section 2.2), that directing the CMG output torque about the X-axis, cases 5-2c and 5-2f, does not provide adequate control capability. Consequently, cases 5-2a and 5-2d appear to be the most suitable CMG orientations. For low control torque levels, the difference between the two orientations can be considered negligible, and for the following analysis case 5-2a was selected. The equations of motion for the control moment gyro in this orientation are derived in Appendix B.

5.2 Wing-Controller Equations of Motion

The dynamical equations of motion for the coupled torsion and bending of a cantilever wing are derived in a number of classic aeroelastic references, including Refs. 20 and 21. These equations, with the inclusion of the CMG terms from Appendix B, can be written

$$m\ddot{h}(y,t)+m_G\ddot{h}(y,t)\,\delta(y-y_G)+EI\frac{\partial^4 h(y,t)}{\partial y^4}+S_\alpha\,\ddot{\alpha}(y,t)$$

$$+S_{\alpha G}\ddot{\alpha}(y,t)\,\delta(y-y_G) \qquad = -L_D - L \qquad (5\text{-}1)$$

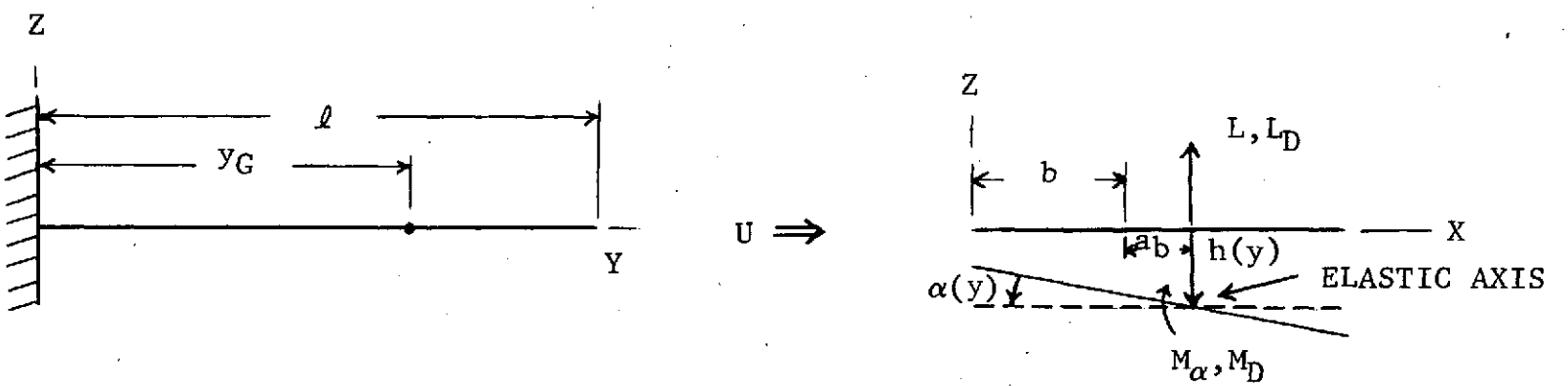

FIG. 5-1 WING GEOMETRY

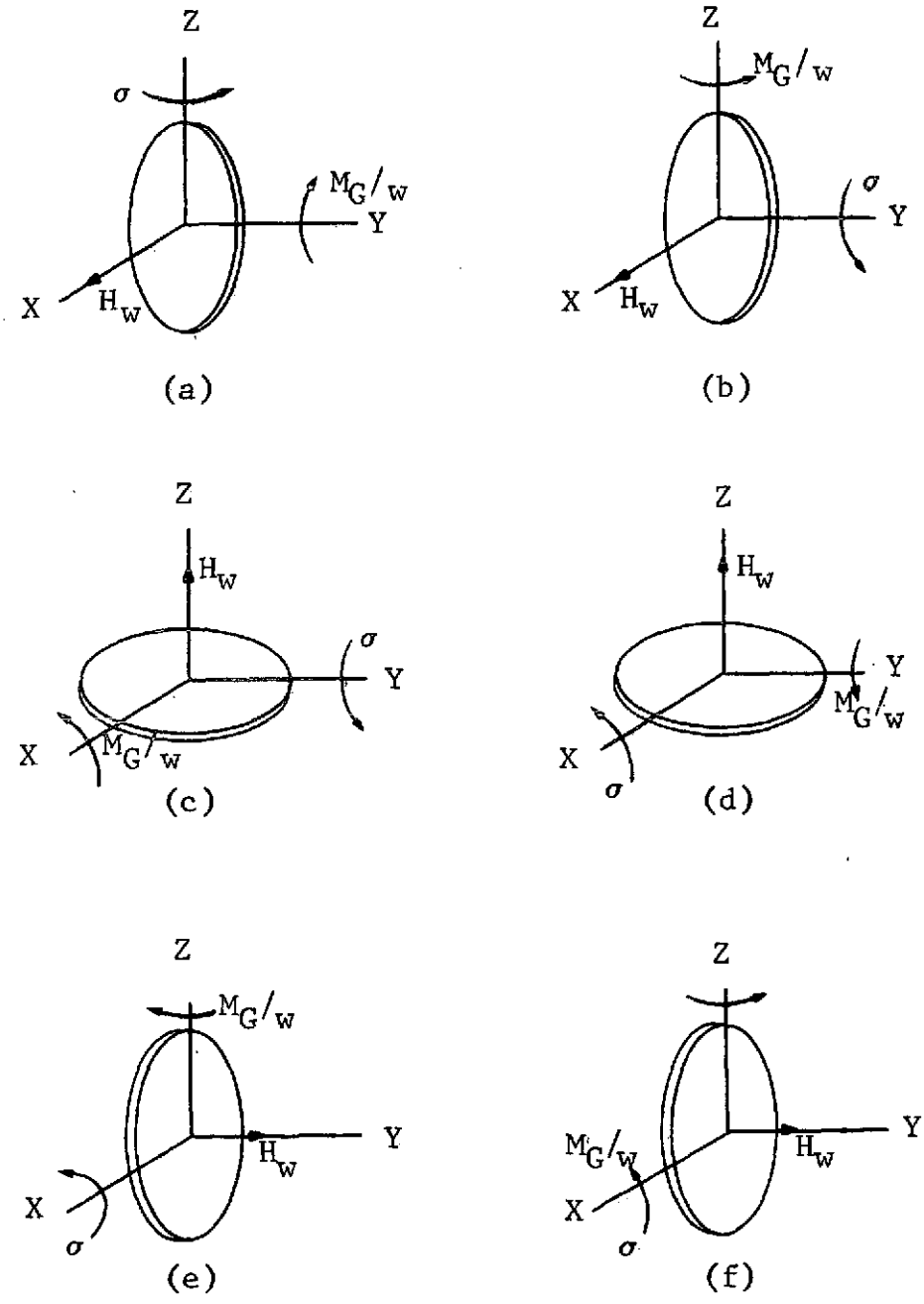

FIG. 5-2 POSSIBLE CMG ORIENTATIONS

$$S_\alpha \ddot{h}(y,t)+S_{\alpha G}\ddot{h}(y,t)\delta(y-y_G)+I_\alpha \ddot{\alpha}(y,t)+I_{\alpha G}\ddot{\alpha}(y,t)\delta(y-y_G)$$
$$- GJ\frac{\partial^2\alpha(y,t)}{\partial y^2} + H_w\dot{\sigma}(y,t)\delta(y-y_G) = M_D + M_\alpha \qquad (5\text{-}2)$$

$$- H_w\dot{\alpha}(y_G,t)+I_{Gz}\ddot{\sigma}(y_G,t) = T_c(y_G,t) \qquad (5\text{-}3)$$

With the boundary conditions of a cantilever beam:

$$\begin{aligned} &\text{at} \quad y = o, \quad h = \frac{\partial h}{\partial y} = \alpha = 0 \\ &\text{at} \quad y = \ell, \quad \frac{\partial^2 h}{\partial y^2} = \frac{\partial^3 h}{\partial y^3} = \frac{\partial \alpha}{\partial y} = 0 \end{aligned} \qquad (5\text{-}4)$$

The CMG is treated as a concentrated mass and is assumed to generate a concentrated torque about the Y-axis. Rotational inertia terms about the X-axis and CMG effects on flexural and torsional rigidity are considered negligible.

A number of methods are available for developing solutions to the above equations. Runyan and Watkins (28) developed a solution for a uniform wing with arbitrarily placed, concentrated masses by extending the treatment of Goland (29), in which the differential equations are attacked directly. To obtain flutter information, this is the most accurate approach for a uniform wing, but it does not allow for a suitable means to determine control gains or to deal with wings having non-uniform properties. A practical method for performing flutter calculations is based on the assumption that the motion of the system can be approximated by a superposition of a finite number of certain selected modal functions. This type of analysis is often referred to as a Rayleigh type or the Rayleigh-Ritz method. Since a continuous system, such as a wing, possesses infinite degrees of freedom, the accuracy of the results depends, in general, on the number and choice of modal functions to be used. The two most common choices for these functions are either the coupled or uncoupled modes of oscillation of the system in a vacuum, since these functions satisfy structural boundary conditions. In determining the uncoupled modes, bending and torsion are assumed independent, such that the inertial coupling terms, those containing S_α, are neglected in the equations of motion. Physically, this is equivalent to assuming, for pure bending, for example, that the mass

distribution acts along the elastic axis with no torsional deformation, and similarly for pure torsion, the wing is assumed to be constrained from bending. A coupled mode usually refers to a combination of torsional and bending deformations appropriate to the natural normal harmonic vibration of a freely oscillating system (30).

On a wing with a true elastic axis and utilizing strip theory aerodynamics, it is computationally more convenient to use uncoupled modes in the analysis (20). Furthermore, Ref. 31, in comparing the coupled and uncoupled methods with experimental results on a straight, uniform, cantilever wing with a large mass placed at various spanwise locations, indicates that using coupled modes analysis shows no better agreement with experiments, and that using uncoupled modes shows a more systematic improvement of accuracy when additional degrees of freedom are used. For these reasons, the uncoupled mode method will be used in this analysis.

The number of modal functions assumed in any flutter analysis generally depends on the complexity of the structure under consideration. Experience has shown, for simple wing models without large concentrated masses, that satisfactory results are obtained with two or three modes. The assumption is made in this analysis that the CMG mass is not large relative to the wing mass, otherwise little benefit in weight savings would result using active control. The CMG does, however, generate a concentrated torque on the wing, whose effect may require the addition of more modes in the analysis for sufficient accuracy. The procedure adopted in the following open-loop analysis will be to assume four uncoupled modes, consisting of the first and second bending and torsion modes of the uniform wing. This results in an 18th order system. To determine whether the complexity of this formulation can be reduced without loss in accuracy, these results will be then compared with a two mode, 10th order, analysis.

The bending and torsion deflections can now be written as

$$h(y,t) = f_{h1}(y)h_1(t) + f_{h2}(y)h_2(t) \qquad (5\text{-}5)$$

$$\alpha(y,t) = f_{\alpha 1}(y)\alpha_1(t) + f_{\alpha 2}(y)\alpha_2(t) \quad * \qquad (5\text{-}6)$$

where f_{h1} and f_{h2} are the first two uncoupled bending modes, and $f_{\alpha 1}$ and $f_{\alpha 2}$ are the first two uncoupled torsion modes of a uniform contilever wing oscillating in a vacuum. The mode shapes are illustrated in Fig. 5-3 and can be represented mathematically by

$$f_{h1}(y) = \cosh(1.875\cdot y)-\cos(1.875\cdot y)-.734\left[\sinh(1.875\cdot y) - \sin(1.875.y)\right] \qquad (5\text{-}7)$$

$$f_{h2}(y)=\cosh(4.694\cdot y)-\cos(4.694\cdot y)-1.018\left[\sinh(4.694\cdot y) -\sin(4.694\cdot y)\right] \qquad (5\text{-}8)$$

$$f_{\alpha 1}(y) = \sin \frac{\pi}{2} y \qquad (5\text{-}9)$$

$$f_{\alpha 2}(y) = \sin \frac{3\pi}{2} y \qquad (5\text{-}10)$$

To develop the ordinary differential equations of motion, the classic approach of Galerkin (32) will be used. Thus, Eq. 5-1 is multiplied by f_{h1} and f_{h2} and Eq. 5-2 is multiplied by $f_{\alpha 1}$ and $f_{\alpha 2}$, and the resulting four equations are integrated over the length of the wing. Assuming two-dimensional strip theory, with the lift and moment per unit span being represented by the expressions defined in the typical section analysis of Chap. 2 , the equations of motion can be written,

$$\begin{aligned} &mF_{h1}\ddot{h}_1+\frac{m_G}{\ell}f_{h1}^2(y_G)\ddot{h}_1+F_{h1}C_{h1}h_1 +F_{h1,\alpha 1}S_\alpha\ddot{\alpha}_1 + \frac{S_{\alpha G}}{\ell}f_{h1}(y_G)f_{\alpha 1}(y_G)\ddot{\alpha}_1 + \\ &\frac{m_G}{\ell}f_{h1}f_{h2}(y_G)\ddot{h}_2 + F_{h1,\alpha 2}S_\alpha\ddot{\alpha}_2 + \frac{S_{\alpha G}}{\ell}f_{h1}(y_G)f_{\alpha 2}(y_G)\ddot{\alpha}_2 \\ &= -\pi\rho b^2\left\{F_{h1}\ddot{h}_1 + U\left[F_{h1,\alpha 1}\dot{\alpha}_1 + F_{h1,\alpha 2}\dot{\alpha}_2\right]\right. \\ &\left. - ba\left[F_{h1,\alpha 1}\ddot{\alpha}_1 + F_{h1,\alpha 2}\ddot{\alpha}_2\right]\right\} -2\pi\rho b\, U\int_o^\tau \frac{d}{d\bar{t}} \\ &\left[F_{h1}h_1 +U(F_{h1,\alpha 1}\alpha_1+F_{h1,\alpha 2}\alpha_2)+b(\tfrac{1}{2}-a)(F_{h1,\alpha 1}\dot{\alpha}_1+F_{h1,\alpha 2}\dot{\alpha}_2)\right] \\ &\times \Phi(\tau-\bar{t})d\bar{t} \end{aligned} \qquad (5\text{-}11)$$

*NOTE: To be consistent with the typical section analysis, h and α are retained to represent the bending and torsion deflections. However, similar subscripts between the two analyses may refer to somewhat different quantities. Hopefully, the formulation is straightforward enough so that no confusion results.

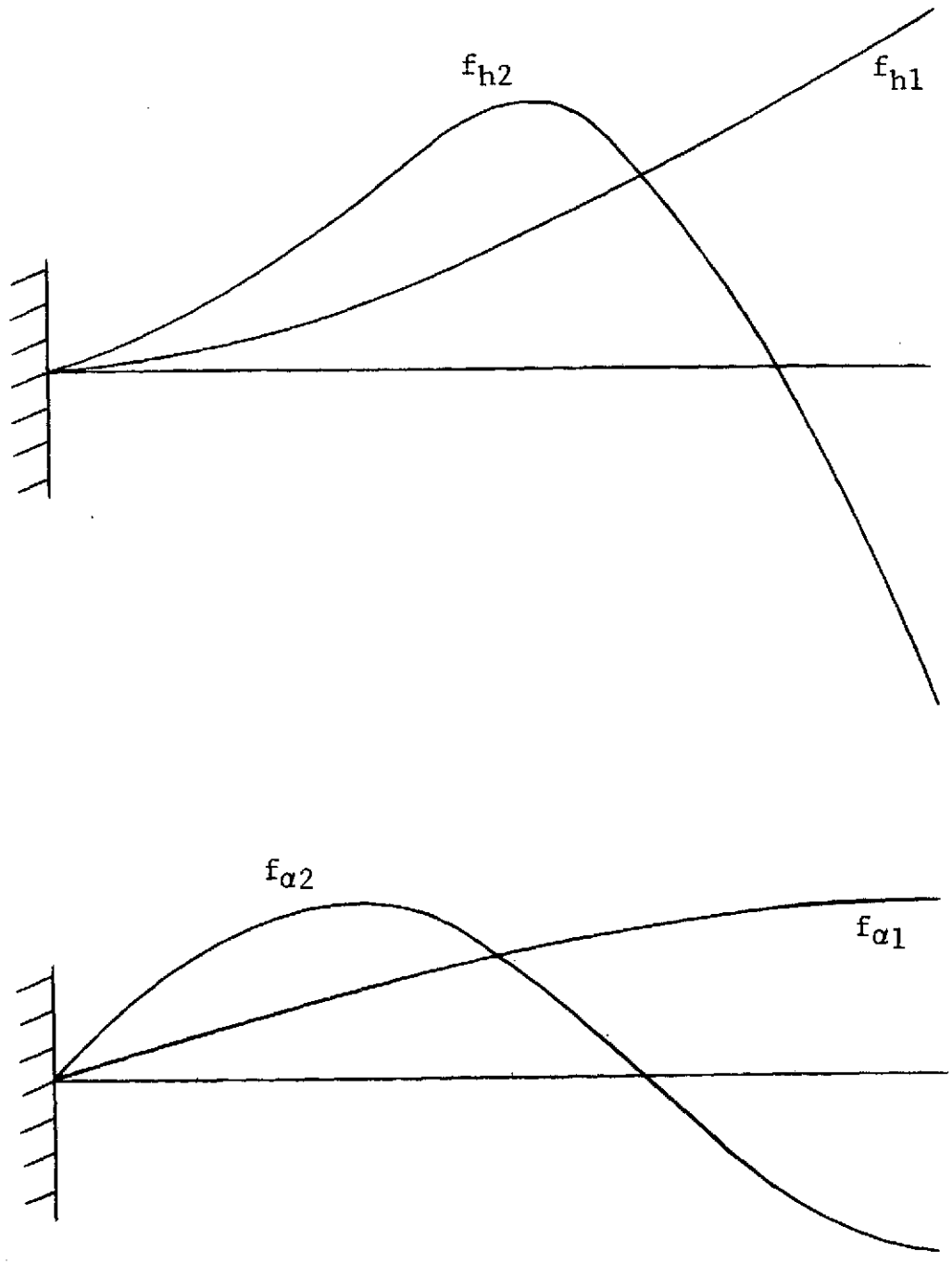

FIG. 5-3 UNCOUPLED BENDING AND TORSION MODES OF VIBRATION OF A UNIFORM CANTILEVER WING

$$mF_{h2}\ddot{h}_2+\frac{m_G}{\ell}f_{h2}^2(y_G)\ddot{h}_2+\frac{m_G}{\ell}f_{h1}f_{h2}(y_G)\ddot{h}_1+F_{h2}C_{h2}h_2+S_\alpha F_{h2,\alpha 1}\ddot{\alpha}_1$$

$$+\frac{S_{\alpha G}}{\ell}f_{h2}f_{\alpha 1}(y_G)\ddot{\alpha}_1+S_\alpha F_{h2,\alpha 2}\ddot{\alpha}_2+\frac{S_{\alpha G}}{\ell}f_{h2}f_{\alpha 2}(y_G)\ddot{\alpha}_2$$

$$=-\pi\rho b^2\left\{F_{h2}\ddot{h}_2+U\left[F_{h2,\alpha 1}\dot{\alpha}_1+F_{h2,\alpha 2}\dot{\alpha}_2\right]\right.$$

$$\left.-ba\left[F_{h2,\alpha 1}\ddot{\alpha}_1+F_{h2,\alpha 2}\ddot{\alpha}_2\right]\right\}-2\pi\rho bU\int_o^\tau\frac{d}{d\bar{t}}$$

$$\left[F_{h2}\dot{h}_2+U(F_{h2,\alpha 1}\alpha_1+F_{h2,\alpha 2}\alpha_2)+b(\tfrac{1}{2}-a)(F_{h2,\alpha 1}\dot{\alpha}_1+F_{h2,\alpha 2}\dot{\alpha}_2)\right]\times$$

$$\Phi(\tau-\bar{t})d\bar{t} \qquad (5\text{-}12)$$

$$S_\alpha F_{h1,\alpha 1}\ddot{h}_1+\frac{S_{\alpha G}}{\ell}f_{h1}f_{\alpha 1}(y_G)\ddot{h}_1+S_\alpha F_{h2,\alpha 1}\ddot{h}_2+\frac{S_{\alpha G}}{\ell}f_{h2}f_{\alpha 1}(y_G)\ddot{h}_2+I_\alpha F_{\alpha 1}\ddot{\alpha}_1$$

$$+\frac{I_{Gz}}{\ell}f_{\alpha 1}^2(y_G)\ddot{\alpha}_1+\frac{I_{Gz}}{\ell}f_{\alpha 1}f_{\alpha 2}(y_G)\ddot{\alpha}_2+C_{\alpha 1}F_{\alpha 1}\alpha_1+\frac{H_w}{\ell}f_{\alpha 1}(y_G)\dot{\sigma}$$

$$=\pi\rho b^2\left\{ba\left[F_{h1,\alpha 1}\ddot{h}_1+F_{h2,\alpha 1}\ddot{h}_2\right]-Ub(\tfrac{1}{2}-a)\left[F_{\alpha 1}\dot{\alpha}_1-b^2(\tfrac{1}{8}+a^2)F_{\alpha 1}\ddot{\alpha}_1\right]\right\}$$

$$+2\pi\rho Ub^2(\tfrac{1}{2}+a)\int_o^\tau\frac{d}{d\bar{t}}\left[F_{h1,\alpha 1}\dot{h}_1+F_{h2,\alpha 1}\dot{h}_2+UF_{\alpha 1}\alpha_1+b(\tfrac{1}{2}-a)F_{\alpha 1}\dot{\alpha}_1\right]\Phi(\tau-\bar{t})d\bar{t}$$

(5-13)

$$S_\alpha F_{h1,\alpha 2}\ddot{h}_1+\frac{S_{\alpha G}}{\ell}f_{h1}f_{\alpha 2}(y_G)\ddot{h}_1+S_\alpha F_{h2,\alpha 2}\ddot{h}_2+\frac{S_{\alpha G}}{\ell}f_{h2}f_{\alpha 2}(y_G)\ddot{h}_2+I_\alpha F_{\alpha 2}\ddot{\alpha}_2$$

$$+\frac{I_{Gz}}{\ell}f_{\alpha 2}^2(y_G)\ddot{\alpha}_2+\frac{I_{GZ}}{\ell}f_{\alpha 2}f_{\alpha 1}(y_G)\ddot{\alpha}_1+C_{\alpha 2}F_{\alpha 2}\alpha_2+\frac{H_w}{\ell}f_{\alpha 2}(y_G)\dot{\sigma}$$

$$=\pi\rho b^2\left\{ba\left[F_{h1,\alpha 2}\ddot{h}_1+F_{h2,\alpha 2}\ddot{h}_2\right]-Ub(\tfrac{1}{2}-a)\left[F_{\alpha 2}\dot{\alpha}_2-b^2(\tfrac{1}{8}+a^2)F_{\alpha 2}\ddot{\alpha}_2\right]\right\}$$

$$+2\pi\rho Ub^2(\tfrac{1}{2}+a)\int_o^\tau\frac{d}{d\bar{t}}\left[F_{h1,\alpha 2}\dot{h}_1+F_{h2,\alpha 2}\dot{h}_2+UF_{\alpha 2}\alpha_2+b(\tfrac{1}{2}-a)F_{\alpha 2}\dot{\alpha}_2\right]\Phi(\tau-\bar{t})d\bar{t}$$

(5-14)

$$- H_w\left[\dot{\alpha}_1 f_{\alpha 1}(y_G)+\dot{\alpha}_2 f_{\alpha 2}(y_G)\right] + I_y \ddot{\sigma} = T_c \qquad (5\text{-}15)$$

where

$$\begin{aligned}
F_{h1} &= \frac{1}{\ell}\int_o^\ell f_{h1}^2(y)dy \\
F_{h2} &= \frac{1}{\ell}\int_o^\ell f_{h2}^2(y)dy \\
F_{\alpha 1} &= \frac{1}{\ell}\int_o^\ell f_{\alpha 1}^2(y)dy \\
F_{\alpha 2} &= \frac{1}{\ell}\int_o^\ell f_{\alpha 2}^2(y)dy \\
F_{h1,\alpha 1} &= \frac{1}{\ell}\int_o^\ell f_{h1} f_{\alpha 1}(y)dy \\
F_{h2,\alpha 1} &= \frac{1}{\ell}\int_o^\ell f_{h2} f_{\alpha 1}(y)dy \\
F_{h1,\alpha 2} &= \frac{1}{\ell}\int_o^\ell f_{h1} f_{\alpha 2}(y)dy \\
F_{h2,\alpha 2} &= \frac{1}{\ell}\int_o^\ell f_{h2} f_{\alpha 2}(y)dy \\
C_{h1} &= \frac{1}{\ell}\int_o^\ell EI f_{h1} f_{h1}^{IV}(y)dy \\
C_{h2} &= \frac{1}{\ell}\int_o^\ell EI f_{h2} f_{h2}^{IV}(y)dy \\
C_{\alpha 1} &= -\frac{1}{\ell}\int_o^\ell GJ f_{\alpha 1} f_{\alpha 1}^{II}(y)dy \\
C_{\alpha 2} &= -\frac{1}{\ell}\int_o^\ell GJ f_{\alpha 2} f_{\alpha 2}^{II}(y)dy
\end{aligned} \qquad (5\text{-}16)$$

Another often used procedure for obtaining the equations of motion is to first develop expressions for the kinetic and potential energies of the system and then apply Lagrange's equations (33). The resulting equations would, of course, be the same.

5.3 Open-Loop Characteristics of Wing-Controller System

Paralleling the procedure of Chap. 2 to determine the characteristic equation, Eqs. 5-11 and 5-12 are divided by $\pi\rho b^3$, Eqs. 5-13 and 5-14 are divided by $\pi\rho b^4$, and the Laplace transform of the resulting equations is taken. The equations become, in matrix form,

$$
\begin{bmatrix}
\left[(\mu_1+1)\bar{s}^2+2\bar{u}\varphi(\bar{s})+\left(\frac{\omega_{h1}}{\omega_{\alpha1}}\right)^2\mu\right]F_{h1} & \mu_G\bar{s}^2 & \left\{(x_{\alpha11}\mu-a)\bar{s}^2+\left[1+(1-2a)\varphi(\bar{s})\right]\bar{u}\bar{s}\right. & \left\{(x_{\alpha12}\mu-a)\bar{s}^2+\left[1+(1-2a)\varphi(\bar{s})\right]\bar{u}\bar{s}\right. & 0 \\
 & & \left.+2\bar{u}^2\varphi(\bar{s})\right\}F_{h1,\alpha1} & \left.+2\bar{u}^2\varphi(\bar{s})\right\}F_{h1,\alpha2} & \\
\mu_G & \left[(\mu_2+1)\bar{s}^2+2\bar{u}\varphi(\bar{s})+\left(\frac{\omega_{h2}}{\omega_{\alpha1}}\right)^2\mu\right]F_{h2} & \left\{(x_{\alpha21}\mu-a)\bar{s}^2+\left[1+(1-2a)\varphi(\bar{s})\right]\bar{u}\bar{s}\right. & \left\{(x_{\alpha22}\mu-a)\bar{s}^2+\left[1+(1-2a)\varphi(\bar{s})\right]\bar{u}\bar{s}\right. & 0 \\
 & & \left.+2\bar{u}^2\varphi(\bar{s})\right\}F_{h2,\alpha1} & \left.+2\bar{u}^2\varphi(\bar{s})\right\}F_{h2,\alpha2} & \\
\left[(x_{\alpha11}\mu-a)\bar{s}^2-\bar{u}(1+2a)\varphi(\bar{s})\bar{s}\right] & \left[(x_{\alpha21}\mu-a)\bar{s}^2-\bar{u}(1+2a)\varphi(\bar{s})\bar{s}\right] & \left\{\left[r_{\alpha1}^2\mu+(\tfrac{1}{8}+a^2)\right]\bar{s}^2\right. & r_{\alpha G}\mu\bar{s}^2 & \\
F_{h1,\alpha1} & F_{h2,\alpha1} & +\bar{u}\left[\tfrac{1}{2}-a-(\tfrac{1}{2}-2a^2)\varphi(\bar{s})\right]\bar{s} & & G_{11}\bar{s} \\
 & & \left.+r_\alpha^2\mu-\bar{u}^2(1+2a)\varphi(\bar{s})\right\}F_{\alpha1} & & \\
\left[(x_{\alpha12}\mu-a)\bar{s}^2-\bar{u}(1+2a)\varphi(\bar{s})\bar{s}\right] & \left[(x_{\alpha22}\mu-a)\bar{s}^2-\bar{u}(1+2a)\varphi(\bar{s})\bar{s}\right]F_{h2,\alpha2} & r_{\alpha G}^2\mu\bar{s}^2 & \left\{\left[r_{\alpha2}^2\mu+(\tfrac{1}{8}+a^2)\right]\bar{s}^2\right. & \\
F_{h1,\alpha2} & & & +\bar{u}\left[\tfrac{1}{2}-a-(\tfrac{1}{2}-2a^2)\varphi(\bar{s})\right]\bar{s} & G_{12}\bar{s} \\
 & & & \left.+r_\alpha^2\mu-\bar{u}^2(1+2a)\varphi(\bar{s})\right\}F_{\alpha2} & \\
0 & 0 & -G_{01}\bar{s} & -G_{02}\bar{s} & \bar{s}^2
\end{bmatrix}
\begin{bmatrix} \frac{h_1}{b} \\ \frac{h_2}{b} \\ \alpha_1 \\ \alpha_2 \\ \sigma \end{bmatrix}
=
\begin{bmatrix} 0 \\ 0 \\ 0 \\ 0 \\ \frac{I_G}{I_{Gz}\omega_{\alpha1}^2} \end{bmatrix}
\tag{5-17}
$$

where, in this case

$$\bar{s} = \frac{s}{\omega_{\alpha 1}}$$

$$\bar{u} = \frac{U}{b\,\omega_{\alpha 1}}$$

In determining the effect of the CMG on the dynamic characteristics of the wing, the values of the nondimensional wing parameters corresponding to those previously used in Section 2.2 have been selected. The effect of the CMG parameter, $\bar{G}_2$, on flutter velocity and flutter frequency is illustrated in Figs. 5-4 and 5-5, respectively. for two different span locations of the CMG, corresponding to the midspan and wing tip. The CMG is assumed to be weightless. Also shown are comparisons between the two mode, four mode, and typical section analyses.

It can be seen from these figures that the two mode analysis appears to provide sufficient accuracy for increases in the flutter velocity parameter up to and beyond 3.0, and that the typical section analysis is seen to correspond closely to the three-dimensional case with the CMG at midspan. A comparison of the root loci, using the three methods of analysis, for particular designs having $\bar{u}_F = 2.5$, is shown in Fig. 5-6. The effectiveness in increasing the flutter velocity by moving the CMG to the wing tip is evident from Fig. 5-4 and is shown more explicitly in Fig. 5-7 for various values of CMG weight. Increases in weight, generally decrease the flutter velocity, except in the vicinity of the wing tip, where the flutter velocity varies only slightly with CMG weight. Although the flutter velocity remains fairly constant, Fig. 5-8 shows that the flutter frequency tends to decrease with CMG weight increases.

From the above analysis, locating the CMG controller at the wing tip appears to provide the most effective control on the system. In Chapter VI, the feedback characteristics of various designs with this CMG location will be determined.

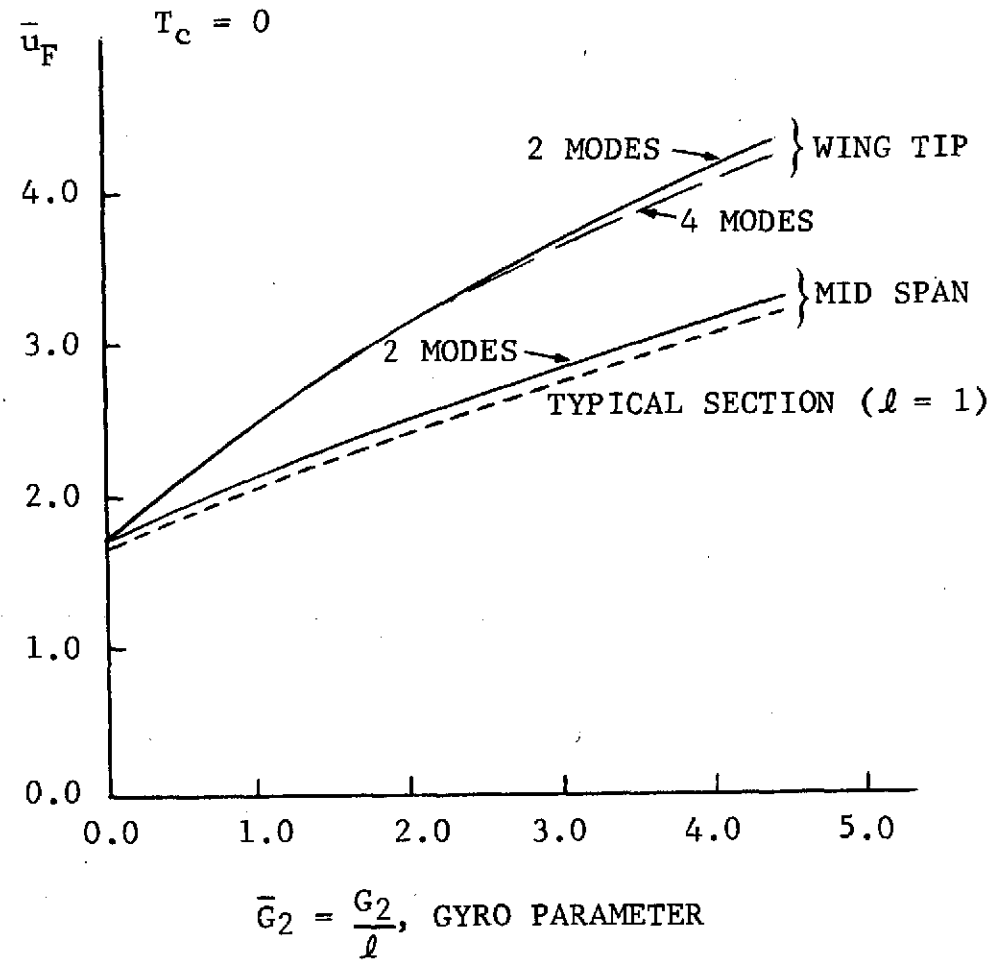

FIG. 5-4 VARIATION IN FLUTTER VELOCITY WITH $\bar{G}_2$

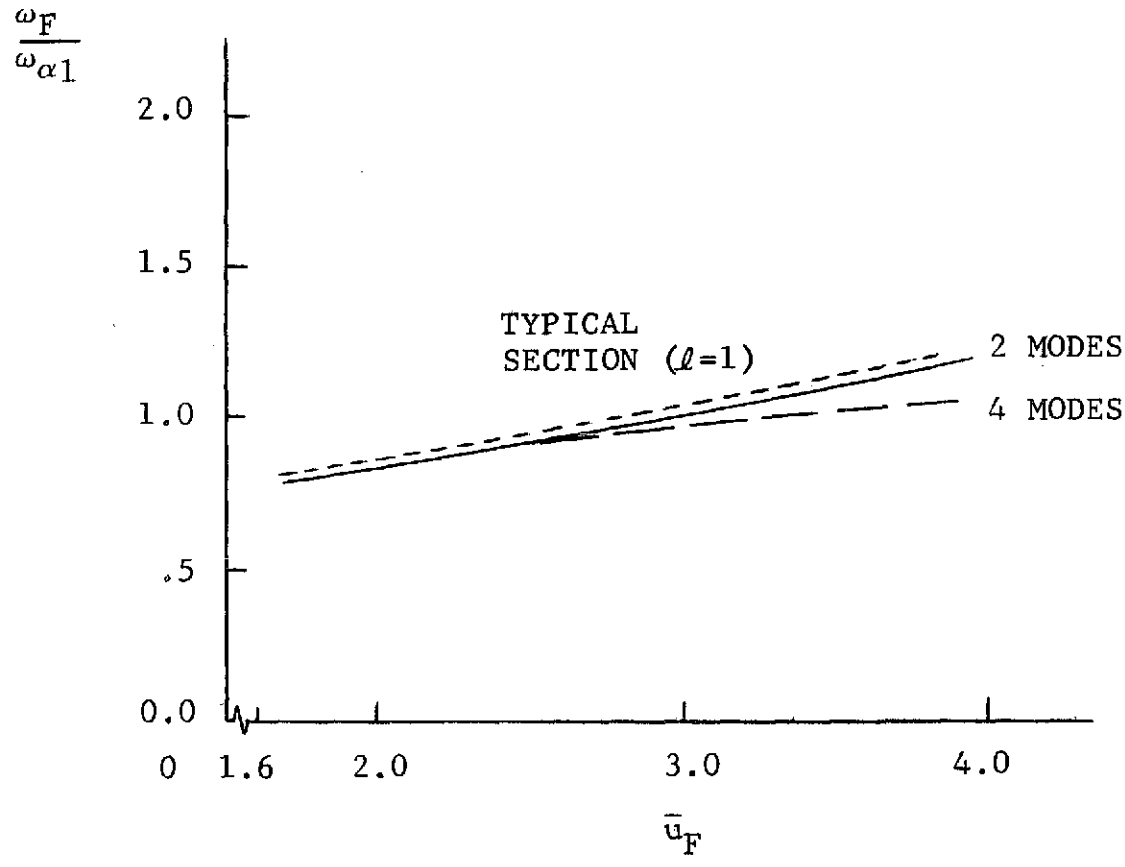

FIG. 5-5 VARIATION OF FLUTTER FREQUENCY WITH FLUTTER VELOCITY

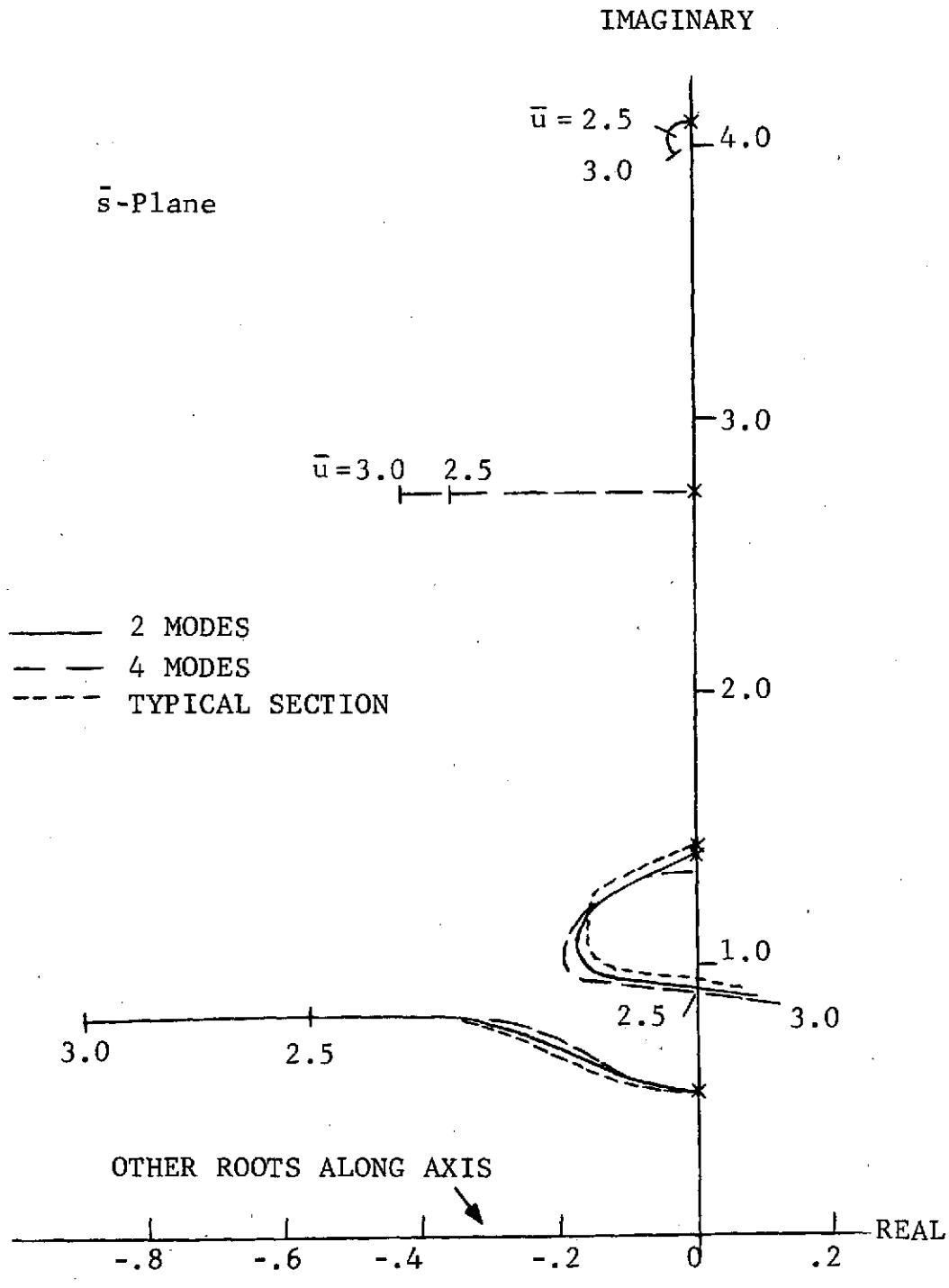

FIG. 5-6 ROOT LOCUS COMPARISON OF 3 METHODS OF ANALYSIS, $\bar{u}_F = 2.5$

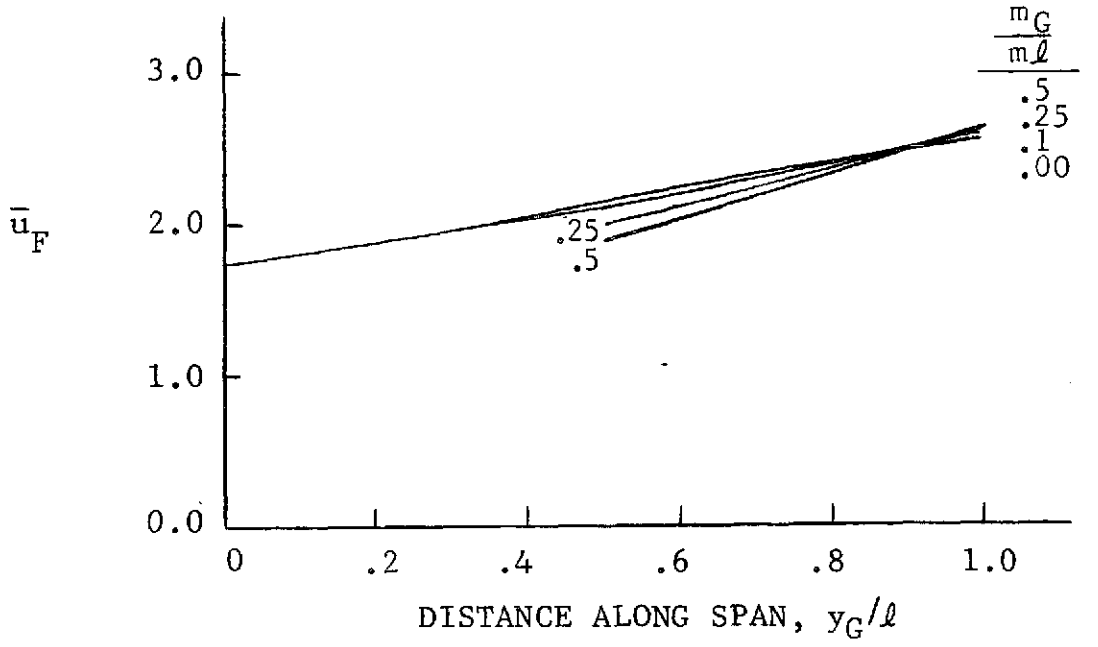

FIG 5-7 EFFECT OF CMG WEIGHT AND SPAN LOCATION OF FLUTTER VELOCITY, $\bar{G}_2$=.952

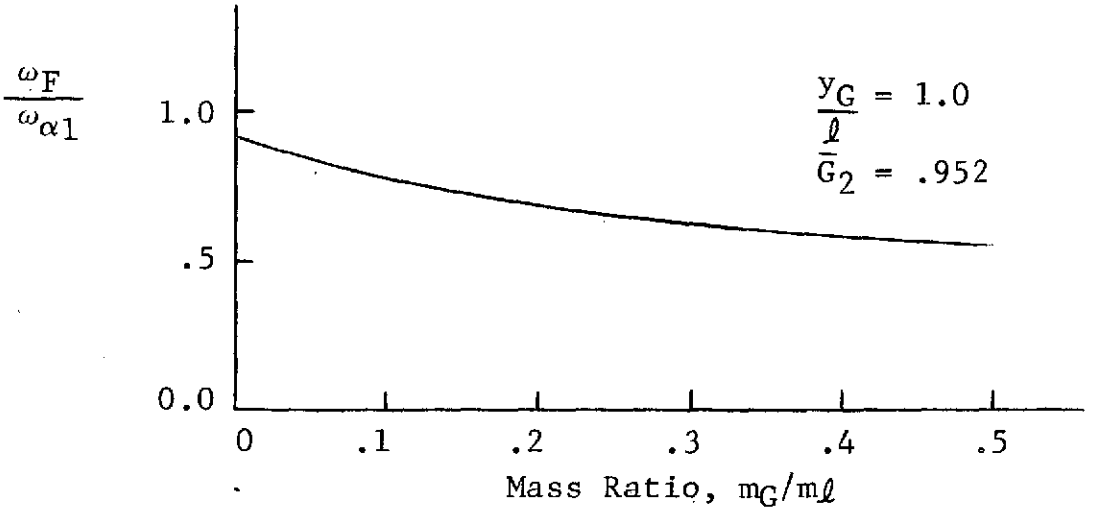

FIG. 5-8 EFFECT OF CMG WEIGHT ON FLUTTER FREQUENCY

VI. FEEDBACK CONTROL OF THE THREE-DIMENSIONAL WING-CONTROLLER SYSTEM

6.1 Introduction

Obtaining solutions to the feedback control problem of a continuous, elastic, unstable system, such as a wing in an airstream travelling faster than the critical flutter velocity, can be most difficult. Exact solutions of just the aeroelastic problem have been developed for only a few special cases. Since the wing is actually an infinite-degree-of-freedom system, and thus has infinite states, new, more realistic, meanings must also be found for the concepts of controllability and observability (34). In Chap. 5, it was shown how the continuous system could be approximated by an equivalent system with finite degrees of freedom, and furthermore, in our particular case, how describing the system with only two modes of vibration can result in reasonable accuracy in determining the system's flutter characteristics. There is no guarantee, however, that this simple model will be valid for the feedback case. Higher modes may be excited and possibly driven unstable in attempting to control the lower modes. Thus, certain questions arise in examining the control problem of even the approximate system: 1) What is the minimum number of modes to be included in the analysis to insure that the controlled system is stable over the required range of velocities?, 2) What is the minimum number of controls needed for controllability and/or stability?, 3) What are the essential feedback parameters to achieve stability?, and 4) How many measurements are needed to establish observability for the system? These questions will be discussed in some detail in the following sections.

6.2 State Variable Selection and Controllability

The method of design using arbitrary dynamics and the concept of controllability were discussed in Chap. 3. For convenience in determining the control characteristics of the three-dimensional system, the system equations, Eqs. 5-17, are first put in standard state variable form. As in the typical section case, a decision as to which quantities are selected as states must be made, with the added complexity for the three-dimensional wing in deciding how many vibrational modes to assume in the analysis. Each additional assumed mode increases the number of states by four, due to the particular modeling of the incompressible

aerodynamics. Thus, for the two mode analysis, the system could be represented by ten states (two states corresponding to the CMG), and eighteen states would be needed if four modes were included in the analysis. It is obvious that the amount of analysis and various design requirements such as sensor and feedback selection, could be substantially reduced if only two modes are necessary to obtain accurate control information. For that reason, and because the two mode analysis proved adequate in determining the open-loop system characteristics, a feedback control design using two modes was first attempted. The gains obtained from this analysis were then used to determine the characteristics of the system, approximated by four modes, to verify the accuracy of the two mode method.

The selection of the ten states defining the two mode system is made consistent with those chosen in the typical section analysis of Chap. 3. They are

$$h_{11} = h_1 \tag{6-1}$$

$$h_{12} = \dot{h}_1 \tag{6-2}$$

$$\alpha_{11} = \alpha_1 \tag{6-3}$$

$$\alpha_{12} = \dot{\alpha}_1 \tag{6-4}$$

$$\sigma_1 = \sigma \tag{6-5}$$

$$\sigma_2 = \dot{\sigma} \tag{6-6}$$

$$\xi_1 = (1+\mu_1)F_{h1}\frac{\dot{h}_{12}}{b} + (x_{\alpha 11}\mu - a)F_{h1,\alpha 1}\dot{\alpha}_{12} \tag{6-7}$$

$$\xi_2 = \dot{\xi}_1 + \left[(1+\mu_1)d_1+1\right]\bar{u}F_{h1}\frac{\dot{h}_{12}}{b} + \bar{u}\left[(x_{\alpha 11}\mu - a) + \tfrac{1}{2}(1-2a)n_2\right] F_{h1,\alpha 1}\dot{\alpha}_{12} \tag{6-8}$$

$$\xi_3 = (x_{\alpha 11}\mu - a)F_{h1,\alpha 1}\frac{\dot{h}_{12}}{b} + \left[r_{\alpha 1}^2\mu + (\tfrac{1}{8}+a^2)\right]F_{\alpha 1}\dot{\alpha}_{12} \tag{6-9}$$

$$\xi_4 = \left[(x_{\alpha 11}\mu - a)d_1 - (1+2a)n_2\right]\bar{u}F_{h1,\alpha 1}\frac{\dot{h}_{12}}{b} + \left\{\left[r_{\alpha 1}^2\mu + (\tfrac{1}{8}+a^2)\right]d_1 + \tfrac{1}{2}(1-2a) - \mu\left(\frac{\omega_{h1}}{\omega_{\alpha 1}}\right)^2 n_2(1+2a)\right\}\bar{u}F_{\alpha 1} - G_{11}\dot{\sigma}_2 + \dot{\xi}_3 \tag{6-10}$$

Following the procedure developed in Section 3.1, the appropriate portions of the set of Eqs. 5-17 are multiplied by $D_{\varphi}(\bar{s})$ and the inverse Laplace transform taken, remembering that in the two mode case

$$f_{h2} = f_{\alpha 2} = F_{h2} = F_{\alpha 2} = F_{h2,\alpha 1} = F_{h2,\alpha 2} =$$

$$F_{\alpha 2,h1} = F_{\alpha 2,h2} = 0$$

The resulting equations are then written using the state variable definitions, Eqs. 6-1 to 6-10, and put in the matrix form, Fig. 6-1, where the matrix elements are defined in Appendix D.

As discussed in Section 3.3, a necessary and sufficient condition for modal controllability is that the controllability matrix be nonsingular. It can be shown that this matrix defined by

$$C = \left[G \vdots FG \vdots \cdots\cdots \vdots F^{n-1}G \right]$$

is non-singular for the parameters selected in this analysis with G_{11}, $G_{01} > 0$, $\bar{u} \geq 0$. Furthermore, the system remains controllable, using just one controller, even when the number of modes in the analysis is increased, so long as the quantities, $f_{hi}(y_G)$ and $f_{\alpha i}(y_G)$ do not equal zero. This requirement is met with the CMG at the wing tip. These results are, of course, theoretical, with the assumed modes and aerodynamic model being approximations. Experimental verification of controllability of any design would be necessary to insure that the control or sensors are not located at the node of a particular mode of vibration.

6.3 Design by Arbitrary Dynamics

To investigate the feedback characteristics of the system defined in Eqs. 6-11, a particular CMG-controller, having a $\bar{G}_2$-value of 1.13 and CMG-to-wing mass and moment of inertia ratios of .05, was selected for analysis. For flutter velocity increases up to 50% (i.e., $\bar{u}_F = 2.55$), this system will have only two critical roots. Based on the typical section analysis in Sect. 4.3, this system will be the design having minimum power requirements, if the critical roots are placed on the real axis. Assuming a control law of the form

$$
\begin{bmatrix} h_{11}/b \\ h_{12}/b \\ \alpha_{11} \\ \alpha_{12} \\ \sigma_1 \\ \sigma_2 \\ \xi_1 \\ \xi_2 \\ \xi_3 \\ \xi_4 \end{bmatrix} = \begin{bmatrix} 0 & 1 & 0 & 0 & 0 & 0 & 0 & 0 & 0 & 0 \\ 0 & 0 & 0 & 0 & 0 & 0 & F(2,7) & 0 & F(2,9) & 0 \\ 0 & 0 & 0 & 1 & 0 & 0 & 0 & 0 & 0 & 0 \\ 0 & 0 & 0 & 0 & 0 & 0 & F(4,7) & 0 & F(4,9) & 0 \\ 0 & 0 & 0 & 0 & 0 & 0 & 0 & 0 & 0 & 0 \\ 0 & 0 & 0 & F(6,4) & 0 & 1 & 0 & 0 & 0 & 0 \\ 0 & 0 & 0 & 0 & 0 & 0 & F(7,7) & 1 & F(7,9) & 0 \\ F(8,1) & F(8,2) & F(8,3) & F(8,4) & 0 & 0 & F(8,7) & 0 & F(8,9) & 0 \\ 0 & 0 & 0 & F(9,4) & 0 & 0 & F(9,7) & 0 & F(9,9) & 1 \\ 0 & F(10,2) & F(10,3) & F(10,4) & 0 & F(10,6) & F(10,7) & 0 & F(10,9) & 0 \end{bmatrix} \begin{bmatrix} h_{11}/b \\ h_{12}/b \\ \alpha_{11} \\ \alpha_{12} \\ \sigma_1 \\ \sigma_2 \\ \xi_1 \\ \xi_2 \\ \xi_3 \\ \xi_4 \end{bmatrix} + \begin{bmatrix} 0 \\ 0 \\ 0 \\ 0 \\ 0 \\ 1 \\ 0 \\ 0 \\ G_{11} \\ d_1\bar{u}G_{11} \end{bmatrix} \frac{T_c}{I_{G_Z}\omega_{\alpha 1}^2}
$$

(6 - 11)

FIG. 6-1 TWO MODE EQUATIONS OF MOTION

$$\frac{T_c}{I_{G_z}\omega_1^2} = K_1\frac{h_1}{b} + K_2\frac{\dot{h}_1}{b} + K_3\alpha_1 + K_4\dot{\alpha}_1 - K_5\,\sigma - K_6\dot{\sigma} \qquad (6\text{-}12)$$

$$+ K_7\,\xi_1 + K_8\,\xi_2 + K_9\,\xi_3 + K_{10}\,\xi_4$$

and utilizing Eq. 3-26 results in feedback gains, varying with velocity, shown in Table 6-1. Since the three-dimensional wing is stable without the CMG for $\bar{u} < 1.7$, only the feedback characteristics for $\bar{u} > 1.7$ were considered of interest.

TABLE 6-1

SCHEDULED GAINS FOR FLUTTER SUPPRESSION TO $\bar{u} = 2.55$

$\bar{u}$	K_1	K_2	K_3	K_4	K_5	K_6	K_7	K_8	K_9	K_{10}
1.9	.006	.009	.057	.014	.006	.080	.0	.001	.001	.005
2.1	.006	.008	.052	.014	.006	.081	0.0	.001	.002	.005
2.3	.005	.006	.048	.016	.006	.084	0.0	.001	.001	.005
2.5	.0045	.006	.043	.017	.007	.086	0.0	.001	.001	.004

As was discussed in the typical section analysis of Sect. 3.4, when there are only two critical roots the gains remain fairly constant with velocity. The relative sizes of the gains indicate that full state feedback may not be necessary. A number of reduced state feedback systems, using constant gains and meeting the stability criterion, are possible, three of which are shown in Table 6-2:

TABLE 6-2

CONSTANT REDUCED GAIN DESIGNS FOR $\bar{u} = 2.55$

a)	b)	c)
$K_3 = .043$	$K_1 = .0045$	$K_3 = .043$
$K_5 = .020$	$K_3 = .03$	$K_4 = .017$
$K_6 = .086$	$K_5 = .04$	$K_5 = .020$

A comparison of the root loci obtained for the scheduled gains of Table 6-1 and the constant reduced gains of Table 6-2, case a), which requires the feedback of α, σ, and $\dot{\sigma}$, is shown in Fig. 6-2. The final selection of any feedback scheme will depend on sensor and power requirements, with any variation from the gains in Table 6-1 resulting in increased power.

The simplest control design would be to just feedback σ. However, the large power increase associated with this design (cf. Fig. 4-5) would probably make it infeasible.

6.4 Higher Mode Instability

Although a number of designs have been developed for suppressing flutter in the system defined by Eqs. 6-11, there is no assurance, as yet, that the gains determined will stabilize this system with higher modes included in the analysis. An example of the occurrence of such a higher order instability is presented in Ref. 35 for a flexible launch vehicle. To guard against such occurrences in a design, usually more modes are included in the control analysis than are necessary to accurately determine the passive flutter characteristics. For example, in Ref. 36, although three modes were sufficient to predict the critical flutter velocity, seven modes were used in the control system design analysis.

To determine the effect on higher modes of the designs developed in the previous section, constant gains, corresponding to $\bar{u} = 2.5$ in Table 6-1, were used, and the second bending and second torsion modes were included in describing the wing-controller system. The resulting root locus is shown in Fig. 6-3. From the figure, the problem of higher order instability appears not to exist. Similar results are found for the gains in Table 6-2. This is not the case, however, if different root locations are selected for the critical roots. Figure 6-4 shows the locations of roots corresponding to different values of the imaginary part of the critical root at a velocity corresponding to $\bar{u} = 2.5$. From Fig. 6-3, it can be seen that, although the roots associated with the first bending and torsion branches remain relatively constant as the imaginary value of the critical root is increased, the higher order roots do vary,

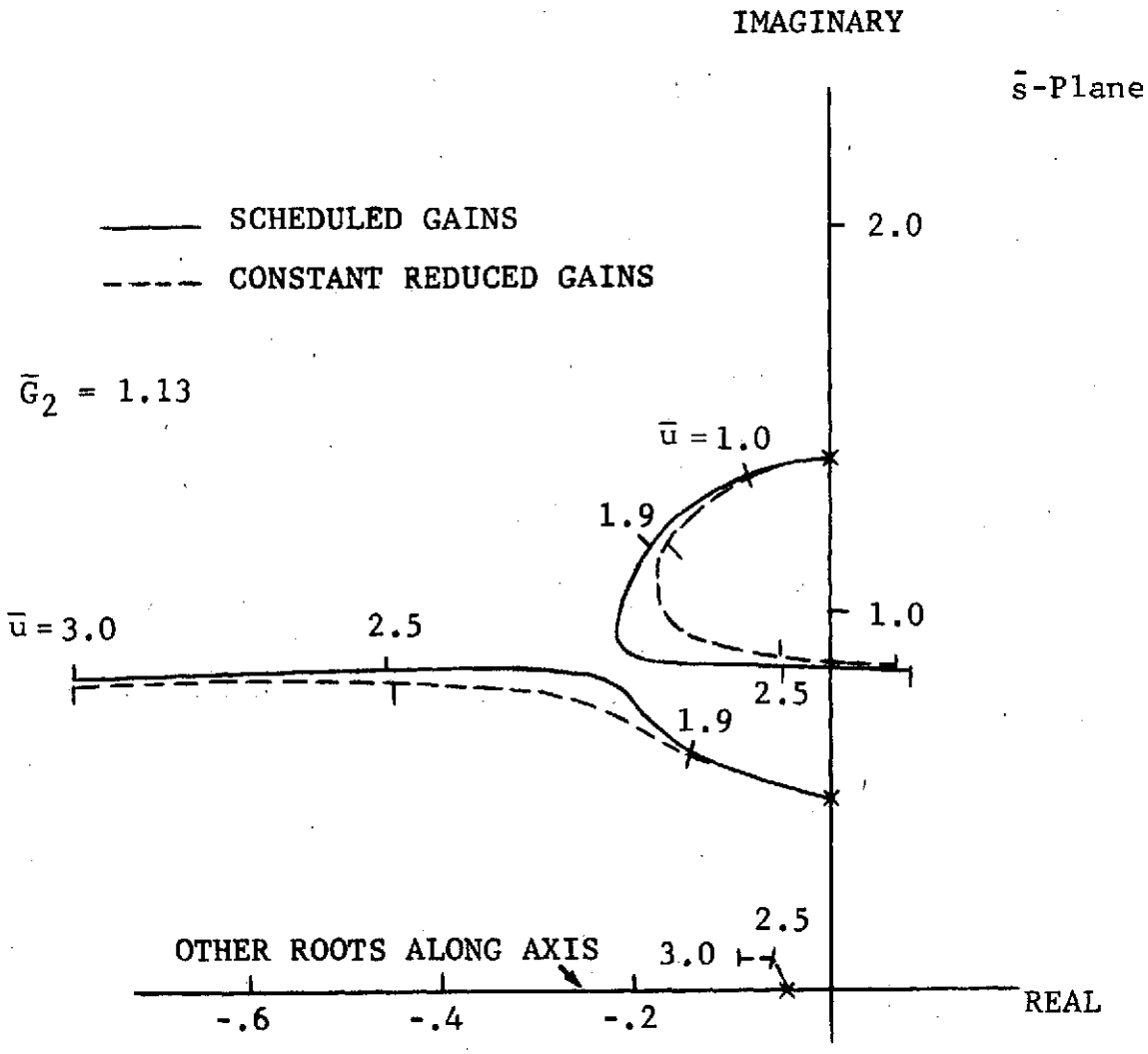

FIG. 6-2 COMPARISON BETWEEN SCHEDULED GAINS AND REDUCED CONSTANT GAINS

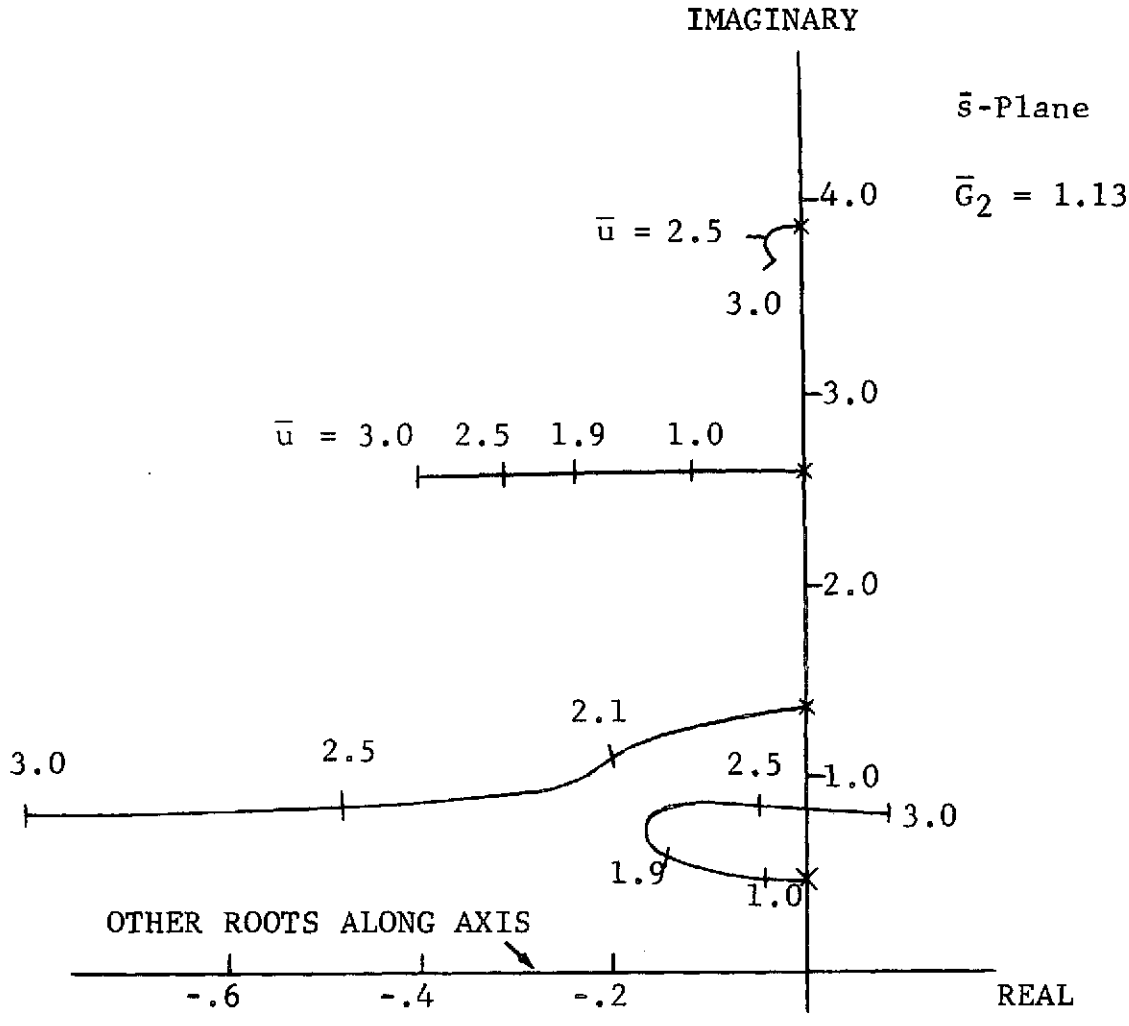

Fig. 6-3 FOUR MODE ROOT LOCUS USING OPTIMIZED CONSTANT GAINS FROM TWO MODE ANALYSIS

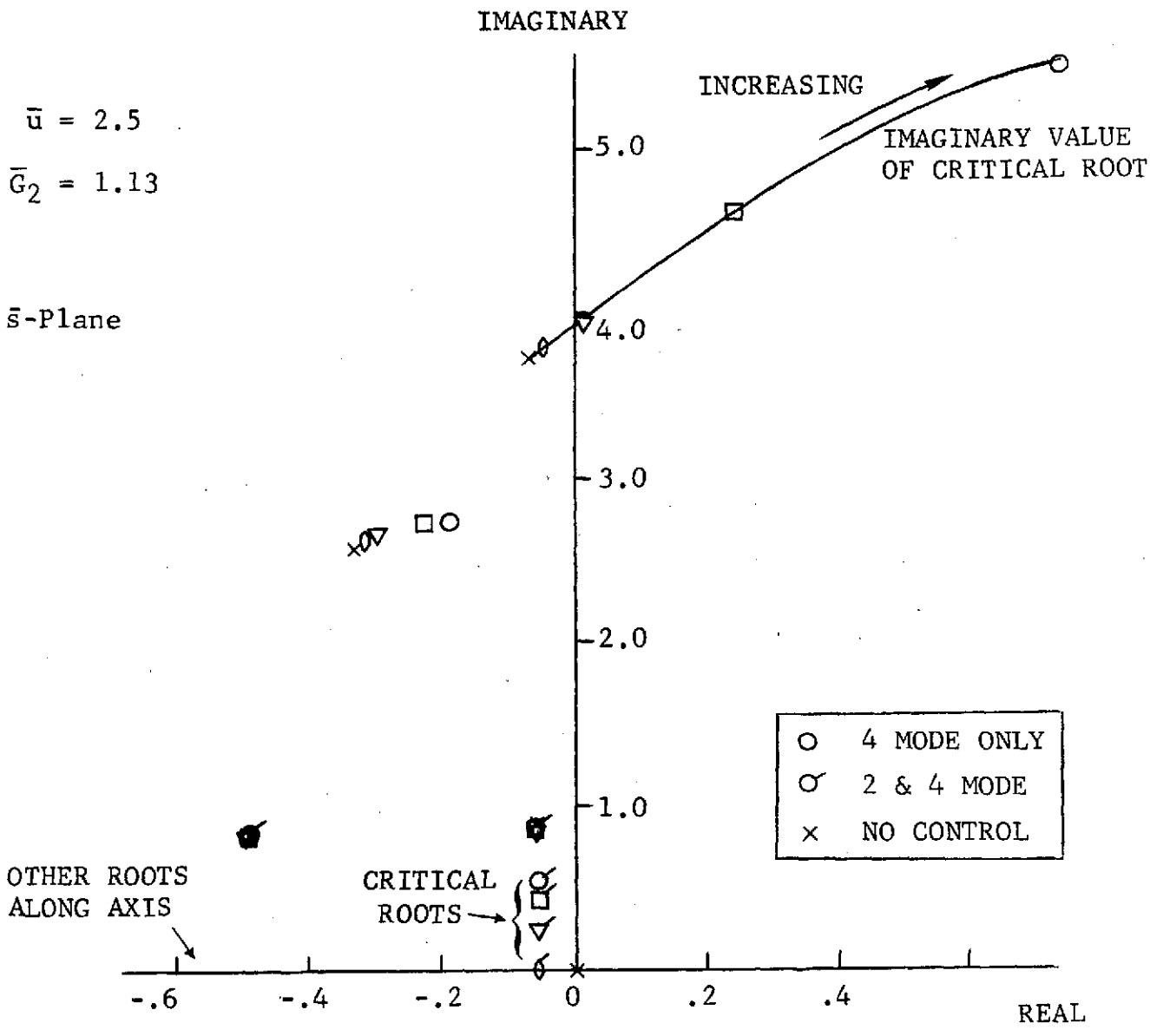

FIG. 6-4 COMPARISON OF FOUR MODE ROOTS USING TWO MODE GAINS FOR DIFFERENT LOCATIONS OF CRITICAL ROOTS

with one root eventually becoming and staying unstable. Similar results will occur, if other prescribed root locations in the two mode analysis cause the gain values, and thus the power requirements to be large. The gains in Table 6-1 were selected by minimizing the value of power required for control upon encountering an impulsive gust disturbance. This criterion caused the minimum perturbation in the non-critical roots and resulted in low gain values. If other optimum criteria are established, for example, by defining certain weighting matrices in the quadratic synthesis analysis discussed in Sect. 4-1, problems in higher mode instability may occur.

6.5 System Observability

As was discussed in Section 3.5, the sensor problem could be reduced if all the states could be estimated from a measurement of σ . The system, Eqs. 6-11, will be observable if the observability matrix, defined in Eq. 3-27, is non-singular. It can be shown that the observability matrix is non-singular for the parameters selected in this analysis for $G_{01}, G_{11}, > 0, \tilde{u} \geq 0$. The system does not remain observable with a single measurement, however, if higher modes are included in the analysis, even if $f_{hi}(y_G)$ and $f_{\alpha i}(y_G)$ do not equal zero. The relationship between the modes (cf. Eqs. 5-5 & 5-6) requires additional measurements as the number of selected modes increases, since only $\alpha(t)$ (or $h(t)$) and not $\alpha_1(t)$ and $\alpha_2(t)$ can be determined from a single measurement. This illustrates another advantage to the design of Sect. 6-3, which required but two modes for a suitable design.

VII. CONCLUSIONS & RECOMMENDATIONS

7.1 Conclusions

An analysis, utilizing modern control techniques for designing active flutter suppression systems with a control moment gyro as the controller, has been presented. The following conclusions can be drawn:

1. The concepts of modern control theory provide a well-organized, systematic, and mathematically powerful approach to the design of active flutter suppression systems. Using the method of arbitrary dynamics, feedback gains, which produce stable systems having satisfactory response characteristics, can be easily obtained in a straightforward manner over a wide range of structural, geometric, and aerodynamic parameters. The solution for optimal gains based on a variety of cost functionals can be incorporated into the design not only for the single input/single output case considered here, but can be adapted to multi-input/multi-output systems. If full state feedback systems are not feasible, these methods provide starting points in obtaining reduced feedback and suboptimal designs.

2. The control moment gyro has certain attractive design features which warrant its consideration as an alternative to aerodynamic surfaces for actively suppressing flutter modes. Controller designs characterized by simplicity, quick response, and low power requirements can be developed.

3. Although the flutter suppression analysis in this thesis was accomplished using a control moment gyro, certain design results can be applied generally to any controller.

   (a) Controllability can be achieved using only one, properly placed, controller for significant increases in flutter velocity.

   (b) When using arbitrary dynamics, noncritical roots should remain constant.

(c) For introductory analyses, relative feedback gain size is a reasonable design criterion for evaluating prospective designs.

(d) Optimization criterion, such as minimizing a quadratic cost function, should be used cautiously, with the possibility of higher order instability kept in mind.

(e) Two-dimensional analysis can provide valuable insight in developing practical design procedures and determining basic system characteristics.

(f) Certain aerodynamic surface parameters, such as flap width and/or length, can play a role similar to $\bar{G}_2$ in selecting optimum designs.

7.2 Recommendations

In the field of active flutter suppression there are many possible areas of further research, many of which are discussed in Ref. 4. Recommendations evolving more directly from the results of this thesis are the following, some of which are presently being pursued at Stanford:

1. Application of the control moment gyro concept as primary control device or in conjunction with aerodynamic surfaces, to an actual wing model, to determine realistic sizing and power requirements.

2. Application of the design techniques, procedures, and tradeoff studies outlined in this thesis to an aerodynamic surface control, to compare power, performance, and complexity of design.

3. Establishment of a practical design optimization criterion, thereby providing a more thorough understanding into the cause and prevention of higher order instability.

4. Development of suitable mathematical modeling of the aerodynamics in subsonic, transonic, and supersonic flow over complex elastic structures to allow the broad application of modern control techniques.

5. Establishment of sensor and estimator requirements to determine the required feedbacks for stable and optimum designs.

APPENDIX A

AERODYNAMIC FORCES ON A TWO-DIMENSIONAL WING SECTION IN UNSTEADY INCOMPRESSIBLE FLOW

Critical to the application of certain design techniques used in this thesis, such as the root-locus diagram and state variable formulation, is the particular modeling of the two-dimensional, transient aerodynamic forces using the Wagner indicial function. Although this concept is familiar to most aeroelasticians, it is felt that a brief description of its derivation is warranted.

First, the aerodynamic forces in two-dimensional, incompressible flow on a surface oscillating in simple harmonic motion are considered. Using potential flow theory, Theodorsen (22) obtained results for lift and moment in which the solution was separated into two components, corresponding to circulatory and non-circulatory portions of the flow field. The resulting equations can be written

$$L = \pi\rho b^2\left[\ddot{h}+U\dot{\alpha}-ba\ddot{\alpha}\right]+2\pi\rho UbC(k)\left[\dot{h}-U\alpha+b(\tfrac{1}{2}-a)\dot{\alpha}\right] \qquad (A\text{-}1)$$

$$M = \pi\rho b^2\left[ba\ddot{h}-Ub(\tfrac{1}{2}-a)\dot{\alpha}-b^2(\tfrac{1}{8}+a^2)\ddot{\alpha}\right] + 2\pi\rho Ub^2(a+\tfrac{1}{2})C(k)\left[\dot{h}+U\alpha+b(\tfrac{1}{2}-a)\dot{\alpha}\right] \qquad (A\text{-}2)$$

The non-circulatory components are contained in the first set of terms in Eqs. A-1 and A-2, and are also valid for arbitrary motion as long as it is small. In the second set of terms, $C(k)$ is commonly known as the Theodorsen function and is evaluated by solving certain complex integrals resulting from the potential flow formulation. The Theodorsen function is complex and can be written after integration

$$C(k) = F(k) + iG(k) = \frac{H_1^{(2)}(k)}{H_1^{(2)}(k)+ iH_o^{(2)}(k)} \qquad (A\text{-}3)$$

where $H_1^{(2)}$ and $H_0^{(2)}$ are Hankel functions of the second kind. A complex polar plot of C(k) is shown below.

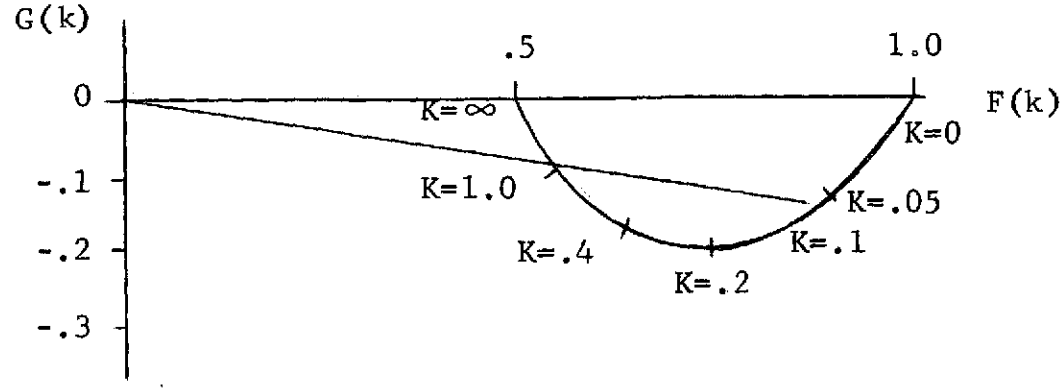

Fig. A-1 COMPLEX POLAR PLOT OF C(k)

These results have been used extensively for flutter prediction for many years, and can still provide a source of relatively reliable reference data for large aspect ratio wings even though they actually have supersonic flutter speeds (20).

Theodorsen's formulation for C(k) is invalid, however, for convergent oscillations in arbitrary motion. One method for solving this problem employs a superposition (Duhamel) integral of the linear results for simple harmonic motion.

Corresponding to the steady state case, Wagner (23) determined the lift on an airfoil considering the growth of circulation about the airfoil as it starts impulsively from rest to a uniform velocity, U. The form of this lift is

$$L = 2\pi\rho b\, Uw\, \Phi(\bar{t})$$

where w is the downwash velocity, $\bar{t}$ is a non-dimensional time, and $\Phi(\bar{t})$ is the Wagner indicial function. Wagner's

function was originally calculated by using a vortex-sheet method (23). The method described here somewhat parallels the approach in Ref. 24.

Because of linearity, it is possible to determine the lift due to circulation for any arbitrary motion of the airfoil by superposition. In an interval $d\bar{t}$ the downwash $w(\bar{t})$ increases by the amount, $\frac{dw(\bar{t})}{d\bar{t}}\, d\bar{t}$. When $d\bar{t}$ is small, this may be regarded as an impulsive increment and the lift can be determined by convolution:

$$L = 2b\pi U\rho\left[w(o)\,\Phi(o) + \int_o^{\bar{t}} \Phi(\bar{t}-\bar{t}')\frac{dw(\bar{t}')}{d\bar{t}'}\, d\bar{t}'\right] \qquad \text{(A-4)}$$

It is a convenient fact that in incompressible flow the circulatory component of force on an airfoil is determined by the downwash velocity at the 3/4-chord (cf Eqs. A-1 & A-2) which has the form

$$w_{3/4c} = \dot{h} + U\alpha + b\,(\tfrac{1}{2}-a)\dot{\alpha} \qquad \text{(A-5)}$$

Thus, only one Wagner function is required to describe the arbitrary motion. The Wagner function is evaluated by assuming

$$w(\bar{t}) = w_o e^{ik\bar{t}}$$

in Eq. A-4 and comparing the results to Theodorsen's form for the oscillatory lift, Eq. A-1, which can be written

$$L = 2\pi b\rho UC(k)w_o e^{ik\bar{t}} \qquad \text{(A-6)}$$

After some manipulation of terms, the Wagner function can be written as

$$\Phi(\bar{t}) = \frac{2}{\pi}\int_o^{\infty} \frac{F(k)}{k} \sin k\bar{t}\, dk \qquad \text{(A-7)}$$

and its behavior as a function of $\bar{t}$ is illustrated in Fig. A-2.

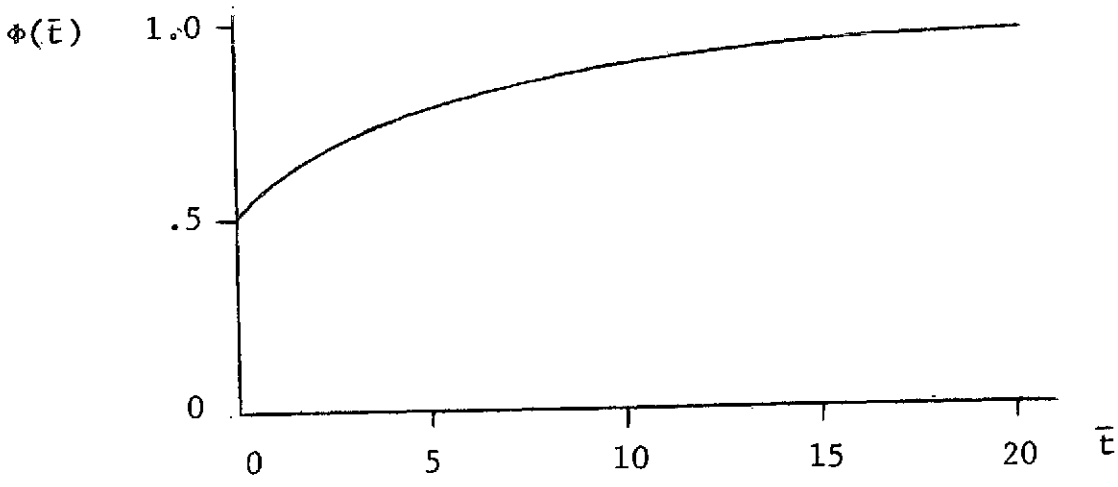

FIG A-2 WAGNER INDICIAL LIFT FUNCTION

Although $\Phi(\bar{t})$ has a relatively simply graphical form, it is not mathematically expressible in terms of well-known functions. Therefore, several accurate approximations have been developed (20). For convenience in taking Laplace transforms, a particularly useful one for application in this thesis, is the form

$$\Phi(\bar{t}) \simeq 1 - .165e^{-.0455\bar{t}} - .335e^{-.3\bar{t}} \qquad \text{(A-8)}$$

Appendix B

GYRO EQUATIONS OF MOTION

In the twin-gyro controller, the equal but opposite precession of the gyro rotors can be obtained by using two torquing motors or by using one motor with proper gearing between the two gyros. The development of the CMG contribution to the typical-section equations of motion follows the derivation in Ref. 19, in which one motor is used. For this analysis, the following assumptions are made:

(1) The CMG twin-gyro controller is rigidly attached to the wing.

(2) The spin speed of each rotor is assumed equal and constant with respect to its respective gimbals.

(3) The rotor spin axes are principal axes.

(4) The moment of inertia of the typical section-controller combination about the elastic axis (y) is independent of the gyro gimbal angle σ (Fig. B-1).

(5) The typical section rotates only about the elastic axis.

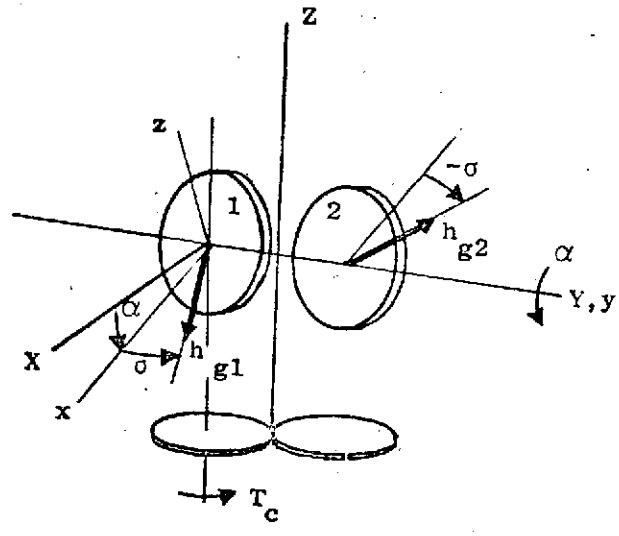

FIG. B-1 TWIN-GYRO CONTROLLER ROTORS

The total angular momentum of the gyro controller is

$$\vec{H}_{TG} = \vec{H}_{G1} + \vec{H}_{G2} + \vec{H}_{F} \tag{B-1}$$

where

$\vec{H}_{TG}$ = total angular momentum of the twin-gyro controller

$\vec{H}_{G1}$ = total angular momentum of gyro 1, including rotor and gimbal

$\vec{H}_{G2}$ = total angular momentum of gyro 2

$\vec{H}_{F}$ = total angular momentum of twin-gyro controller "fixed" elements.

From Fig. B-1

$$\vec{H}_{G1} = h_{g1} \cos\sigma \, \hat{x} + (h_{g1} \sin\sigma + I_{1y}\dot{\alpha})\hat{y} + I_{1z}\dot{\sigma}\hat{z} \tag{B-2}$$

where

h_{g1} = angular momentum of gyro rotor 1

I_{1y} = moment of inertia of gyro 1 about y axis

I_{1z} = moment of inertia of gyro 1 about z axis.

Similarly,

$$\vec{H}_{G2} = -h_{g2} \cos\sigma \, \hat{x} + (h_{g2} \sin\sigma + I_{2y}\dot{\alpha})\hat{y} - I_{2z}\dot{\sigma}\hat{z}; \tag{B-3}$$

also

$$\vec{H}_{F} = I_{F}\dot{\alpha}\hat{y} \tag{B-4}$$

where I_F is the moment of inertia of the fixed components about the y axis. Combining Eqs. B-1, B-2, B-3, and B-4 and letting $h_{g1} = h_{g2}$, $I_{1z} = I_{2z}$ yield

$$\vec{H}_{TG} = (H_w \sin\sigma + I_y\dot{\alpha})\,\hat{y} \tag{B-5}$$

where

$$H_w = 2h_{g1} = 2h_{g2}$$

$$I_y = I_{1y} + I_{2y} + I_F.$$

Equation B-5 illustrates the features of the twin-gyro controller in which the momentum change will occur about the y axis and crosscoupling terms cancel.

To obtain the contribution of the controller to the typical-section equations of motion, Eq. B-5 is differentiated with respect to time in an inertial reference frame and expressed in the wing reference frame by the theorem of Coriolis as

$$\overset{i}{\vec{H}}_{TG} = \overset{w}{\vec{H}}_{TG} + \vec{\omega} \times \vec{H}_{TG} = \vec{M}_{w/G}. \qquad \text{(B-6)}$$

Here the superscript i indicates differentiation with respect to time in an inertial frame; the superscript w indicates time differentiation in the wing frame; $\vec{\omega}$ is the angular velocity of the wing frame with respect to the inertial frame which is this analysis equals $\dot{\alpha}\hat{y}$; and $M_{w/G}$ is the reaction moment of the wing on the controller.

Equation B-6 can be written in scalar notation since the momentum and rotation are about the y axis. It becomes

$$\overset{i}{H}_{TG} = I_y \ddot{\alpha} + H_w \dot{\sigma}\cos\sigma = M_{w/G} . \qquad \text{(B-7)}$$

An equation involving the control torque and the gyro parameters can be obtained by differentiating Eqs. B-2 and B-3 and applying the theorem of Coriolis. This results in

$$\overset{i}{\vec{H}}_{G1} = (I_{1z}\dot{\alpha}\dot{\sigma}+h_{g1}\dot{\sigma}\sin\sigma)\hat{x}+(h_{g1}\dot{\sigma}\cos\sigma+I_{1y}\ddot{\alpha})\hat{y}$$

$$+ (I_{1z}\ddot{\sigma}-h_{g1}\dot{\alpha}\cos\sigma)\hat{z} = \vec{T_1} \qquad \text{(B-8)}$$

$$\frac{i}{H_{G2}} = (-I_{2z}\dot{\alpha}\dot{\sigma}+h_{g2}\,\dot{\sigma}\sin\sigma\,)\hat{x}+(h_{g2}\,\dot{\sigma}\cos\sigma+I_{2y}\ddot{\alpha})\hat{y}$$

$$+\,(-I_{2z}\ddot{\sigma}+h_{g2}\,\dot{\alpha}\cos\sigma\,)\hat{z} = \overrightarrow{T_2} \qquad \text{(B-9)}$$

where $\overrightarrow{T_1}$ and $\overrightarrow{T_2}$ are the torques on gyro 1 and 2 respectively.

Subtracting Eq. B-9 from Eq. B-8 and taking the component in the Z direction gives

$$I_{Gz}\,\ddot{\sigma} - H_w\,\dot{\alpha}\cos\sigma = T_{1z} - T_{2z} \qquad \text{(B-10)}$$

where

$$I_{Gz} = I_{1z} + I_{2z}$$

$$\left.\begin{matrix} T_{1z} \\ T_{2z} \end{matrix}\right\} = \text{torques about } z \text{ axis on gyros 1 and 2 respectively.}$$

Since the gyros are geared together,

$$T_{1z} = -T_{2z}.$$

Therefore, let

$$T_{1z} - T_{2z} = 2T_{1z} = T_c$$

where T_c is defined as the control torque supplied by the torque motor on the twin-gyro system about the z axis. Equation B-10 becomes

$$I_{Gz}\,\ddot{\sigma} - H_w\,\dot{\alpha}\cos\sigma = T_c. \qquad \text{(B-11)}$$

With the assumption of small gimbal-angle oscillations about $\sigma = 0$, Eqs. B-7 and B-11 can be linearlized by setting $\cos\sigma \approx 1$. The linearized equations are

$$I_y\,\ddot{\alpha} + H_w\,\dot{\sigma} = M_{w/G} \qquad \text{(B-12)}$$

$$-H_w\,\dot{\alpha} + I_{Gz}\ddot{\sigma} = T_c. \qquad \text{(B-13)}$$

Equations B-12 and B-13 are now used in conjunction with the equations of motion for the typical section to describe the motion of the wing-controller system and are applicable for use in the three-dimensional case under the assumptions of Chap. 5.

APPENDIX C

TYPICAL SECTION OPEN-LOOP CHARACTERISTIC EQUATION

The characteristic equation described in Chapter II is

$$\bar{s}^2\Big\{A_6\bar{s}^6+\bar{u}A_5\bar{s}^5+(\bar{u}^2A_{41}+A_{42}+A_{43}G_2)\bar{s}^4+\bar{u}(\bar{u}^2A_{31}+A_{32}+A_{33}G_2)\bar{s}^3$$
$$+\Big[\bar{u}^4A_{21}+\bar{u}^2A_{22}+A_{23}+(\bar{u}^2A_{24}+A_{25})G_2\Big]\bar{s}^2$$
$$+\ \bar{u}\Big[\bar{u}^2A_{11}+A_{12}+(\bar{u}^2A_{13}+A_{14})G_2\Big]\bar{s}$$
$$+\ \bar{u}^2(\bar{u}^2A_{01}+A_{02}+A_{03}G_2)\Big\} = 0$$

where

$$A_6 = (1+\mu)(r_\alpha^2\mu+\tfrac{1}{8}+a^2)-(x_\alpha\mu-a)^2$$

$$A_5 = d_1A_6+\Big[\tfrac{1}{2}(1+\mu)-\mu(x_\alpha+a)\Big]+n_2\Big[2\mu(r_\alpha^2+a^2)+(4x_\alpha a-\tfrac{1}{2})\mu-\tfrac{1}{4}\Big]$$
$$= d_1A_6+A_{5D}+n_2A_{5N}$$

$$A_{41} = d_oA_6+d_1A_{5D}+n_1A_{5N}+n_2\Big[1-\mu(1+2a+2x_\alpha)\Big]$$

$$A_{42} = \left[\left(\frac{\omega_h}{\omega_\alpha}\right)^2(r_\alpha^2\mu+\tfrac{1}{8}+a^2)+r_\alpha^2\mu(1+\mu)\right]$$

$$A_{43} = (1+\mu)$$

$$A_{31} = d_oA_{5D}+n_oA_{5N}+n_1\Big[1-\mu(1+2a+2x_\alpha)\Big]$$

$$A_{32} = d_1A_{42}+\left(\frac{\omega_h}{\omega_\alpha}\right)^2\mu(\tfrac{1}{2}-a)+n_2\left[2r_\alpha^2\mu-\left(\frac{\omega_h}{\omega_\alpha}\right)^2\mu(\tfrac{1}{2}-2a^2)\right]$$

$$A_{33} = 2n_2+(1+\mu)d_1$$

$$A_{21} = n_o\Big[1-\mu(1+2a+2x_\alpha)\Big]$$

$$A_{22} = d_oA_{42}+d_1\left(\frac{\omega_h}{\omega_\alpha}\right)^2\mu(\tfrac{1}{2}-a)+n_1\left[2r_\alpha^2\mu-\left(\frac{\omega_h}{\omega_\alpha}\right)^2\mu(\tfrac{1}{2}-2a^2)\right]$$
$$-\ n_2\left(\frac{\omega_h}{\omega_\alpha}\right)^2\mu(1+2a)$$

$$A_{23} = \left(\frac{\omega_h}{\omega_\alpha}\right)^2 \mu^2 r_\alpha^2$$

$$A_{24} = 2n_1 + (1+\mu)d_o$$

$$A_{25} = \left(\frac{\omega_h}{\omega_\alpha}\right)^2 \mu$$

$$A_{11} = d_o\left(\frac{\omega_h}{\omega_\alpha}\right)^2 \mu(\tfrac{1}{2}-a) + n_o\left[2r_\alpha^2\mu - \left(\frac{\omega_h}{\omega_\alpha}\right)^2 \mu(\tfrac{1}{2}-2a^2)\right] - n_1\left(\frac{\omega_h}{\omega_\alpha}\right)^2 \times \mu(1+2a)$$

$$A_{12} = d_1 A_{23}$$

$$A_{13} = 2n_o$$

$$A_{14} = d_1 A_{25}$$

$$A_{01} = -n_o\left(\frac{\omega_h}{\omega_\alpha}\right)^2 \mu(1+2a)$$

$$A_{02} = d_o A_{23}$$

$$A_{03} = d_o A_{25}$$

$$F_{71} = \frac{\bar{u}}{A_6}(B_1+A_{5D})B_4(\tfrac{1}{2}+a)$$

$$F_{73} = \frac{\bar{u}}{A_6}(B_1+A_{5D})r_\alpha^2\mu$$

$$F_{74} = \frac{\bar{u}^2}{A_6}(B_1+A_{5D})$$

$$F_{76} = \frac{\bar{u}}{A_6} G_1 (B_1+A_{5D})$$

$$F_{77} = -\frac{\bar{u}}{A_6}\left\{n_2 A_{5N} + d_1 A_6 - \left[B_2 + B_1\left(\tfrac{1}{2}+a\right)\right]\right\}$$

$$F_{81} = \frac{B_4}{A_6}\left\{\bar{u}^2\left[\left(\tfrac{1}{2}+a\right)\left(2n_1 A_{5D} + B_1 d_1 + B_1\right) - A_6 d_o\right] - B_2 B_4\left(\tfrac{1}{2}+a\right)\right\}$$

$$F_{82} = -\left(2n_o\bar{u}^2 + B_4 d_1\right)\bar{u}$$

$$F_{83} = \frac{1}{A_6}\left\{r_\alpha^2\mu\left[2n_1\bar{u}^2 A_{5D} + \bar{u}^2 B_1\left(d_1+1\right) - B_2 B_4\right] - 2A_6 n_o \bar{u}^4\right\}$$

$$F_{84} = \frac{1}{A_6}\left\{\bar{u}\left[2n_1\bar{u}^2 A_{5D} + \bar{u}^2 B_1\left(d_1+1\right) - B_2 B_4\right]\right.$$

$$\left. - A_6\bar{u}^2\left[d_o + B_3 n_o + 2n_1\right]\right\}$$

$$F_{86} = \frac{G_1}{A_6}\left\{2n_1\bar{u}^2 A_{5D} + \bar{u}^2 B_1\left(d_1+1\right) - B_2 B_4\right\}$$

$$F_{87} = -\frac{1}{A_6}\left(\bar{u}^2\left\{d_o A_6 + n_1 A_{5N} - \left(d_1+1\right)\left[B_2 + B_1\left(\tfrac{1}{2}+a\right)\right]\right\}\right.$$

$$\left. + B_4\left[B_2\left(\tfrac{1}{2}+a\right) + r_\alpha^2\mu + \tfrac{1}{8} + a^2\right]\right)$$

APPENDIX D

ELEMENTS OF TWO MODE, OPEN-LOOP DYNAMICS MATRIX

The open loop dynamics matrix, developed using two uncoupled modes of vibration, is written in Eq. 6-11. The elements of that matrix are defined as follows:

$$F(1,2) = 1.0$$

$$F(2,7) = (r_{\alpha 1}^2 \mu + \frac{1}{8} + a^2) F_{\alpha 1}/\Delta$$

$$F(2,9) = -(x_{\alpha 11}\mu - a) F_{h1,\alpha 1}/\Delta$$

$$F(3,4) = 1.0$$

$$F(4,7) = -(x_{\alpha 11}\mu - a) F_{h1,\alpha 1}/\Delta$$

$$F(4,9) = (1+\mu_1) F_{h1}/\Delta$$

$$F(5,6) = 1.0$$

$$F(6,4) = -G_{o1}$$

$$F(7,7) = \left\{ \left[(1+\mu_1) d_1 + 1 \right] F(2,7) F_{h1} + \left[(x_{\alpha 11}\mu - a) d_1 + 1 + B_3 n_2 \right] F(2,9) F_{h1,\alpha 1} \right\} \bar{u}$$

$$F(7,8) = 1.0$$

$$F(7,9) = -\left\{ \left[(x_{\alpha 11}\mu - a) d_1 + 1 + B_3 n_2 \right] F(4,9) F_{h1,\alpha 1} + \left[(1+\mu_1) d_1 + 1 \right] F(4,7) F_{h1} \right\} \bar{u}$$

$$F(8,1) = -\mu \left(\frac{\omega_{h1}}{\omega_{\alpha 1}} \right)^2 d_o F_{h1} \bar{u}^2$$

$$F(8,2) = -\left[2n_o \bar{u}^3 + \mu \left(\frac{\omega_{h1}}{\omega_{\alpha 2}} \right)^2 d_1 \bar{u} \right] F_{h1}$$

$$F(8,3) = -2n_o \bar{u}^4 F_{h1,\alpha 1}$$

$$F(8,4) = -\left[d_o + B_3 n_o + 2n_1 \right] \bar{u}^3 F_{h1,\alpha 1}$$

$$F(8,7) = -\left\{ \left[\bar{u}^2 \left((1+\mu_1) d_o + 2n_1 \right) + \mu \left(\frac{\omega_{h1}}{\omega_{\alpha 1}} \right)^2 \right] F_{h1} F(2,7) + \left[(x_{\alpha 11}\mu - a) d_o + d_1 + B_3 n_1 + 1 \right] \bar{u}^2 F_{h1,\alpha 1} F(2,9) \right\}$$

$$F(8,9) = -\left\{\left[(x_{\alpha 1}1\mu - a)d_o + d_1 + B_3 n_1 + 1\right]\bar{u}^2 F_{h1,\alpha 1}F(4,9) + \left[\bar{u}^2\left((1+\mu_1)d_o + 2n_1\right) + \mu\left(\frac{\omega_{h1}}{\omega_{\alpha 1}}\right)^2\right]F_{h1}F(4,7)\right\}$$

$$F(9,4) = -G_{o1}\, G_{11}$$

$$F(9,7) = -\left\{\left[(x_{\alpha 1}1\mu - a)d_1 - (1+2a)n_2\right]F_{h1,\alpha 1}F(2,7) + \left[(r^2_{\alpha 1}\mu + \tfrac{1}{8} + a^2)d_1 + \frac{B_3}{2} - (\tfrac{1}{2} - a^2)n_2\right]F_{\alpha 1}F(2,9)\right\}\bar{u}$$

$$F(9,9) = -\left\{\left[(r^2_{\alpha_1}\mu + \tfrac{1}{8} + a^2)d_1 + \frac{B_3}{2} - (\tfrac{1}{2} - 2a^2)n_2\right]F_{\alpha 1}(4,9) + \left[(x_{\alpha 1}1\mu - a)d_1 - (1+2a)n_2\right]F_{h1,\alpha 1}F(4,7)\right\}\bar{u}$$

$$F(9,10) = 1.0$$

$$F(10,2) = (1+2a)n_o\bar{u}^3 F_{h1,\alpha 1}$$

$$F(10,3) = -\left[r_\alpha{}^2\mu d_o\bar{u}^2 - (1+2a)n_o\bar{u}^4\right]F_{\alpha 1}$$

$$F(10,4) = -\left\{\bar{u}^3\left[\frac{B_3}{2}\, d_o - (\tfrac{1}{2} - 2a^2)n_o - (1+2a)n_1\right] + r_\alpha{}^2\mu d_1\bar{u}\right\}F_{\alpha 1} - G_{o1}\, G_{11} d_1\bar{u}$$

$$F(10,6) = G_{11} d_o\bar{u}^2$$

$$F(10,7) = -\left\{\left[(x_{\alpha 1}1\mu - a)d_o - (1+2a)n_1\right]\bar{u}^2 F_{h1,\alpha 1}F(2,7) + \left[\bar{u}^2\left[(x_{\alpha 1}1\mu - a)d_o + \frac{B_3}{2}d_1 - (\tfrac{1}{2} - 2a^2)n_1 - (1+2a^2)n_2\right] + r_\alpha{}^2\mu\right]F_{\alpha 1}F(2,9)\right\}$$

$$F(10,9) = -\left\{\left[\bar{u}^2\left[x_{\alpha 1}1\mu - a)d_o + \frac{B_3}{2}\, d_1 - (\tfrac{1}{2} - 2a^2)n_1 - (1+2a)n_2\right] + r_\alpha{}^2\mu\right]F_{\alpha 1}F(4,9) + \left[(x_{\alpha 1}1\mu - a)d_o - (1+2a)n_1\right]\times \bar{u}^2 F_{h1,\alpha 1}F(4,7)\right\}$$

Where

$$\Delta = (1+\mu_1)(r_{\alpha 1}^2\mu+\tfrac{1}{8}+a^2)F_{h1}F_{\alpha 1}-(x_{\alpha 11}\mu-a)^2F_{h1,\alpha 1}^2$$

REFERENCES

1. Johannes, R. P., "Performance Advantages Offered by Advanced Flight Control Technology", AIAA Paper No. 70-874, July 1970.

2. Johannes, R. P., "Active Flutter Control-Flight Test System Synthesis", JACC Paper No. 7-B1, August 1971.

3. Swaim, R. L., "Aircraft Elastic Mode Control", Journal of Aircraft, Vol. I, No. 2, February 1971, pp. 65-71.

4. Thompson, G. O. and Kass, G. J., "Active Flutter Suppression -- An Emerging Technology", Journal of Aircraft, Vol. 9, No. 3, March 1972, pp. 230-235.

5. Topp, L. J., "Potential Performance Gains by Use of a Flutter Suppression System", JACC Paper No. 7-B3, August 1971.

6. Thiesen, J. G., and W. C. Robinette, "Servo Control of Flutter", AIAA Structural Dynamics and Aeroelastic Specialist Conference Proceedings, April 1969, pp. 228-240.

7. Moon, F. C., and Dowell, E. H., "The Control of Flutter Instability in a Continuous Elastic System using Feedback", AIAA/ASME 11th Structures, Structural Dynamics, and Materials Conference, Volume of Technical Papers on Structural Dynamics, Denver, April 1970.

8. Kalmbach, C. F., "Feedback Control of Flutter Instability in a Continuous Elastic System", AIAA Journal, Vol. 10, No. 5, May 1972, pp. 711-712.

9. Hodges, G. E., "Active Flutter Suppression - B-52 Controls Configured Vehicle", AIAA Paper No. 73-322, 1973.

10. Triplett, W. E., Kappus, H. F., and Landy, R. J., "Active Flutter Control: An Adaptable Application to Wing/Store Flutter", AIAA Paper No. 73-194, 1973.

11. Nissim, E., "Flutter Suppression Using Active Controls Based on the Concept of Aerodynamic Energy", NASA TN D-6199, March 1971.

12. Miller, B., "USAF Plans Advanced Fighter Program", Aviation Week & Space Technology, July 16, 1973, pp. 14-16.

13. White, J. S. and Hansen, Q. M., "Study of a Satellite Attitude Control System Using Integrating Gyros as Torque Sources", NASA TN D-1073, September 1961.

14. Cannon, R. H., Jr., "Basic Response Relations for Satellite Attitude Control Using Gyros", Proceedings of IFAC, Butterworths, London, 1963, pp. 535-544.

15. Havill, J. R. and Ratcliff, J. W., "A Twin-Gyro Attitude Control System for Space Vehicles", NASA TN D-2419, August 1964.

16. Liska, D. J. and Jacot, A. D., "Control Moment Gyros in Attitude Control", Journal of Spacecraft and Rockets, Vol. 3, No. 9, September 1966, pp. 1313-1320.

17. Huston, R. L., "Twin-Gyro Attitude Control Systems", Journal of Spacecraft and Rockets, Vol. 3, No. 7, July 1966, pp. 1136-1138.

18. Campbell, R. A., "Performance of a Twin-Gyro Attitude Control System Including Passive Compensation and a Nonlinear Control Law", NASA TN D-5868, August 1970.

19. Pasternack, S., Jr., "Attitude Control of Hopping Vehicles", Ph.D. Dissertation, May 1971, Dept. of Aeronautics and Astronautics, Stanford University, Stanford, Calif.

20. Bisplinghoff, R. L., Ashley, H., and Halfman, R. L., Aeroelasticity, Addison-Wesley, Cambridge, Mass., 1955.

21. Bisplinghoff, R. L. and Ashley, H., Principles of Aeroelasticity, John Wiley, New York, 1962.

22. Theodorsen, T., "General Theory of Aerodynamic Instability and the Mechanism of Flutter", NACA Report 496, April 1935.

23. Wagner, H., "Uber Die Entstehung Des Dynamischen Auftriebes von Tragflugeln," Z. Angew. Math. Mech., Bd5, Heft 1, Feb. 1925.

24. Garrick, I. E., "On Some Reciprocal Relations in the Theory of Nonstationary Flows", NACA TR 629, 1938.

25. Gopinath, B., "On the Identification and Control of Linear Systems", Ph.D. Dissertation, 1968, Dept. of Electrical Engineering, Stanford University, Stanford, Ca.

26. Bryson, A. E., Jr., and Y.-C. Ho, Applied Optimal Control, Blaisdell, Waltham, Mass., 1969.

27. Hall, W. E., Jr., and Bryson, A. E., Jr., "Optimal Control and Filter Synthesis by Eigenvector Decomposition", SUDAAR No. 436, November 1971, Dept. of Aeronautics and Astronautics, Stanford University, Stanford, Calif.

28. Runyan, H. L., and Watkins, C. E., "Flutter of a Uniform Wing with an Arbitrarily Placed Mass According to a Differential-Equation Analysis and a Comparison with Experiment", NACA TN 1848, 1949.

29. Goland, M., "The Flutter of a Uniform Cantilever Wing", Journal of Applied Mechanics, Vol. 12, No. 4, Dec. 1945, pp. 197-208.

30. Woolston, D. S. and Runyan, H. L., "Appraisal of Method of Flutter Analysis Based on Chosen Modes of Comparison with Experiment for Cases of Large Mass Coupling", NACA TN 1902, 1949.

31. Woolston, D. S. and Runyan, H. L., "On the Use of Coupled Modal Functions in Flutter Analysis", NACA TN 2375, 1951.

32. Fung, Y. C., An Introduction to the Theory of Aeroelasticity, Dover, New York, 1969.

33. Scanlan, R. H. and Rosenbaum, R., Introduction to the Study of Aircraft Vibration and Flutter, Dover, New York, 1968.

34. Wang, P. K., "Control of Distributed Parameter Systems", Advances in Control Systems, Vol. 1, Chap. 3, pp. 75-172, Academic Press, N. Y., 1964.

35. Rynaski, E., Whitbeck, R., and Dolbin, B., Jr., "Sensitivity Considerations in the Optimal Control of a Flexible Launch Vehicle", CAL Report No. BE-2311-F1, Cornell Aeronautical Laboratory, Inc., Buffalo, N. Y., June 1967.

36. Triplett, W. E., "A Feasibility Study of Active Wing/Store Flutter Control", JACC Paper No. 7B4, August 1971.